UiT THE ARCTIC UNIVERSITY OF NORWAY

Faculty of Engineering Science and Technology

Institute of Industrial Engineering

Research on Optimization of Freeform Surface Operation

Dingjun Liu

Master thesis in Industrial Engineering - May 2017

Title: Research on Optimization of Freeform Surface Operation	*Date:* 01/06/2017 *Classification: *)* *OPEN*
Author: Dingjun Liu *Student no:* *540661*	*Number of Pages:* 89 pages *Number of Attachments:* 6 NC files
Subject Name: Master's Thesis	*Subject Code:* SHO6266
Department: Faculty of Engineering Science and Technology	
Master Program: Industrial Engineering	
Supervisor: Gabor Sziebig	
Co-supervisor: Sibul Lazar	
External Organization/Company:	
External Organization's/Company's Liaison:	

Keywords (max 10):

Iso parametric, Iso planar, Iso scallop, prediction of operation, energy consumption optimization

Abstract (max 150 words):

Nowadays, many manufacturing companies need to face competition both in domestic and international level. Due to this circumstance, manufacturers recognize that one useful method to enhance their competence is reducing the lead-time of manufacturing.

There are many researchers focused on minimize the time of actual cutting, tool path optimization and energy consumption optimization etc. However, few researchers have investigated the operation optimization of CNC machine that integrating multiple ways to reduce the operation time of freeform surface cutting. For example, integrating tool path calculation optimization and machining parameters optimization together for the sake of providing an optimization solution package to enhance the efficiency of manufacturing.

This master thesis will investigate the main optimization methods of tool path (Iso parametric, Iso planar and Iso scallop), as well as prediction of operation time and energy consumption optimization. Then we will provide several approaches for machining a surface on a metal rectangle to research the effect of different tool paths generation such as Iso parametric and Iso scallop etc. depend on NC code on machining time and quality.

Table of Contents

List of Tables

List of Figures

Preface

Since the industrial revolution, many manufacturers need to enhance their production efficiency in order to increase their competitiveness. Because CNC machine is the Irreplaceable production tool of the manufacturing, so improving the production efficiency of CNC machine is the main way to improve the competitiveness of the entire manufacturing company.

This master thesis will focus on three-axis CNC machine and the research direction is free surface operation. The three-axis machine is widely applied in machining free form surface parts. Many researchers have done several researches on free form surface operation, such as tool path optimization methods, energy consumption optimization, prediction methods etc. In the second part of this master thesis, there will be a detailed research report about three different main types of tool path optimization algorithm, which are iso parametric, iso planar and iso scallop, as well as prediction model and also including the optimization of energy consumption etc. In the case study part, a free form surface will be machined on a metal rectangle to test the effect of different tool path optimization methods.

In the process of making my master thesis, I received lots of help from different people. I would like to say thank you to my supervisor Gabor Sziebig and co-supervisor Sibul Lazar, I appreciate their selfless help and patient.

Dingjun Liu

Abstract

Nowadays, many manufacturing companies need to face competition both in domestic and international level. Due to this circumstance, manufacturers recognize that one useful method to enhance their competence is reducing the lead-time of manufacturing.

There are many researchers focused on minimize the time of actual cutting, tool path optimization and tool change time optimization etc. However, few researchers have investigated the operation optimization of CNC machine that integrating multiple ways to reduce the operation time of freeform surface cutting. For example, integrating tool path calculation optimization, prediction method and machining parameters optimization together for the sake of providing an optimization solution package to enhance the efficiency of manufacturing.

This master thesis will investigate the main optimization methods of tool path (Iso parametric, Iso planar and Iso scallop), as well as prediction of operation time and energy consumption optimization. Then we will provide several approaches for machining a surface on a metal rectangle to research the effect of different tool paths generation such as Iso parametric and Iso scallop etc. depend on NC code on machining time and quality.

1 Introduction

Three-axis machine is widely used in manufacturing parts within the world. The manufacturers are committed to achieve the highest production efficiency so as to enhance their competitiveness. To improve the CNC machines' production efficiency, we need to first know what is CNC machine and understand its working principle.

Today CNC machines have replaced manual machines that all paths and movements can be programed and controlled by computer and codes, which is more convenience than by hand, as well as decrease the total operation time and avoiding human errors [1]. CNC machine can also significantly increase the productivity by integrating Computer Aided Design (CAD), Computer Aided Manufacturing (CAM) and Numerical Control (NC), which are described in the below Fig.1. Normally, the G code can be generated by CAD/CAM packages automatically from the specific software. However, the parameters such as tool path, feed rate and tool selection are obtained automatically from the program of the software that is not the optimized solution. Due to this circumstance, we will find some place to insert in our optimization program after analysis.

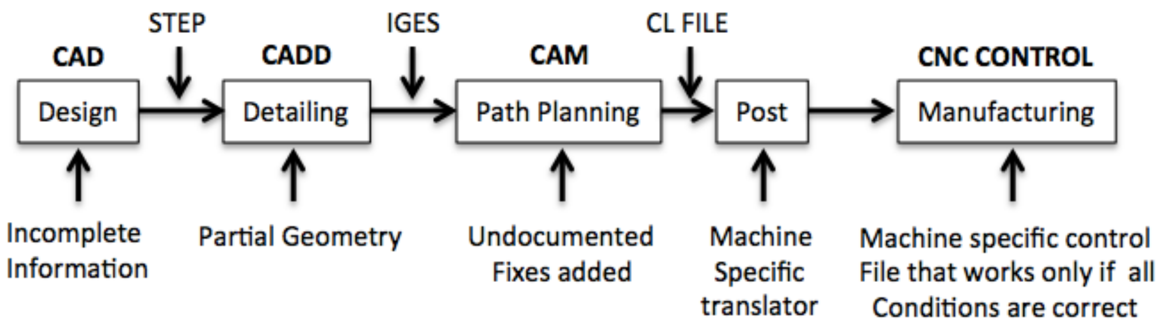

Figure 1 –Manufacturing process: CAD-CAM-PP-CNC

CNC machine (Computer Numerical Control) is a sort of production tool that encompasses different types of machines with variety of shapes, sizes and functions [2]. CNC machines can be divided into two distinct types, which are turning machines and milling machines. A turning machine is generally used to remove materials from the workpiece by spinning the workpiece at a high speed and then use the sharp edge of cutting tool to achieve the desired form [3]. A milling machine is a kind of machine that holds the workpiece with a clamp and then remove the materials to get the need shape with a special high-speed rotation cutting tool to spin and cut in many directions and move in three distinct directions along the x, y and z axis [4].

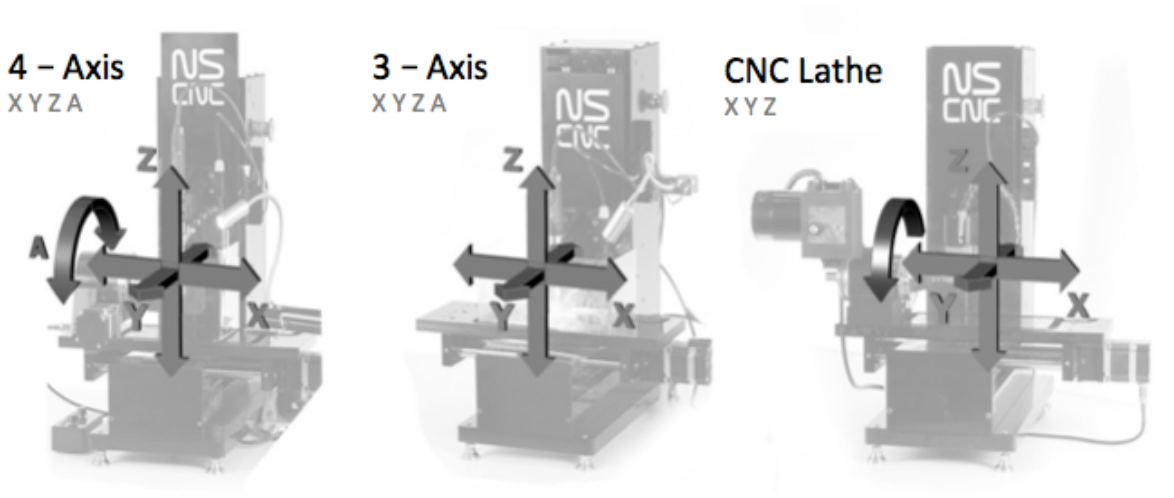

Figure 2 – Four-axis CNC machine, Three-axis CNC machine and CNC lathe.

Fig.2 shows the 4-axis CNC machine, three moving directions of a real CNC machine (3-axis) and CNC Lathe. The difference between those three types of CNC machine can be seen obviously. 3-axis CNC machine has no function of rotation in any axis. However, cutting tool can move in x, y and z directions to produce the required free-form surface. Three-axis CNC machine is not the most advanced machine nowadays, but it has variety of advantages such as high stability, simple operation etc. so that we decided to focus on 3-axis CNC machine.

Because at present there is an increasing demand of complex parts with aerodynamic shapes. Therefore, this master thesis will mainly focus on researching sculpture free-form surfaces with 3-axis Computer Numerical Control machine. In this master paper, an efficient methodology to calculate tool-moving path in order to minimize the total operation time will be conducted, as well as other methods that can contribute to optimize the operation will be investigated in the main chapter.

This master thesis will be organized as follow: chapter one will brief introduce the CNC machine, as well as the background of the research, which includes three algorithms in machining surface, prediction methods and tool path generation according to energy consumption. These three research fields will be discussed detailed in the chapter two with three distinct sub-chapters. Finally, some of the research content will be utilized in the case study part in the chapter three for the sake of researching the effects of different tool path on surface machining.

1.1 Background

In order to achieve the highest production efficiency, there are plenty of methods that can help manufacturers, such as optimizing the energy consumption, tool path generation methods and prediction of operation cycle time etc. This master thesis will mainly focus on sculpture free form surface machining. These surfaces are usually produced by three-axis CNC machine by using ball-end tools.

In this report we will use the sort of ball-end milling of surface machining and then discuss about plenty of possible methods that can effect the total operation time such as three algorithms (iso parametric, iso planar and iso scallop) in machining free form surface, optimization of energy consumption and prediction method during the machining process.

1.1.1 Three Algorithms in Machining Surface

There is variety of algorithms for three-axis tool path generation that has been researched, among those methods the three most popular algorithms in machining free form surface adopted in practice are the iso planar algorithm [5-9], the iso parametric algorithm [10-12] and the iso scallop algorithm [13-21]. Each of these algorithms has its own calculation methods and characteristics.

If we discuss about the first two tool path algorithms, the iso parametric algorithm can only be used to parametric surface but the iso planar algorithm has no restriction as iso parametric method. Either of them is able to calculate a tool path that shows the good surface finishing performance. However, overlap always occurs between the machining areas of adjacent CC curves on the surface if applying these two algorithms to generate tool path, sometimes it will lead to cost more machining time when severe on complicated surfaces. Iso scallop algorithm can eliminate the overlap cause it will start from an initial CC curve and then create the CC curves continuously so that any two neighboring CC curves can be maintained. By using this method, the overlap can be reduced dramatically.

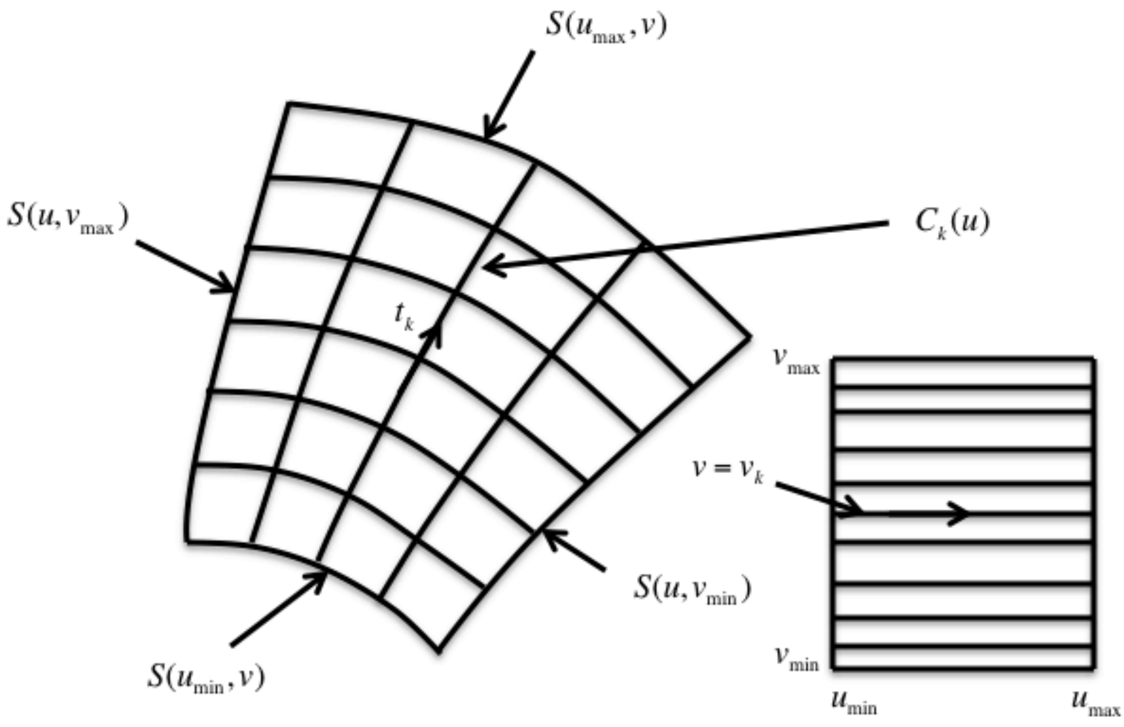

Figure 3 – Iso parametric machining path

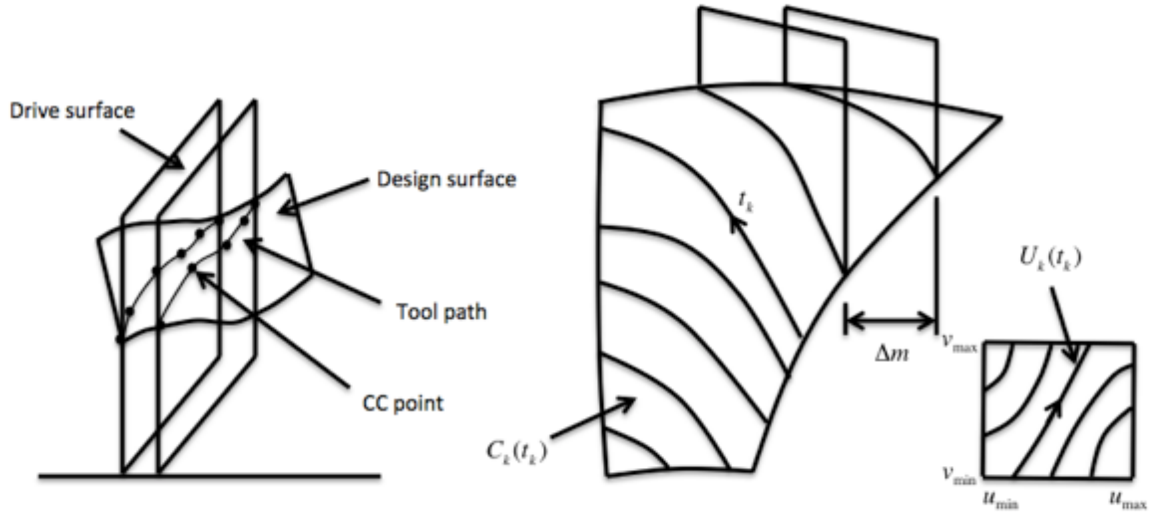

Figure 4 – Iso planar machining path

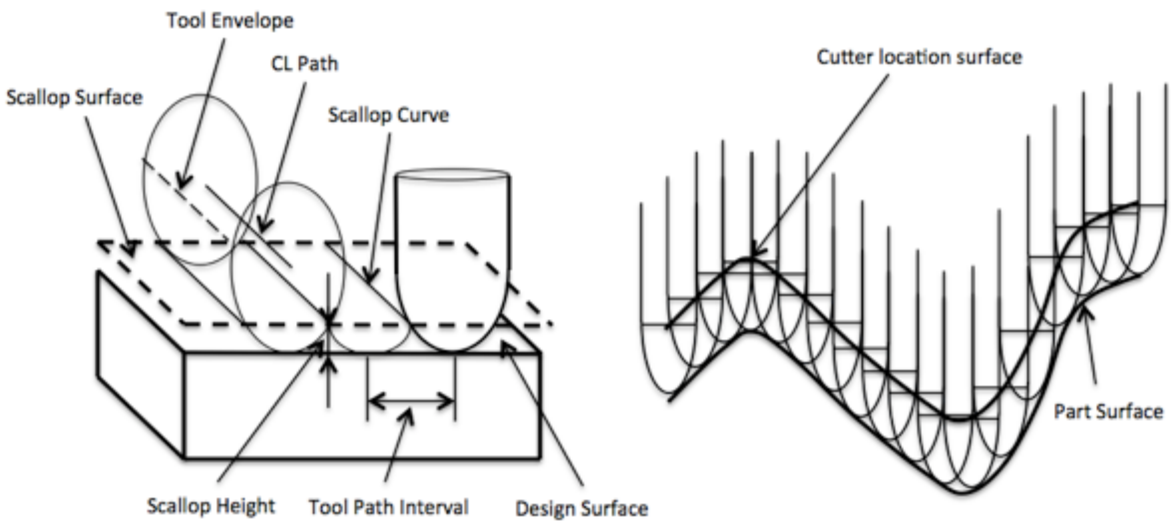

Figure 5 – Iso scallop machining path

Fig. 3, 4 and 5 are schematic illustrations of the iso parametric machining path, iso planar machining path and iso scallop machining path. It can be seen from these figures that different machining method has its own features and ways to generate the tool path. Iso parametric method is selecting one of the surface parameters as the forward direction (it is u in Fig. 3) and the initial path will be another parameter v [22], while iso planar method captures the intersection between the free form surface and a parallel vertical planes as the CC paths [23]. The process of generating the tool path with iso scallop method is more complicated than the other two algorithms. The CC path (cutter contact) performs a tangential trajectory of the ball end machining and the free form surface. In the case of 3D surface machining, it is necessary to generate an offsetting surface in the normal direction with a distance equal to the cutter radius so as to get the CL path that is shown in Fig. 5 [24].

In the chapter 2 there will be a more specific explanation of these three tool path generation algorithms with illustration and calculation.

1.1.2 Prediction of Part Machining Times

The purpose of digital engineering is to simulate the operation systems by researching the corresponding mathematical models based on physical principles. This prediction of part machining times model can predict the structural dynamic behaviour of machine tools by finite element and multibody dynamics methods [25]. The interaction between the structure and manufacturing processes is modelled by feeding back the resulting deflections to the process, predicting the process forces and applying them on the machine structure [26]. The process forces and optimal cutting conditions can be predicted in a virtual model of machining part operations ahead of pricy physical trials [27]. All the methods that mentioned above are important in designing better performance machines and manufacturing operations, the actual machining time of the part is essential in designing and selecting cutting tools to machine specific part geometry, specially in the aerospace industry that the physical test are prohibitive because of the high costs of the parts.

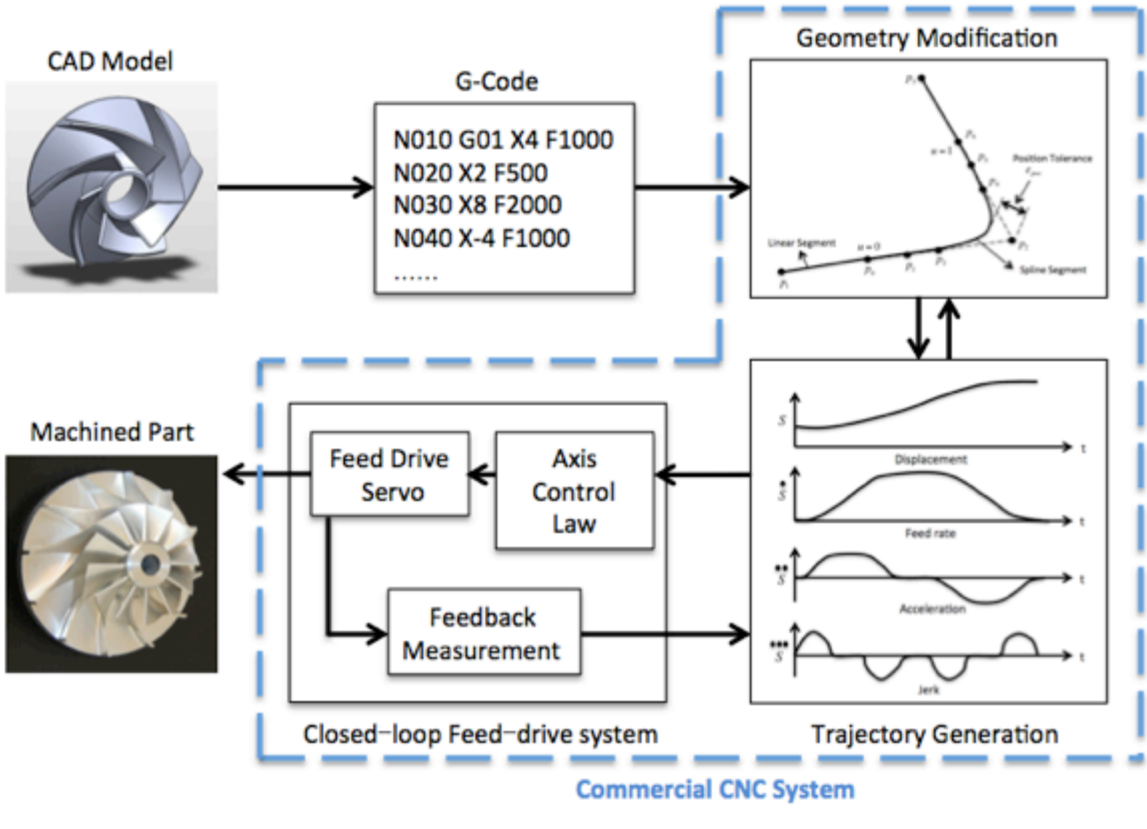

Figure 6 – Action order processing in CNC systems

The total operation time of the part in not only decided by the feeds commanded in the NC program but also by the CNC machine cutting tool's ability. The machining cycle times are predicted by the NC programs that are never accurate due to the CAM systems do not consider the rigid body dynamics of the machining tool. In order to obtain the accurate prediction of cycle time, it should be processing the part's NC tool path by the real CNC of the machine or its own simulation model. Despite of these, it is impossible to copy the commercial CNC's interpolation, smoothing, trajectory generation, compensation and control algorithms, which are hidden in the CNC software.

There are several essays about prediction of machining time from NC programs. The travel time of circular and linear paths are estimated by the path lengths [28] and transition directions between them with the deceleration and acceleration constants of the machine [29,30].

The reference [31] has developed a five-axis research of CNC system in real that is used to validate different smooth trajectory generations, interpolation, active vibration damping and high speed tracking control of feed drives. When the physical machine's drives are changed by their closed loop transfer function blocks, the corresponding CNC changes to a Virtual CNC, which can predict the exact cycle time of a part [32].

In chapter 2 of this master thesis the cycle time prediction model, which is mainly determined by the trajectory module of the CNC that can be decided by acceleration, velocity and jerk elements and limits of the machine will be researched. The trajectory profiles can be obtained from the CNC manufacturer or simple linear motion test. The path is treated by the trajectory generation module, which contains kinematic configuration of the cutting tool. The discrete position orders are generated from the trajectory profiler through the path that determines the cycle time.

1.1.3 Tool Path Generation Regard to Energy Consumption

A typical three axis machining process includes three independent parts. In the computer-aided manufacturing (CAM), a tool path can be generated on different strategies in the workpiece coordinate system (WCS), which can setup virtually aligned and fixed on the operation table. Then at the computer numerical control (CNC) part, the tool path can be transformed into the machine coordinate system (MCS) by inverse kinematics transformation (IKT) and obtains a part program such as G code part program, in which the feedrate is adjusted per the machine's kinematic capacity by the controller. At the final stage, the cutting stage, the part program is conducted and the energy is consumed.

In this paragraph, the energy consumption and related works will be introduced. In order to improve the energy efficiency for a given machining process, the investigation of relationship between the energy consumption and machining parameters. It is important to realize the main contributors to the energy among all the relevant parameters. In reference [33] has made an overall review of existing energy consumption models and found that the cutting process contributes the main energy consumption, which is highly related to the cutting parameters and material removal rate. Reference [34] made a complete evaluation for various machine tools and made a conclusion that the idle power can take about 50% of the total power, which consumes more energy than needed. Reference [35] suggested an empirical way to calibrate the energy consumption model according to their models and they found that material removal rate (MRR) will result in a significant energy saving and cutting in a dry condition is more efficient than in a wet condition. Reference [36] established a model efficiency and specific energy as a unary intention of various parameters and they found that a given set of parameters could decide the specific energy. Energy reduction was researched by [37], with the power pattern for the X, Y and Z axis that is got to be linearly to the feedrate in a certain proportion. In mention to the feedrate, reference [38] has compared the average energy consumption between distinct feedrate and they found that either small or large feedrate could cause high total energy consumption.

Finally, they suggested a medium feedrate that can save about 25% of the total energy cost. Furthermore, such as [39] focused on optimizing different machining parameters by using distinct cutting tool for the sake of reducing energy consumption. Reference [40] also introduced a prediction model that can provide more accurate result of energy consumption by analysing the effect of the feedrate, spindle speed and cutting depth. The connection between the particular power, cutting width and cutting height is studied in [41]. In order to reduce the plunging energy, the relationship between particular cutting energy and cutter swept angle is investigated in reference [42]. Recently, a research for the purpose of minimizing the energy consumption was conduct in [43]. Other investigations such as [44] and [45] have done various production planning methods for the sake of making the control process more efficient.

In the chapter 2 of this master thesis, more details about energy consumption optimization will be introduced in the third sub chapter and it will be organized as follows. Firstly, an energy potential field on the specific surface will be researched, and then an energy consumption model will be build in order to obtain the quotient of energy consumption over the swept area. Sequentially, two essential parameters that used to determine the amount of total energy consumption will be calculated as well. Finally, the optimal feed direction and principle curve generation will be mentioned for the sake of optimize the whole machining process.

2 Research of Optimization Methods

In this chapter, three parts such as tool path algorithm optimization, prediction of operation cycle time and minimizing of energy consumption that related to optimize the machining would be researched for the sake of better balancing between the surface operation performance and machining time. This second chapter is including three axis and five axis CNC machine with ball end and flat end cutting tool in order to cover all the processing situation as much as possible in this not long master thesis.

The three tool path algorithms focus on optimizing the tool path by calculation in mathematical way and try to obtain a theoretical value that can be executed in the real operation, which will be conduct in the case study part as well. The methods in this master thesis have some limit in the real application due to the optimization method is based on the G code. In the G code optimization process, we can only adjust the cutting spacing, which will be calculate by using distinct algorithms. Furthermore, the surface in the real operation at CNC machine is a plane rather than a free form surface. The part that this master thesis did not contain will be accomplished in the future.

The prediction of machining cycle time is the method to predict the total operation time of the part with action order processing steps that has been mentioned in Fig.6. The prediction model will utilize the trajectory generation and corner smoothing models to provide a high accuracy result. In this part, the trajectory generation profiles will be introduced as the key function of the CNC and 3-axis corner smoothing will be mentioned in this part as well.

The third part is about the energy consumption model to find out the most efficient energy cost way, which can also be a part of optimization solution for machining. It should be mentioned that this part research is based on 5 axis CNC machine with the flat end cutter in order to cover a more comprehensive range of research. This part will contain a detailed and exhaustive explanation such as pre determination of tool orientation, establishment of energy consumption model, optimization of feed direction, principle curve generation and expansion algorithm based on Iso-scallop height. At the end of this part there will be a brief conclusion of this method.

The tool path algorithm optimization including iso parametric, iso planar and iso scallop will be the main part of utilization in the real operation. The prediction part should be a theoretical tool for the purpose of predicting the total operation cycle time and the tool path generation regards to energy consumption optimization will be used as a theoretical basis in future research work.

2.1 Tool Path Algorithm Optimization

Producing a part with free form surface is one of the most important technologies that are widely utilized in CAD/CAM software. In order to cut the free form surfaces, ball end cutting tool is the most popular type of tool that is utilized in three axis CNC milling machines. In the current approach, the CAM software response for scheduling the CC (cutter contact) path over the free form surface, and then calculate out their offset curves, which is the CL (cutter location) path [46, 47]. Fig.7 shows the differences between CC (cutter contact) path and CL (cutter location) path, as well as the location and direction of normal vector, which will be introduced in the following part. As Fig.7 described, the CC path represents the contact or intersection point between the cutter edge and the free form surface, while the CL path denotes the path that made up by a mount of consecutive linear sectors of the centre of the ball end cutter.

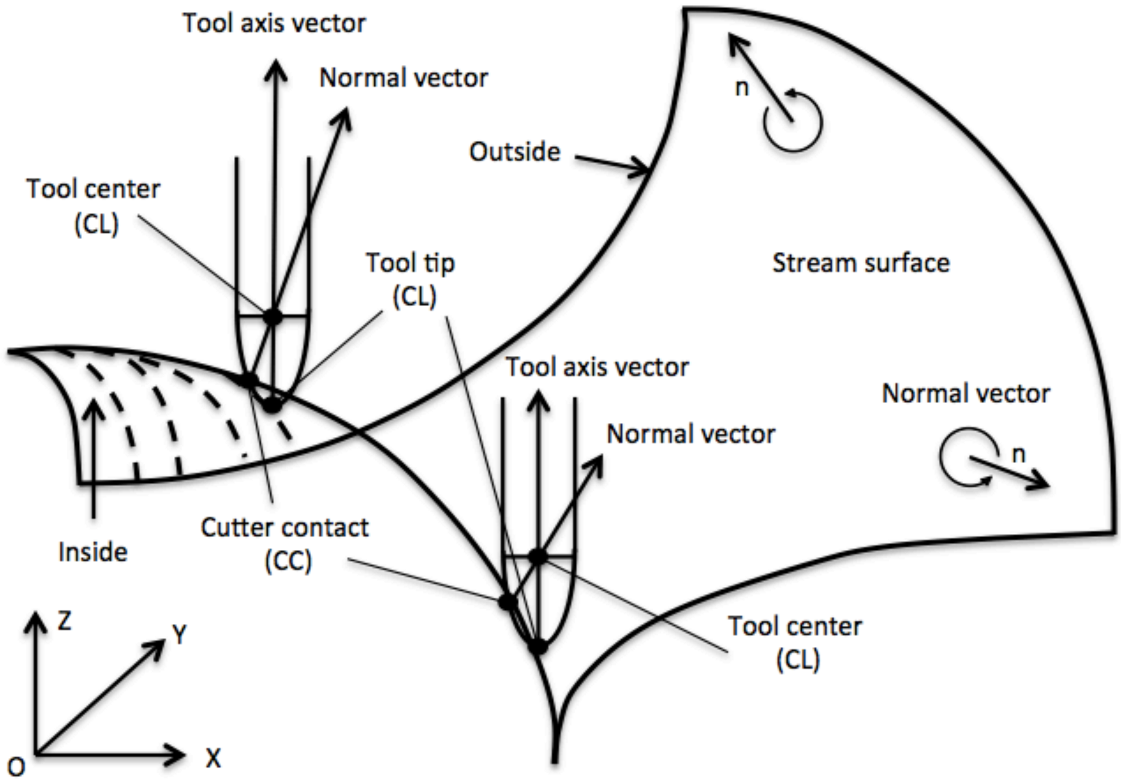

Figure 7 – Illustration of CC path, CL path, Tool axis vector and Normal vector.

Table.1 is the nomenclature of calculation in the following section. It should be noted that some of the parameters in the table.1 are illustrated in Fig.7 as well for the sake of better understanding of the parameters.

Table 1 - Nomenclature

B	Unit vector in the side-step or path-interval direction
C	Cutter-contact path
h	Scallop-height limit
L	Cutter-location path
M	Unit normal vector to the planes in iso-planar machining
N	Unit normal vector to the surface
r	Radius of the ball-end cutter
S	Parametric surface
T	Unit tangent vector in the CC path direction
t	Spatial parameter along the CC path

U	u–v curve in the parametric domain
u, v	Surface parameters
V	Feedrate along the CC path
Δl	Distance of the side step
Δm	Step distance of the planes in iso-planar machining
ρ	Radius of surface curvature in the side-step direction
τ	Sampling period

In order to generate the tool path, it needs to first define the free form surface, and then choose the algorithm to generate the parametric curve. After which the cutting tool will be offsite depends on the surface geometry and the cutting tool's radius. Finally the CC path will be calculated by three different algorithms, which are iso parametric, iso planar and iso scallop. The following sections will describe all the steps in a more detailed way.

2.1.1 Definition of the free form surface

In this master thesis, the free form surface will be machined in the case of ball end milling that can be defined as:

$$S = S(u, v), \tag{1}$$

Where u and v are the surface parameters that are shown in Fig.8, notice that the scope of the u and v domain ($u_{min} \leq u \leq u_{max}$ and $v_{min} \leq v \leq v_{max}$).

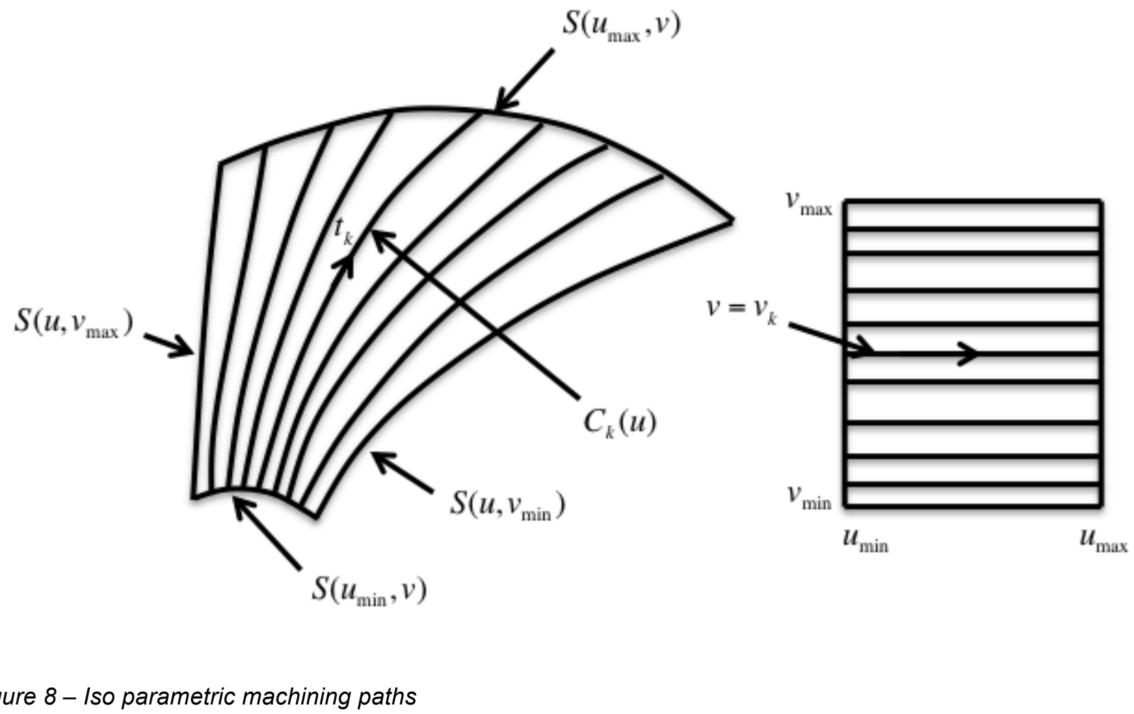

Figure 8 – Iso parametric machining paths

2.1.2 CC path scheduling algorithm and cutting tool offsetting

The algorithm for the CC path interpolation and the cutting tool offsetting will be explained in this section and it should be mentioned that these algorithms are essentially derived from the current methods [48].

2.1.2.1 CC path scheduling algorithm

The CNC system has the sampling rate function that can create a sequence of CC dots in order to follow the CC path at a specific CC velocity and feedrate. At present there are many algorithms about the parametric curve generation have been researched. One of these researched algorithms will be used [49]. Before the calculation of CC path interpolation, a $C(t)$, where t is the spatial parameter that denotes CC path on the free form surface should be introduced. It should be noted that $t = u$ or v for iso parametric machining. Then let t_{i+1} and t_i to be the amounts of the path parameter t at two continuous sampling instants, $(i+1)\tau$ and $i\tau$, where τ is the sampling time. Then:

$$t_{i+1} = \emptyset t^*_{i+1} + (1 - \emptyset)t_i \,, \tag{2}$$

Where,

$$t^*_{i+1} = 2.5t_i - 2t_{i-1} + 0.5t_{i-2} \,, \tag{3}$$

$$\emptyset = \frac{\tau V}{|C(t^*_{i+1}) - C(t_i)|} \,, \tag{4}$$

where V is the specific CC velocity or feedrate. It should be mentioned that at the beginning of the CC path, t_{-1} and t_{-2} need to be calculated by:

$$t_{-1} = t_0 - \frac{\tau V}{|dC/dt|_{t=t_o}} \,, t_{-2} = t_{-1} - \frac{\tau V}{|dC/dt|_{t=t_{-1}}} \tag{5}$$

Then parameter t can be calculated by using Eqs. (2)-(5), recursively, at each sampling rate in order to get the CC point.

2.1.2.2 Tool offsetting

The cutting tool's radius and the surface geometry can decide the cutter offsetting. L is defined as the centre of the ball end cutter at the location of cutter.

$$L = C + r \cdot N \cdot sign(N_z) \,, \tag{6}$$

where r is the radius of the cutting tool, N is the unit normal vector at point C to the surface, N_z is the component of N at z axis and $sign(N_z)$ is the sign function that can keep the tool offsetting on the top side of the free form surface all the time. Then unit normal of the free form surface can be calculated by:

$$N = \frac{\frac{\partial S}{\partial u} \times \frac{\partial S}{\partial v}}{|\frac{\partial S}{\partial u} \times \frac{\partial S}{\partial v}|}, \tag{7}$$

2.1.3 Three algorithms of CC path scheduling

In this part the three different algorithms of CC path scheduling, which are iso parametric, iso planar and iso scallop machining methods, respectively will be discussed and then find out the best proposal for machining free form surface.

2.1.3.1 Iso parametric machining

In the previous section, Fig.8 has described the iso parametric path and introduced the values that should be used in the calculation. In this part, attending to select one of the surface parameters u as the forward direction, therefore another boundary curves, which is $v = v_{min}$ will be the initial CC path. Let kth CC path can be expressed by $C_k(u) = S(u, v_k)$. It should be noted that the curve $v = v_k$ in the domain that constitute by u and v according to the CC path C_k in the *x-y-z* domain (Cartesian domain). The value of the side parameter can be decided one by one,

i.e., $v_{k+1} = v_k + \Delta v_k$,

where Δv_k (the parametric side interval between two neighboring CC paths) can be determined depends on the scallop height limit, h (generally from 0.001 mm to 0.01 mm).

In the general case, the CC path of iso parametric algorithm does not correspond to a constant scallop height h and Δv_k. For this reason, the maximum scallop height on the CC path will not exceed h.

The calculation of Δv_k can be executed on line the generation of the kth CC path. During this generation process, every sampled point, which is $C_{i,k} = C_k(u_i)$, are evaluated in order to get a corresponding value, $\Delta v_{i,k} = \Delta v_k(u_i)$. At the final point of the kth CC path, the minimum value of these corresponding values has chosen, i.e., $\Delta v_k = min(\Delta v_{i,k}'s)$. According to the $v_{k+1} = v_k + \Delta v_k$, the next CC path can be settled consequently. The formulas that can calculate the corresponding value, $\Delta v_{i,k}$, are shown as follows.

Given a sample point on the parametric surface $C_{i,k} = S(u_i, v_k)$, the radius of curvature in the side direction ρ need to find first, which can be calculated by [50]:

$$\rho = \frac{e\alpha^2 + 2f\alpha + g}{a\alpha^2 + 2b\alpha + c}, \tag{8}$$

Where,

$$\alpha = \frac{\frac{\partial S}{\partial v}T}{\frac{\partial S}{\partial u}T}, e = \frac{\partial S}{\partial u}\cdot\frac{\partial S}{\partial u}, f = \frac{\partial S}{\partial u}\cdot\frac{\partial S}{\partial v}, g = \frac{\partial S}{\partial v}\cdot\frac{\partial S}{\partial v}, a = \frac{\partial^2 S}{\partial u^2}\cdot N, b = \frac{\partial^2 S}{\partial u \partial v}\cdot N, c = \frac{\partial^2 S}{\partial v^2}\cdot N,$$

where *N* is the unit normal vector to the parametric surface and *T* is the unit tangent vector on the CC path direction. Then T will be obtained since the tool path is used in the *u* direction:

$$T = \frac{\partial S}{\partial u}/|\frac{\partial S}{\partial u}|,$$

then, side step distance Δl can be calculated for each evaluated point [51]:

$$\Delta l = \sqrt{\frac{8\rho r h}{\rho \pm r}}, \tag{9}$$

where *h* is the scallop height that has introduced in the previous description, *r* is the cutting tool radius, the plus minus sign depends on the case of the surface shape is convex or concave that is illustrated in Fig.9.

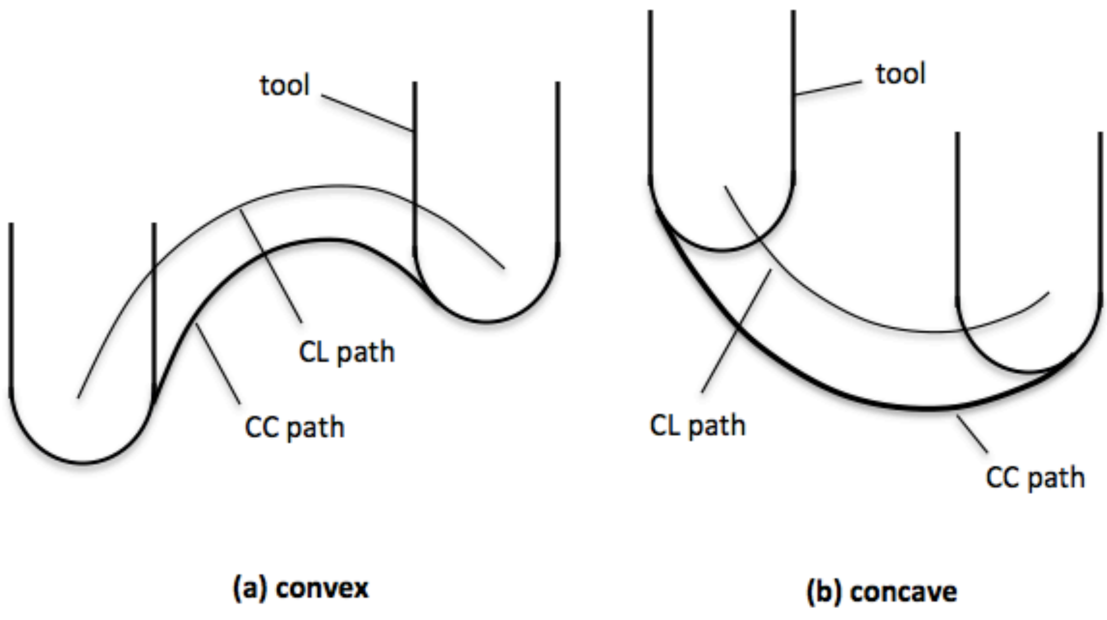

Figure 9 – Convex and concave surface

It should be noted that the CC path direction (*T*) and the surface normal (*N*) are orthogonal to the side step direction. Since Δl is in mm unit distance and it is generally not in the *v* direction, a transformation from Δl to the parametric side Δv is necessary.

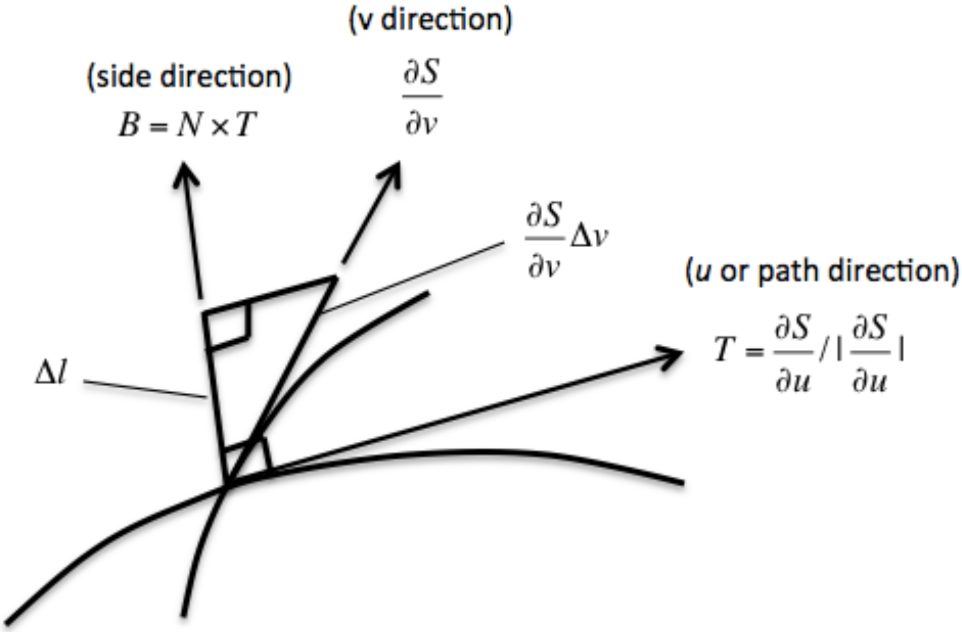

Figure 10 – Side step distance Δl and parametric side interval Δv

This transformation process is described in Fig.10. Depends on the geometrical relationship that illustrate in Fig.10,

$$\Delta l = B \cdot (\frac{\partial S}{\partial v})\Delta v \, ,$$

where,

$$B = N \times T,$$

where B is a unit vector in the side direction. In the end part, the corresponding path interval $\Delta v_{i,k}$ for the ith sampled point on the kth path can be obtained by:

$$\Delta v_{i,k} = \frac{\Delta l}{(N \times T \cdot \frac{\partial S}{\partial v})} \, , \tag{10}$$

By using the CC path scheduling algorithm and tool offsetting that have described above, as well as the iso parametric algorithm presented in the above section, the iso parametric algorithm can be implemented in a CNC machine tool. More details and the process of calculation are shown in appendix.

2.1.3.2 Iso scallop machining

The iso scallop machining path is shown in a schematic illustration in Fig.11. The scallop height is produced by two neighboring CC path that equal to the assigned limit h. It can be seen from the figure below that each CC path $C(t)$ has a corresponding specific curve $U(t)$ in the domain made up by u and v. In the general case, the curve does not follow a constant u and v.

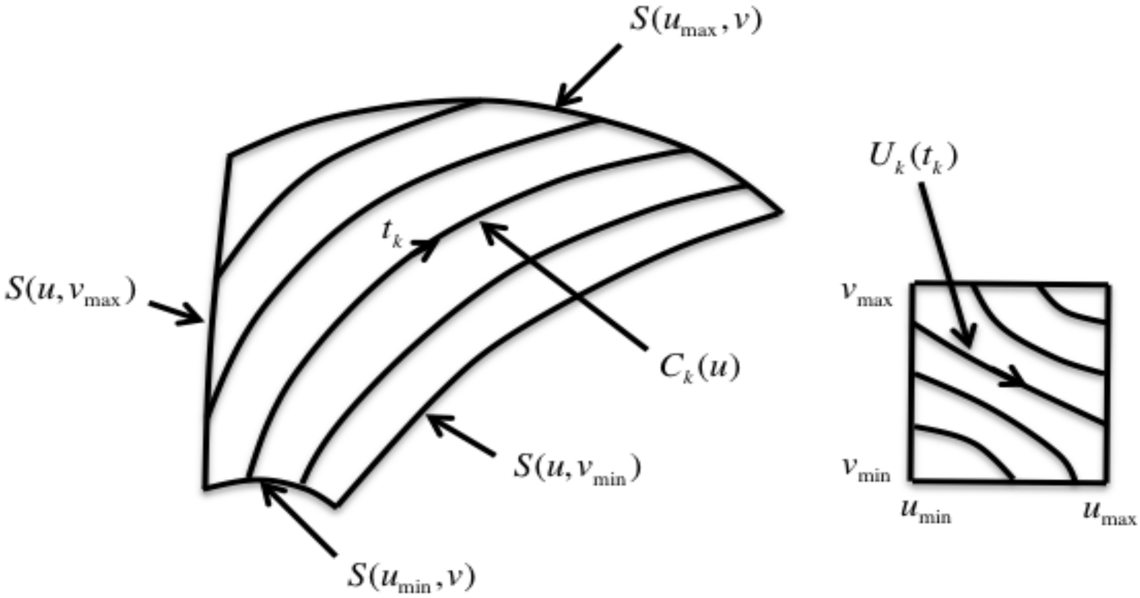

Figure 11 – Iso scallop machining path

There is a existing method that generate the $(k+1)$th CL or CC path based on the curve fitting of the increment points $x_{k+1}, y_{k+1}, z_{k+1}$ from a set of chosen points x_k, y_k, z_k on the kth path. The 3D curve is fitting [51]:

$$L(t) = (x(t), y(t), z(t)),$$

where *t* is the time consuming of the path parameter. Furthermore, in order to obtain sufficient position accuracy, a lot of points need to be evaluated, as well as several spine segments to fit a machining path. Therefore a proposed method is suggested that makes the machining path by 2D curve $U(t) = (u(t), v(t))$ in the parameter domain. It is obvious that the 2D curve fitting for $U(t)$ is uncomplicated for calculation compares with $L(t)$. Fig.12 compares the existing and the proposed methods for the machining path generation.

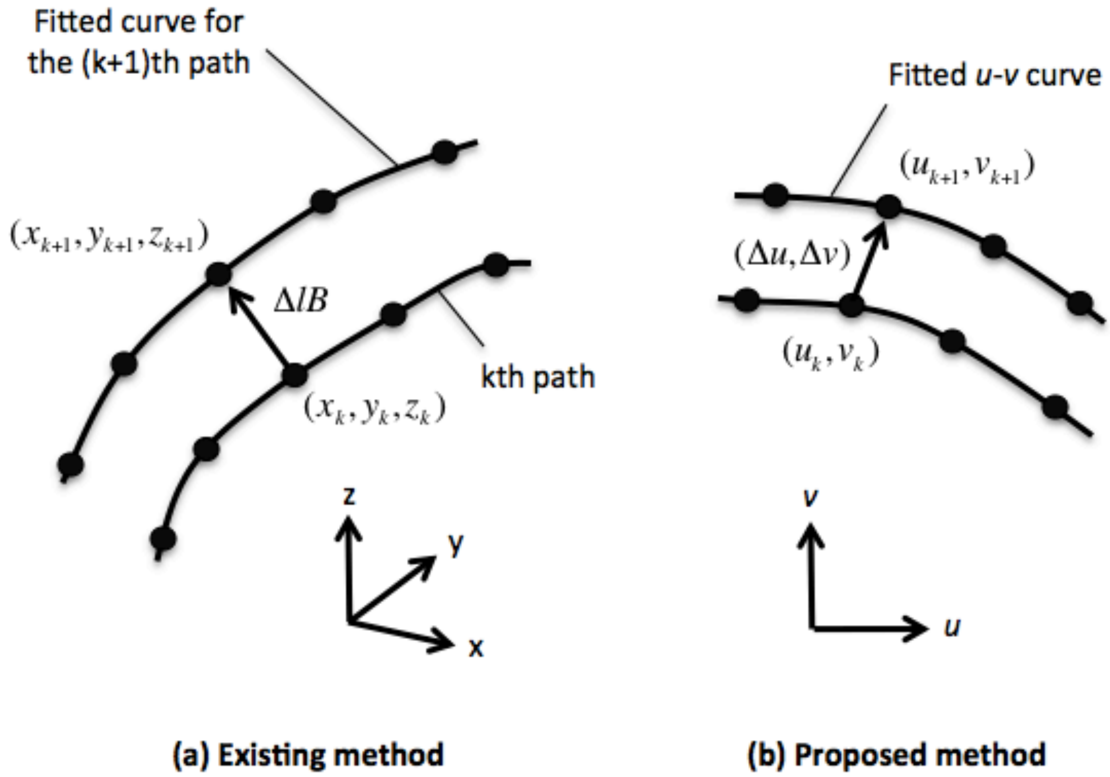

Figure 12 – A comparison of the existing and the proposed methods

In addition, the proposed method does not need tolerance or allowable error to fit $U(t)$. The reasons of this are:

(1) Even though an inaccurate value is applied into the surface function, the CC point is still located on the surface because of 2D curve.

(2) The parameter error can only result in the deviation in the scallop height, which is extremely less than the path interval.

As same as the iso parametric method, the surface parameter u is chosen as the forward machining direction. Therefore another boundary curves, which is $v = v_{min}$ will be the initial CC path and the initial curve is $U_0(t_o) = (u(t_0), v_{min})$ in the domain that consist of u and v. In order to explain it in a more simplicity way, the initial path parameter need to be defined as $t_0 = u$, which can also represented as $U_0(t_0) = U_0(u)$. So that $U_k(t_k) = (u_k(t_k), v_k(t_k))$ means the kth curve in the $u - v$ domain and the two components $u_k(t_k)$ and $v_k(t_k)$ express t_k through curve fitting as polynomials. Then in consequent, the kth CC path becomes to $C_k(t_k) = S_k(U_k(t_k))$ and a cubic spline is used to fit $U(t)$ for a exact CC path because a tight curve fitting for $U(t)$ is not required.

As mentioned in the above section and the illustration in Fig.12 (b), $U_{k+1}(t_{k+1})$ is obtained based on $U_k(t_k)$. In the existing method, four set of (U_{k+1}, t_{k+1}) should be calculated to fit the curve U_{k+1}. While the proposed method will finish this process by generating the kth and the $(k+1)$th CC path. In addition, the four sets path parameter are selected as:

$$t_k = t_k^s + j(t_k^e - t_k^s)/3, \ (j=0,1,2,3),$$

where t_k^e and t_k^s are the end and the start of the path parameter for U_k. For each of the four sets, they have:

$$U_{k+1} = U_k + \Delta U_k,$$

where $\Delta U_k = (\Delta u_k, \Delta v_k)$.

Let $t_{k+1} = t_k$ to define the path parameter for the subsequent path. Then the key issues can be focused to calculated in order to determine an iso scallop machining path, which are the increment of the surface parameters $(\Delta u_k, \Delta v_k)$, as well as the end and the start of the path parameter t_k^e and t_k^s.

After the explaination, the proposed algorithm can be started. Given a set of (U_k, t_k), the first step is to calculate N (the unit surface normal) and T (the tangent vector). N can be obtained by using Eq. (7) and T can be calculated by:

$$T = \frac{\frac{dS}{dt}}{|\frac{dS}{dt}|} = \frac{\frac{\partial S}{\partial u}\frac{du}{dt} + \frac{\partial S}{\partial v}\frac{dv}{dt}}{|\frac{\partial S}{\partial u}\frac{du}{dt} + \frac{\partial S}{\partial v}\frac{dv}{dt}|}, \tag{11}$$

Then Δl (the side step distance) can be calculated by utilizing a given scallop height h based on Eqs. (8) and (9). The transformation from $\Delta l$to the increment of the surface parameters $(\Delta u_k, \Delta v_k)$ can be obtained by:

$$\Delta l B = \frac{\partial S}{\partial u}\Delta u_k + \frac{\partial S}{\partial v}\Delta v_k\ , \tag{12}$$

where $B = N \times T$ is the unit vector in the side step direction.

In the calculation process, the end and the start path parameter t_k^e and t_k^s for U_k are correlating to the intersections of the curve U_k and $u = u_{min}$, $u = u_{max}$, $v = v_{min}$ and/or $v = v_{max}$ (the boundaries of the parametric domain). There are some numerical methods that have been researched to have these intersection points [52]. In this master thesis, a more advance and fast algorithm will be researched for determining t_k^e and t_k^s and the proposed algorithm is introduced in the following.

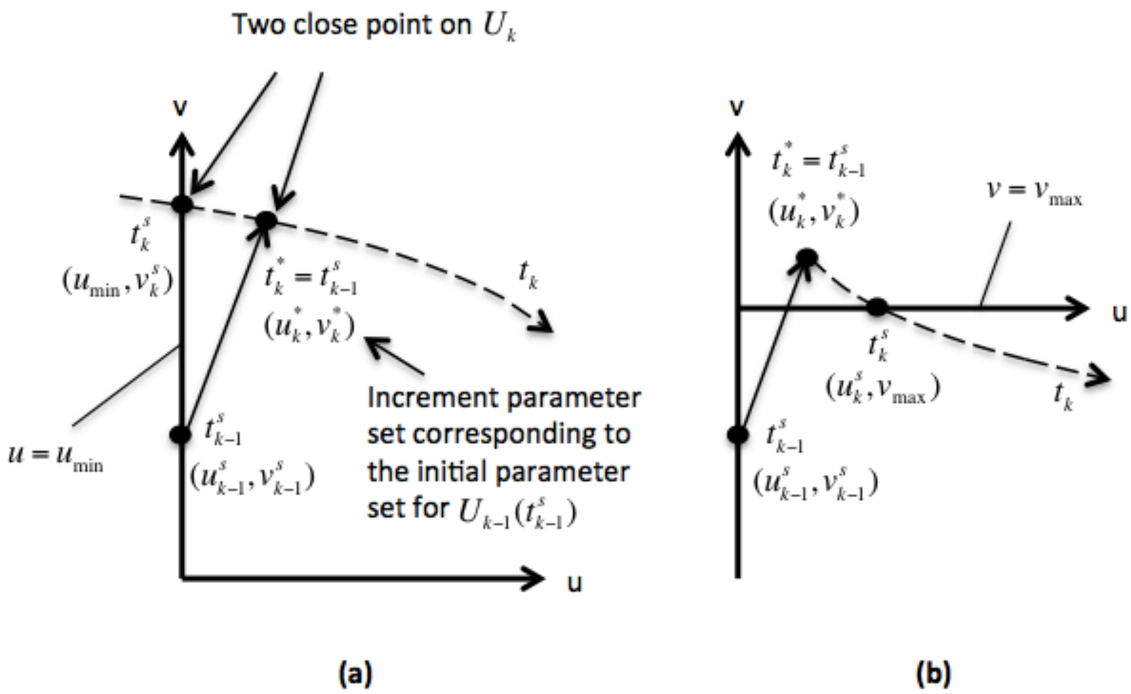

Figure 13 – Schematic description for determining t_k^s

Fig.13 is the schematic description for determining t_k^s. As the explanations above, $U_k(t_k)$ is an iso-scallop increment curve that is obtained from $U_{k-1}(t_{k-1})$. The initial parameter set $U_{k-1}(t_{k-1}^s)$ is defined that has a corresponding increment parameter set (u_k^*, v_k^*). As shown in the Fig.13 (a), t_k^s is corresponding to the intersection of U_k and $u = u_{min}$. Therefore, (u_k^*, v_k^*) and (u_{min}, v_k^s) are two adjacent point on U_k. Then t_k^s can be calculated by:

$$t_k^s = t_k^* - \frac{u_k^* - u_{min}}{\frac{du_k}{dt_k}(t_k = t_k^*)}, \tag{13}$$

where $t_k^* = t_{k-1}^s$. Eq. (13) gives us a good method to find approximation value for t_k^s, it can be approached to the real solution additionally by changing t_k^* by the presently calculated t_k^s and repeating the calculation through Eq. (13). It should be mentioned that Fig.13 (b) illustrate the value t_k^s may be corresponding to the junction of U_k and $v = v_{max}$. In this circumstance, Eq. (13) should be changed by:

$$t_k^s = t_k^* - \frac{v_k^* - v_{min}}{\frac{dv_k}{dt_k}(t_k = t_k^*)}, \tag{14}$$

The algorithm for obtaining the end of the path parameter t_k^e is as same as t_k^s.

By using the CC path scheduling algorithm and tool offsetting that have described above, as well as the iso scallop algorithm presented in the above section, the iso scallop algorithm can be implemented in a CNC machine tool. More details and the process of calculation are shown in appendix.

2.1.3.3 Iso planar machining

The iso planar machining path is shown in a schematic illustration in Fig.14. It can be seen from the figure that the CC path are obtained form the intersections of a series of parallel vertical planes and the parametric surface.

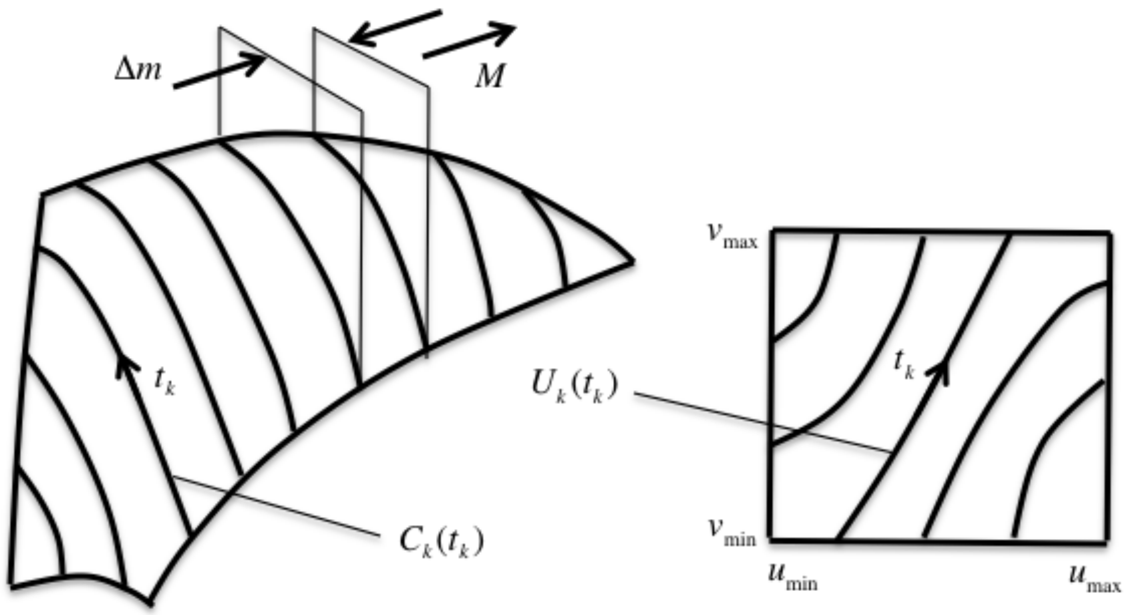

Figure 14 – Iso planar machining paths

In this master report, the unit normal vector perpendicular to the vertical planes that can be denoted by $M = (m_x, m_y, 0)$, and the distance between two close parallel planes is represented by Δm as shown in Fig.14 as well. The proposed algorithm for the iso planar is as same as the iso scallop method, which can be seen from Fig.10 and Fig.14 that each CC path $C\ (t)$ corresponds to a unique curve $U(t)$ in the parametric domain. For instance, $C(t) = S(U(t))$.

In the processing, $U(t)$ can be obtained recursively by :

$$U_{k+1} = U_k + \Delta U_k,$$

where $\Delta U_k = (\Delta u_k, \Delta v_k)$.

The main difference between the iso scallop approach and iso planar algorithm is the method to calculate the parameter increment, which is $(\Delta u_k, \Delta v_k)$.

The kth curve is defined as $U_k(t_k)$, and then the iso planar increment curve can be obtained:

$$U_{k+1}(t_{k+1}),$$

where $t_{k+1} = t_k$.

For two adjacent points on U_k and U_{k+1}, the related CC points $C_k = S(U_k)$ and $C_{k+1} = S(U_{k+1})$ are both placed on the surface. The different vector between these two points, which is $(C_{k+1} - C_k)$ can be obtained approximately by:

$$\frac{\partial S}{\partial u}\Delta u_k + \frac{\partial S}{\partial v}\Delta v_k ,$$

In the geometrical consideration, this distinction vector is placed on a cross section that is developed by the side vector M and the tool axis vector Z. Therefore,

$$\frac{\partial S}{\partial u}\Delta u_k + \frac{\partial S}{\partial v}\Delta v_k = \Delta mM + \Delta zZ , \tag{15}$$

Depends on the components x and y, Δu_k and Δv_kcan be solved, and then $U_{k+1} = (u_k + \Delta u_k, v_k + \Delta v_k)$ can be obtained.

The same as the above section and the illustration in Fig.12 (b), $U_{k+1}(t_{k+1})$ is obtained based on $U_k(t_k)$. In the existing method, four set of (U_{k+1}, t_{k+1}) need to be calculated to fit the curve U_{k+1}. While the proposed method will finish this process by generating the kth and the $(k+1)\ th$ CC path. In addition, the four sets path parameter are selected as:

$$t_k = t_k^s + j(t_k^e - t_k^s)/3, \ (j=0,1,2,3),$$

where t_k^e and t_k^s are the end and the start of the path parameter for U_k. For each of the four sets, they have:

$$U_{k+1} = U_k + \Delta U_k,$$

where $\Delta U_k = (\Delta u_k, \Delta v_k)$.

An initial curve U_0 should be created first in the case of this value does not correspond to a boundary of the $u - v$ domain for the iso planar scheduling. There is an uncomplicated method that can get U_0. Lets say there exist four representative points on four directions from the left bottom corner (u_{min}, v_{min}) on U_0, and the four directions are 0^o, 30^o, 60^o and 90^o, respectively. The original CC path, $C_0 = S(U_0)$, is placed on a vertical plane and deviate from the surface corner $S(u_{min}, v_{min})$ by the distance of ΔmM. Correspondingly, all the points on $U_0 = (u_0, v_0)$ should satisfy:

$$[\frac{\partial S}{\partial u}(u_0 - u_{min}) + \frac{\partial S}{\partial v}(v_0 - v_{min})] \cdot M = \Delta m, \tag{16}$$

Therefore, $(u_0, v_0) = (\lambda, 0)$, $[(\sqrt{3}/2)\lambda, (1/2)\lambda]$, $[(1/2)\lambda, (\sqrt{3}/2)\lambda]$ and $(0, \lambda)$ can be inserted into Eq. (16) in order to obtain the four solutions.

By using the CC path scheduling algorithm and tool offsetting that have described above, as well as the iso planar algorithm presented in the above section, the iso planar algorithm can be implemented in a CNC machine tool. More details and the process of calculation are shown in appendix.

2.2 Prediction of Part Machining Times

The prediction model is introduced in this sub chapter based on researching of trajectory generation profiles and corner smoothing algorithm, which can determine the total cycle time. The trajectory module will be divided into acceleration, velocity and jerk in order to better explain the influence of these parameters. This prediction model will give us the theoretical basis of prediction field in the future utilization.

2.2.1 Trajectory Generation

The action order processing in a CNC system is mentioned before in Fig.6. The G code, which is the main optimization part in this master thesis that belongs to the NC program, can be parsed into linear, circular and spline path section. The total travel distance L for every path section can be calculated and divided into acceleration, constant feed and deceleration area that are shown in Fig. 15. The discrete displacement will be calculated through the path, which is a function of the trajectory profile at continuous interpolation time intervals T_{int} and then dissolve the constant interpolation time intervals into axis position orders. The function is implemented by the interpolator functions and sent the information to drive servo controllers over the cutting tool's inverse kinematic module.

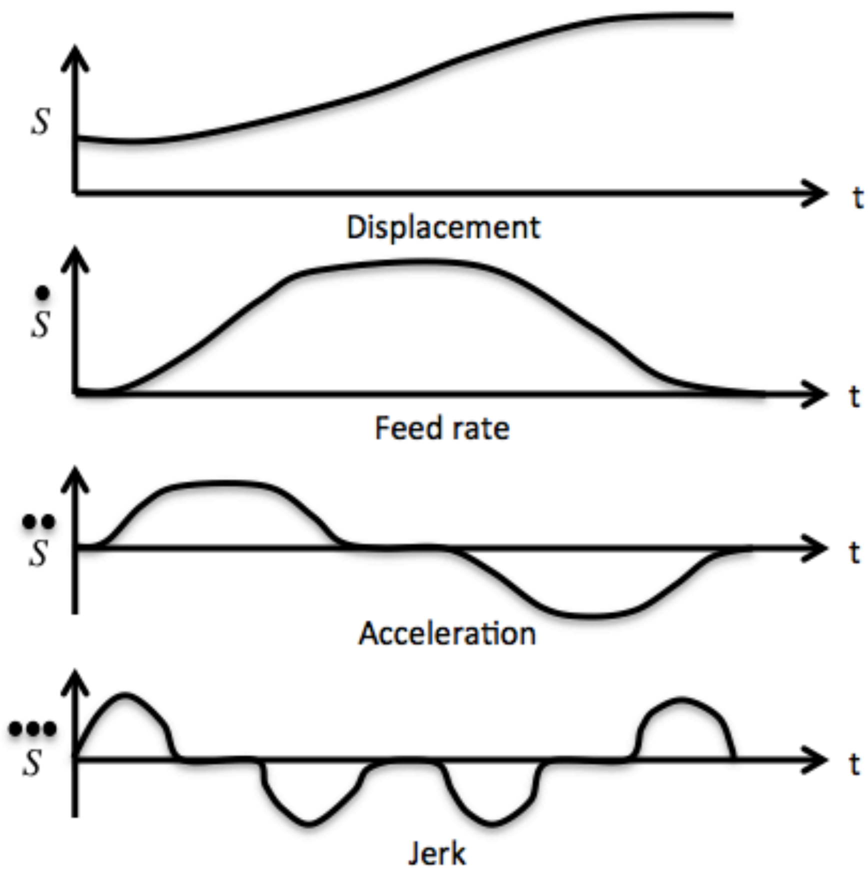

Figure 15 – Jerk continuous trajectory command generation profile

There is a replacement of a fifth order polynomial function of time when the CNC system attend to maintain the continuous velocity, acceleration and jerk profiles that is shown in Fig. 15. The less proportion content can be obtained is the acceleration and jerk are smooth and this will decrease the vibrations during high-speed contour operation [31].

The most CNC machine system has a double exponential feed profile that is illustrated in Fig.16. The three time zones including acceleration, constant feedrate and deceleration can be expressed in the mathematical way as following:

$$f(t) = \begin{cases} \dfrac{f_s - f_c}{T_1 - T_2}\left(T_1 e^{-(t/T_1)} - T_2 e^{-(t/T_2)}\right) + f_c, & t \in [0, t_1) \\ f_c, & t \in [t_1, t_1 + t_2) \\ \dfrac{f_c - f_e}{T_1 - T_2}\left(T_1 e^{-((t-t_1-t_2)/T_1)} - T_2 e^{-((t-t_1-t_2)/T_2)}\right) + f_e, & t \in [t_1 + t_2, t_1 + t_2 + t_3] \end{cases} \quad (17)$$

where $t = kT_{int}, k = 1,2, \ldots, N$ and T_1, T_2 are specified time constants.

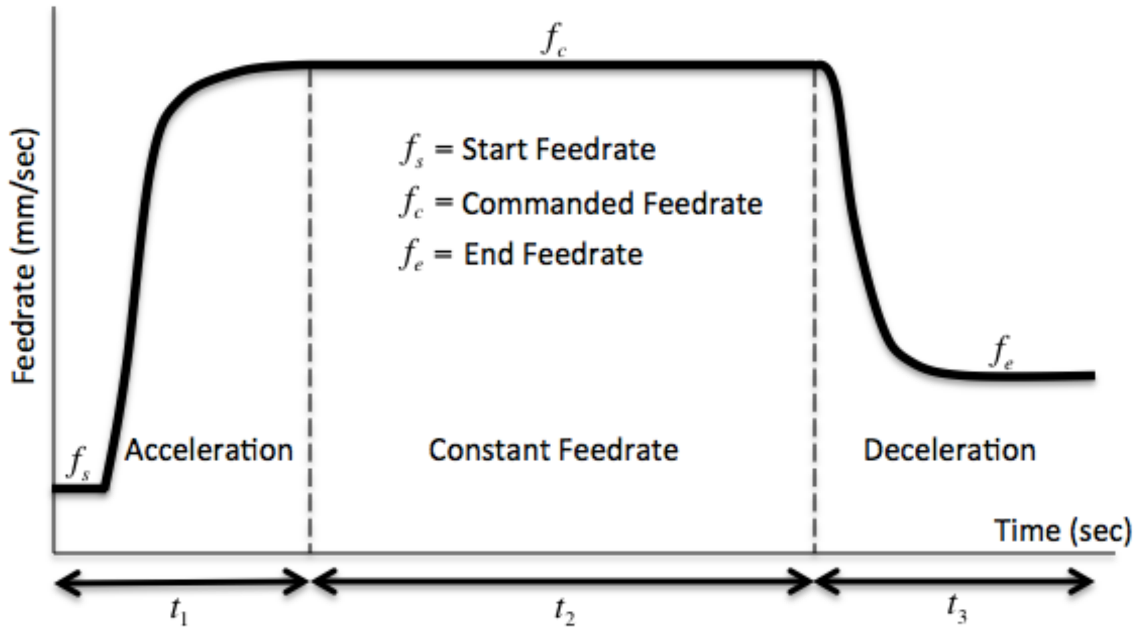

Figure 16 – Exponential feed generation profile

T_1, T_2 are specified time constants that obtained from a series of linear travel commands, which are conducted on each drive, as well as the real velocities are obtained and measured by using the CNC's internal data storage part over the application of programming interface.

The time constants are determined by a non-linear least squared identification method in this research. So that the corresponding travel length $l(t)$ can be obtained by integrating the feed from Eq. (17) along the path.

$$l(t) = \begin{cases} \frac{f_s - f_c}{T_1 - T_2}\{T_1^2(1 - e^{-(t/T_1)}) - T_2^2(1 - e^{-(t/T_2)})\} + f_c t + l(0), & t \in [0, t_1) \\ f_c(t - t_1) + l(t_1)\,, & t \in [t_1, t_1 + t_2) \\ \frac{f_c - f_e}{T_1 - T_2}\left(T_1^2 - T_2^2 - T_1^2 e^{-((t-t_1-t_2)/T_1} + T_2^2 e^{-\left(\frac{t-t_1-t_2}{T_2}\right)}\right) & \\ +f_e(t - t_1 - t_2) + l(t_1 + t_2), & t \in [t_1 + t_2, t_1 + t_2 + t_3] \end{cases} \quad (18)$$

It should be mentioned that the time t is discretised as $t = kT_{int}$ at the interpolation interval time T_{int}. The part machining cycle time can be predicted by the machining time if assuming each path segment length is finished, for instance $L = l(t_1 + t_2 + t_3)$.

The CNC systems have several trajectory generation modules, they are infinite and constant profiles, as well as continuous and exponential jerk profiles as shown in Fig. 15 and Fig. 16.

In order to evaluate the machining time, the main influencing factors should be known first. From reference [31] and [53] the operation time is influenced by the feed speed transitions between the smoothing feed and NC blocks to avoid high frequency jitters that may causes inertial vibrations. Nonetheless, the trajectory generation profile and corner smoothing calculations are the main factors that affect the machining time.

Fig. 17 is the three-axis corner smooth algorithm in order to increase the accuracy of prediction. The initial path has a sharp corner regarding to a tool tip coordinate of p_2 for a three-axis machining application. For the sake of avoiding the dimensional rightness, the corner path can be adjusted. In another hand, the CNC can be adjusted as well to stop at the end of each action so as to achieve zero error. A five order micro spline can be fitted by locating 7 points, which are $P_0, P_1, P_2, P_3 \dots, P_6$ through the path sectors when maintaining the part tolerance ε_{pos} at the corner that can be seen in Fig. 17.

The tool path through the corner spline can be calculated by the following equations:

$$P(u) = \begin{cases} P_0 \sum_{n=0}^{5} C_{0n} u^n + \cdots P_5 \sum_{n=5}^{5} C_{5n} u^n + P_6 \cdot 0, & 0 \le u \le 0.5 \\ P_0 \cdot 0 + P_5 \sum_{n=1}^{5} D_{5n} u^n + \cdots P_6 \sum_{n=1}^{5} D_{6n} u^n + P_6\,, & 0.5 \le u \le 1 \end{cases} \quad (19)$$

where $u = 0.5$ according to the corner point.

In order to make sure the jerk and acceleration continuity at the union points $P_0(u = 0)$ and $P_6(u = 1)$, the parameters of the spline and the locations of the control points should be defined.

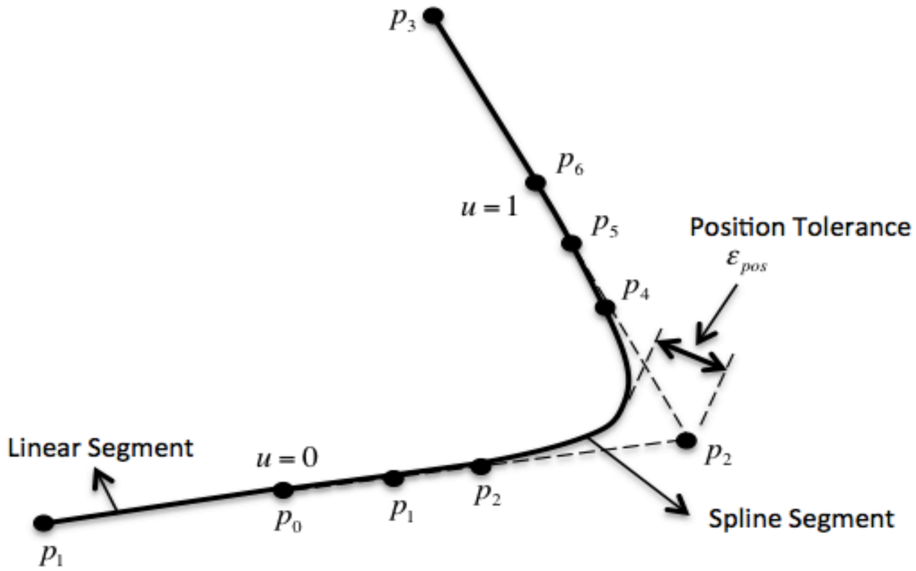

Figure 17 – 3-axis corner smoothing of sharp corner

It should be mentioned that some of the CNC systems start executing the next block earlier than while the machine reaches at the corner. It will be explained in the following example:

The example NC Program is:

N010 G01 X4 F1000

N020 X2 F500

N030 X8 F2000

N040 X-4 F1000

The Fig. 18 [60] is the commanded feedrate in four subsequent NC blocks. The next NC block will start moving when the previous block is finished.

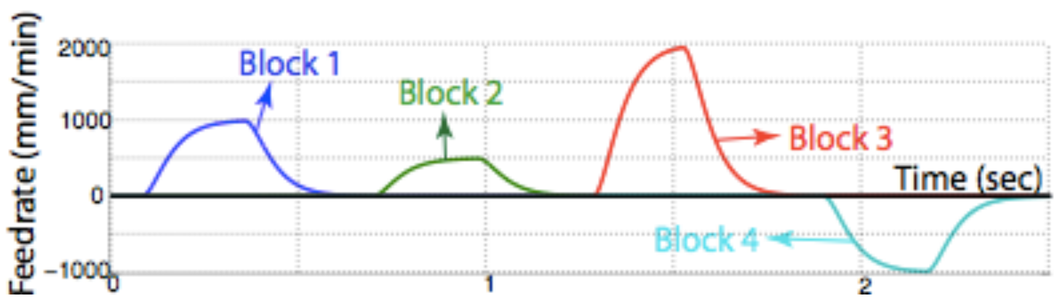

Figure 18 – Four subsequent NC blocks [60]

The time shifting of action blocks of CNC can be obtained and it can be seen from Fig. 19 that when the linear command begin to decelerate, the next NC block, for instance linear motion command, is shifted advanced of its schedule time.

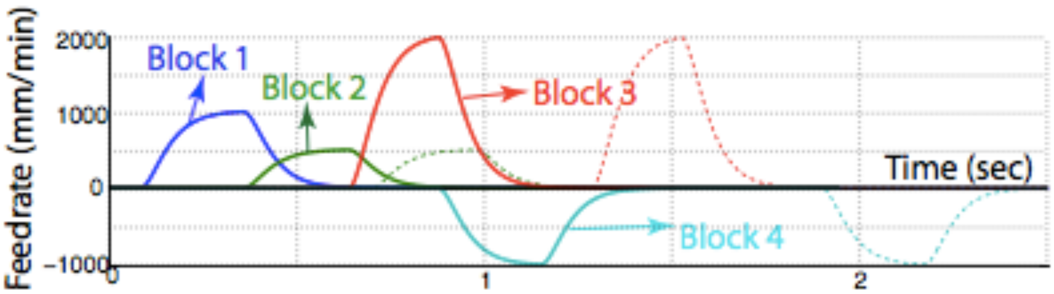

Figure 19 –Time shifting of motion blocks [60]

This scheme mixes the sharp corners in a smooth way but the disadvantage of this is ignoring the constraint of the path error with the tolerance of the machining part. The block shifting strategy can be executed in the virtual CNC by mixing the block transitions that is shown in Fig. 20.

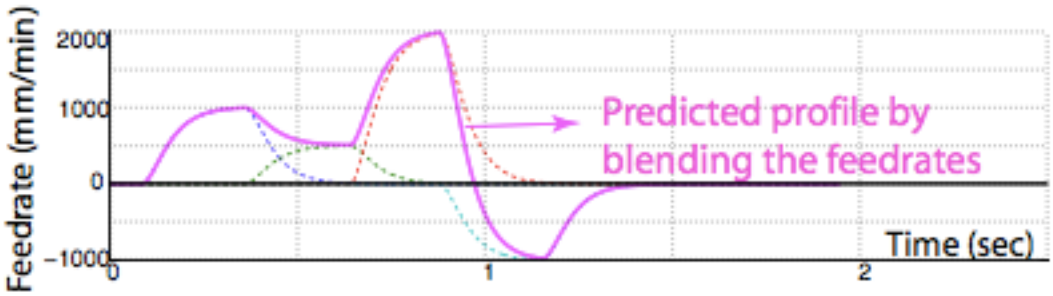

Figure 20 – Fixed feed profiles for continuous block transitions [60]

In this part of study, the two main factors have been researched that can affect the total machining cycle time in three-axis CNC system, which is not the limitation of the virtual CNC system. More descriptions are in the appendix. The virtual CNC system cannot only simulate three-axis tool path but also all range systems from one to five axis. All the servo states can be simulated including torque, position and acceleration etc., as well as total machining time and contouring errors. Despite that, the two main factors that have been studied still affect the total cycle time most.

2.3 Tool Path Generation Consider to Energy Consumption

This part of research is based on a five-axis CNC system for the purpose of making this master thesis study a wider range of coverage, then some useful part will be researched to utilize in the case study part. The case study part will only focus on three-axis surface machining optimization and the five-axis machining will be researched in the future work.

Table 2 is the nomenclature for the calculation in this section. The factors are listed according to the sequence of appearance.

Table 2 - Nomenclature

α	Lead angle (rad)
β	Tilt angle (rad)

r_f	Surface radius of curvature through feed direction (mm)
r_e	Effective cutting radius of a flat-end mill (mm)
r_k	Surface radius of curvature that perpendicular to feed direction (mm)
f	Feedrate (mm/min)
S	Spindle speed (rad/s)
P_{idle}	Idle power (W)
P_T	Cutting power (W)
P_D	Driving power (W)
J_k	Inertia of each axis
F_k	Viscosity friction coefficient of each axis
μ_k	Friction coefficient of each axis
v	Axis velocity
a	Axis acceleration
E_T	Energy consumption due to cutting power (J)
$E_{\boldsymbol{D}}$	Energy consumption due to driving power (J)
w_i	Effective cutting width (mm)
A_i	Swept area (mm^2)
U	Specific energy (J/mm^2)
d_f	Forward step (mm)
$\mathrm{d_s}$	Side step (mm)

The five-axis milling is widely used in machining complicated surfaces with high accuracy needs. It is implemented in many industries such as aerospace and shipbuilding etc. This part will study the optimization method regarding to energy consumption by the following sectors:

1. Build an energy potential field on the known surface that includes the distinct power demand through any feed directions at random cutter contact point.

    a. Determinate the tool orientation before establishing the energy consumption model

    b. Make a energy consumption model to find out the parameters that can determine the energy consumption

2. Find an optimal tool path generation that fits to the minimum directions of the field and meet the maximum scallop height needs at the same time.

2.3.1 Energy Potential Field

2.3.1.1 Determination of tool orientation

Generally, in a five-axis machining, a tool path is consisting of cutter location curve (CL), which is the trajectory of the tool tip and a tool orientation T. Sequentially, the surface normal n can be used and feed direction f, as well as the cross product k corresponding to n and f to determine a local reference frame.

Where, $k = f \times n$.

It is obvious to see in the Fig. 21 that the tool orientation T can be defined by two angles α (lead angle) and β (tilt angle).

In this part, the flat-end cutter will be considered to use because it has close tool surface contact and large cutting width. Furthermore, the flat-end cutter is intrinsically related to orientation of the tool and the work of analysis will be complex, specially considering the side and rear gouging that is illustrated in Fig. 22.

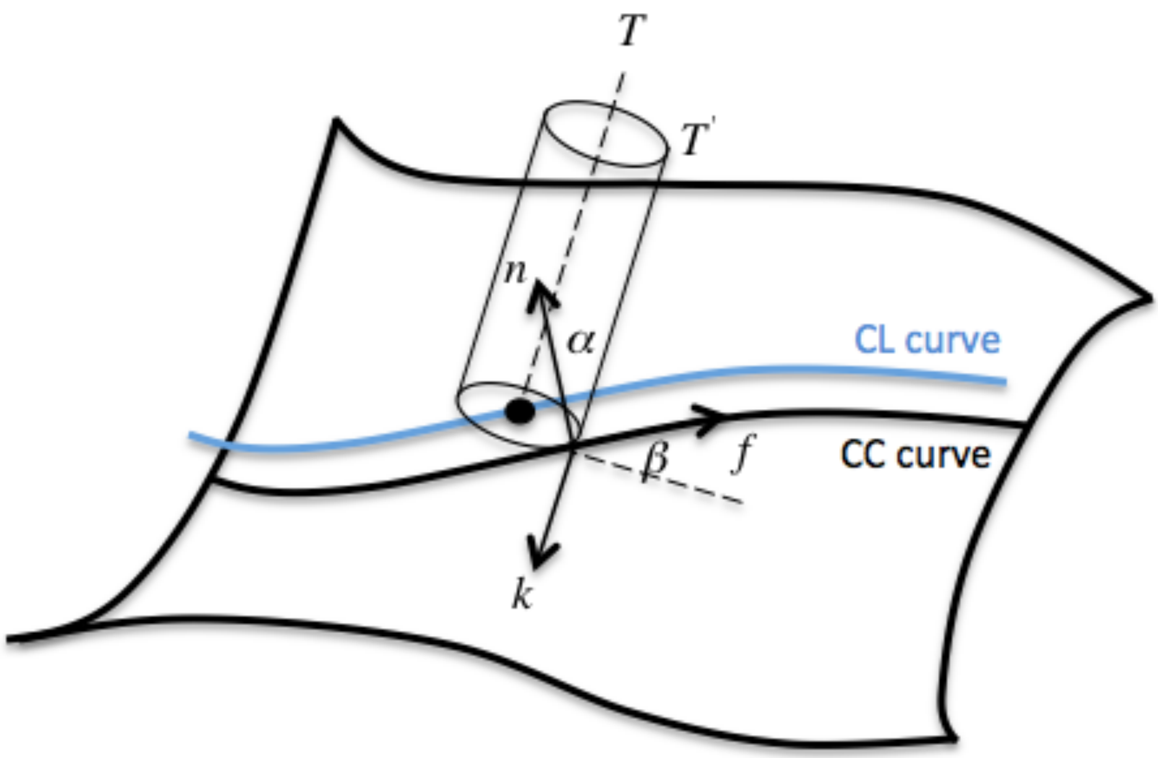

Figure 21 – Parameters define the local frame

If CC point p is given, the lead angle α should be positive so as to protect the rear gouging when the surface radius of curvature r_f through the feed direction f is negative. The relationship of these parameters is shown in Fig. 22 as well.

The lead angle α should be:

$$\alpha \geq sin^{-1}(\frac{r}{-r_f}) \,, \tag{20}$$

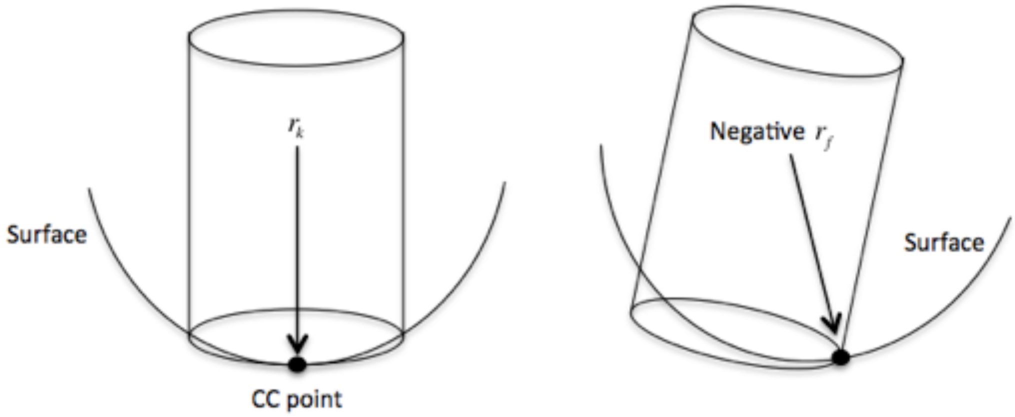

Figure 22 – Side and rear gouging considering a flat-end cutter

The real cutting profile of a flat-end cutter is a kind of ellipse and its effective cutting radius r_e (as shown in schematic figure 23) can be calculated refer to reference [54]:

$$r_e = t^2 r^2 (\frac{1 + tan^2\theta}{t^2 + r^2 tan^2\theta})^{3/2} \,, \tag{21}$$

where $t = rsin\alpha \cdot cos\beta = \theta = tan^{-1}(tan\alpha \cdot sin\beta)$.

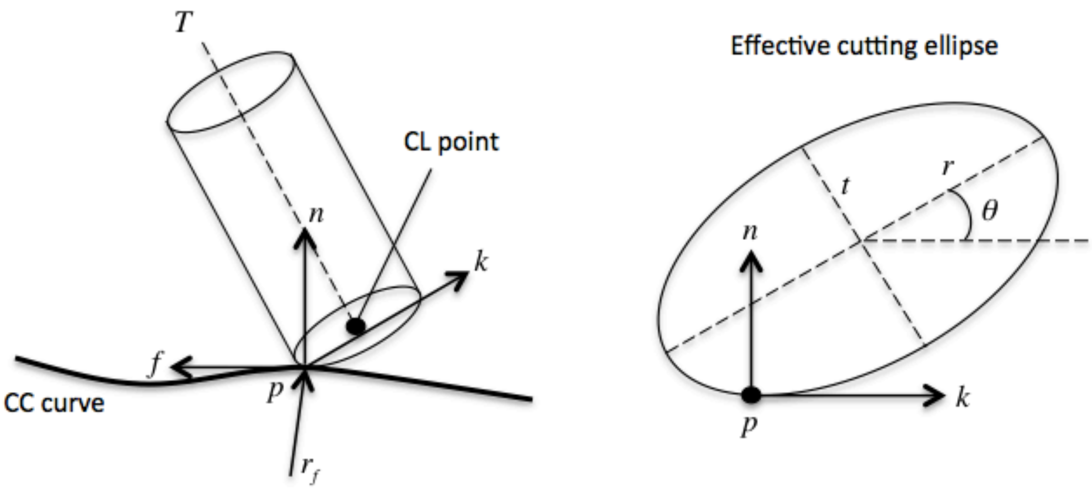

Figure 23 – The effective cutting shape (ellipse)

In order to meet the side gouging free needs, the lead angle α and the tilt angle β need to be optimized by the following equation:

$$r_e(\alpha,\beta) = \frac{1}{Max(-\frac{1}{r_k},0)} \; , \tag{22}$$

where r_k is the radius of curvature on the surface at point p through k.

Then the concave case can be known, in which the lead angle α is positive when r_k is negative in order to protect the local gouging. On the contrary, the lead angle α can be infinitely closed to 0 for the sake of having the largest cutting width.

In the case that the global collision has been maintained, the tilt angle β is set to 0 so as to have a more regular cutting strip. Then the pre-determined the tool orientation can be implemented by using the following equation:

$$(\alpha,\beta) = (Max(0, sin^{-1}(\frac{r}{-r_f}), sin^{-1}(\frac{r}{-r_k})),0) \; , \tag{23}$$

In the workpiece coordinate system, the tool orientation can be expressed as:

$$T_i = (a_i, b_i, c_i) = n\ cos\alpha + f\ sin\alpha cos\beta\ -\ k\ sin\alpha sin\beta \; , \tag{24}$$

The tool orientation can be a unary function of feed direction f because of the different feed directions can cause the changing of r_f and r_k, which means the known CC curve can define a unique tool orientation of the flat-end cutter.

If we consider the ball-end tool that will be utilized for our case study, Eq. (24) will be simplified if a positive and fixed lead angle α has been take care as invariant when the tilt angle β becomes to zero.

2.3.1.2 The model of energy consumption

We know that the feedrate is the tool tip's speed when the tool moves through the tool path. This speed is usually changed in process by the controller of the machine so as to avoid from exceeding the machine's kinematic or dynamic constraints when transforms the tool tip's speed to the speed of the machine's axis.

In order to make such similar system, a reference constant feedrate f should be assigned to simulate the machine in verse kinematic and then the machine axis's velocity and acceleration can be calculated in advance to ensure whether the given feedrate is conservative, and then decrease it if the virtual numerical controller is unaccepted. When the above work is finished, the energy consumption model can be build with both the feedrate and tool orientation specified.

In general, there are three main contributing factors to the power demand that are power demand P_{idle}, cutter power demand P_T and driving power demand P_D, respectively according to reference [38] and [55].

If assuming the tool moves an infinitesimal distance from CC point P_i to P_{i+1} by the specified feedrate f, then the total consumed energy of the cutting movement can be calculated:

$$E = (P_{idle} + P_T + P_D) * \frac{||p_{i+1} - P_i||}{f}, \tag{25}$$

where $\frac{||p_{i+1} - P_i||}{f}$ is the time consuming between P_i and P_{i+1}, to be denoted as Δt.

Each machine tools have their own intrinsic characteristic that can be calibrated. For example the inertia of each axis J_k, the idle running power P_{idle} and the viscosity friction coefficient μ_k. The energy requirement according to cutting power demand P_T for compensating the cutting force is:

$$E = P_T * \frac{||p_{i+1} - P_i||}{f} = \int_0^{\Delta t} \int_0^{h_0} (F_t(h,t) r S) dh\, dt, \tag{26}$$

where $F_t(h,t)$ is the intensity of the tangential force at a given height h and a given time t. S is the spindle speed and r is the tool radius. Therefore, the part $\int_0^{h_0}(F_t(h,t)rS)dh$ of the equation is the cutting power at time t.

Each axis's power demand P_D should be independent to each other, so other variable power demand in the machine coordinate system needs to be investigated. The internal friction force and the torque in the machine coordinate system require extra energy for acceleration. Therefore, the velocity v_k and acceleration a_k should be calculated of each axis at the first step. Suppose that the chord error e is known, and then the two adjacent CC points can be found out due to the feed direction f.

Fig. 24 is the illustration of the parameters that are needed to the calculation. Assume that the cutter posture at point p_i in the workpiece coordinate system can be expressed as:

$$(x_i, y_i, z_i, a_i, b_i, c_i),$$

where $T_i = (a_i, b_i, c_i)$ is the tool orientation that determined previously.

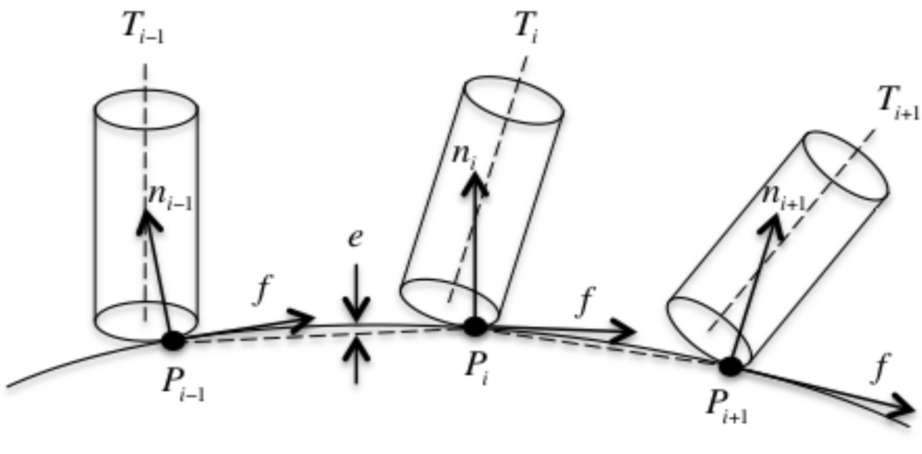

Figure 24 – Three adjacent cutter postures with the chord error

Then the cutter postures p_{i-1}, p_i and p_{i+1} can be converted into their corresponding machine coordinates by utilizing the inverse kinematics transformation:

$$(m_{i,1}, m_{i,2}, m_{i,3}, m_{i,4}, m_{i,5}) = IKT(x_i, y_i, z_i, a_i, b_i, c_i) \,, \tag{27}$$

For more information about IKT is given in the appendix. Then the velocity v_k and acceleration a_k of each axis can be calculated by following:

$$v_k = (m_{i+1,k} - m_{i,k})/\Delta t \,, \tag{28}$$

$$a_k = (m_{i+1,k} - 2m_{i,k} + m_{i-1,k})/\Delta t^2, \qquad k = 1,2,3,4,5 \,, \tag{29}$$

According to the Eq. (28) and Eq. (29), the total energy cost of the driving power demand can be obtained by:

$$\begin{aligned} E_D &= P_D \Delta t \\ &= \sum_{k=1}^{5} (\mu_k J_k v_k \Delta t + F_k v_k^2 \Delta t + \{\tfrac{1}{2} J_k((v_k + a_k \Delta t)^2 - v_k^2), if\ a_k > 0 \\ &\qquad\qquad\qquad\qquad\qquad\qquad\qquad\qquad 0, if\ a_k \leq 0\}) \end{aligned} \tag{30}$$

It should be mentioned that the part kinetic energy demand $\frac{1}{2} J_k((v_k + a_k \Delta t)^2 - v_k^2$ is 0 for any axis when $a_k \leq 0$ is following the laws of energy conservation. In the contrary, the motor has to provide more energy to accelerate the whole inertia that related with the axis.

Until now the three main factors of energy consumption have been calculated. In order to obtain the infinitesimal energy consumption of any neighboring two CC points, the three main factors, which are Eq. (25), Eq. (26) and Eq. (30) can be simply summed up as follows:

$$E = P_{idle} \Delta t + E_T + E_D \,, \tag{31}$$

There is a new factor named the area swept A_i by the cutter from p_i to p_{i+1} that is used to better evaluate the energy efficiency. The area swept value A_i can be determined by the equation as following:

$$A_i = \frac{1}{2}(w_i + w_{i+1})||p_{i+1} - p_i|| \,, \tag{32}$$

where w_i is the effective cutting width on the surface at point p_i that is determined by the length of the effective cutting chip from the nominal surface S to the tolerance surface S'. Fig. 25 illustrates the two distinct cases according to the effective cutting width.

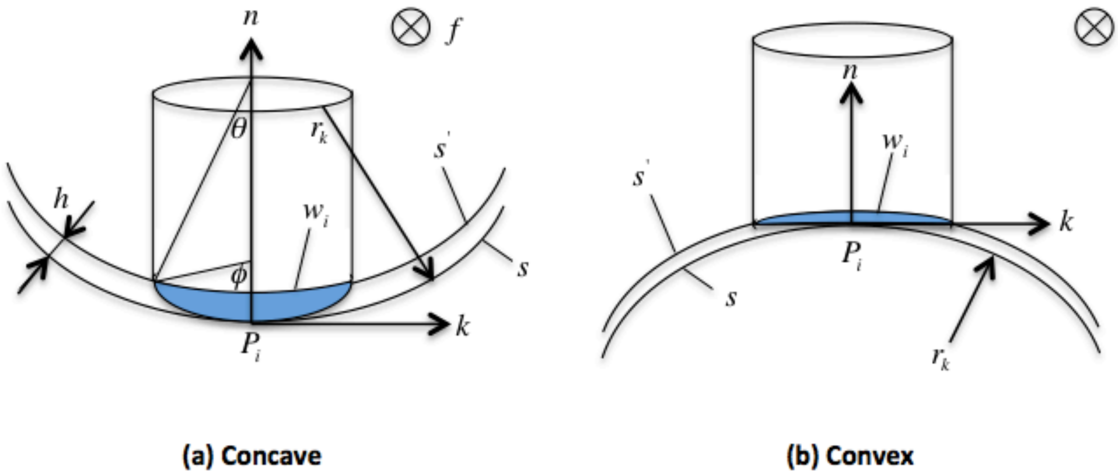

Figure 25 – The two different cases considering of effective cutting width of flat-end milling

It is obvious to distinguish the difference between the concave and convex considering of the effective cutting width of flat-end milling. The distance of cutting width of concave case is defined between the two intersection points from the ellipse shape to the local arc of the tolerance surface S' that can be determined by solving the two parameters θ and φ of the following equations:

$$r_k - (r_k - h)cos\theta = rsin\alpha - rsin\alpha cos\varphi ,$$

$$r_k sin\theta = rsin\varphi , \tag{33}$$

The effective cutting width w_i of the concave case can be simply calculate as follows and the illustration of the relationship between r and φ can be seen in appendix:

$$w_i = 2rsin\varphi , \tag{34}$$

Similarly, it is obvious to see from the Fig. 25 that the distance of cutting width of convex case is degenerated into the cord length between the nominal surface S and the tolerance surface S'. Then the effective cutting width w_i of the convex case can be calculated by the following formula:

$$w_i = min(2r, \sqrt{8r_k h}) , \tag{35}$$

After determination of the effective cutting width w_i, the specific energy can be obtained at a random CC point and through any feed direction is then the quotient of the energy consumption over the swept area:

$$U = E/A = \frac{P_{idle}\Delta t + E_T + E_D}{\frac{1}{2}(w_i + w_{i+1})p_{i+1} - p_i} , \tag{36}$$

2.3.1.3 Energy consumption based on tool path generation

In a five-axis machining, the tool path is composed of a series of discrete CL curves that dominate the tool tip position and the relevant tool orientation in the workpiece coordinate system. In general, the CC curves are composed of groups of discrete CC points. Usually, the CC curves are decided at first on the nominal surface, and then a tool orientation is decided subsequently, and then calculates the CL curves according to the CC curves, the corresponding tool orientation and the nominal surface.

According to the requirements of machining accuracy, two important constraints should be defined while planning a tool path:

1. The maximum value of scallop height should be keeping below a threshold.

2. The chord error e of any two neighboring CC points cannot exceed a known tolerance.

Fig. 26 shows the definition of the side step and forward step. There are two important factors d_s and d_f in this figure require to explain: the side step d_s is the distance between any two adjacent CC points and the forward step d_f is the maximum distance between any two subsequent CC points. Both the side step d_s and the forward step d_f are depending on the local surface curvature. In Eq. (35) the effective cutting width w_i is being the side step when calculating d_s. The forward step d_f can be calculated by the following formula [56]:

$$d_f = min(\sqrt{8e|r_f| - 4e^2}, d_{f0}) , \tag{37}$$

where r_f is the curvature radius of the surface along the feed direction and d_{f0} is a constant that can be set to bound the forward step in the situation r_f is infinite.

As mentions and explanations above, the feed direction, which is the direction orthogonal to the CC curve at the CC point, can determine the tool orientation at any CC point. The target of this sub chapter is not only satisfying d_s and d_f at each CC point, but also attend to optimize the total energy consumption according to the Eq. (36). The final solution should be the iteration of the principle curve generation and iso scallop height that will be introduced in the next part.

2.3.1.4 Feed direction optimization

The specific energy term is a pure quantity which changes continuously versus different feed directions, this means a vector field about the energy cost efficiency embedded on the entire surface, which is extremely dependent on the machine's configuration. It can be called as the machine based energy potential field. There is a distinct feed direction f_i through the specific energy cost is the lowest between all the others for each CC point p_i. Furthermore, this feed direction can be named as the optimal specific energy direction.

There are two properties of the potential field that is described as below:

1. For any point on the surface, it has two opposite optimal directions. However, if the specific energy U in Eq. (36) for arbitrary point on the surface is a constant, there is an exception for the case of flat surface.

2. The flow lines on the surface are continuous and will never interact to itself.

When the potential field is defined, the tool path should be defined in a way that the feed directions are as close as possible to the individual optimal directional flow lines of the machine based energy potential field in order to minimize the energy consumption. There is some of the research such as reference [57] and [58] that attended to fit a tool path into a known vector field. A better way to balance between the best fitting to the machine based energy potential field and the demand regular patterns of CC curves can be found.

If a free-form surface is defined as:

$$S(u,v) = (X(u,v), Y(u,v), Z(u,v)\,,$$

a discrete $N \times N$ grid of the machine based energy potential field is created upon the parametric uv domain $[0,1] \times [0,1]$ of the surface.

For each point $\mu_{ij} = (u,v)$ on the grid, the specific energy U that is calculated in Eq. (36) at point $S(u,v)$ can be obtained for every k radian of feed direction from 0 to 2π, where

$$k = \frac{\pi}{180},$$

this can be recorded as a value of vector U_{ij} that is shown in Fig. 26.

the machine based energy potential field is required to constantly calculate at an random $S(u,v)$ in the process of computation of CC curves. This is better than directly calculating it for the case of a grid point μ_{ij}. To be more clear, for an arbitrary node:

$$p = S(u,v)\,,$$

then let:

$$U_i, \quad i = 1,2,3,4 \quad ,$$

which is the machine based energy potential field of the four neighboring grid nodes of (u,v). Then the machine based energy potential field vector u of $S(u,v)$ can be calculated by:

$$u = \frac{1}{\sum_{i=1}^{4} \frac{1}{||p - \mu_i||^2}} \sum_{i=1}^{4} \frac{U_i}{||p - \mu_i||^2}, \tag{38}$$

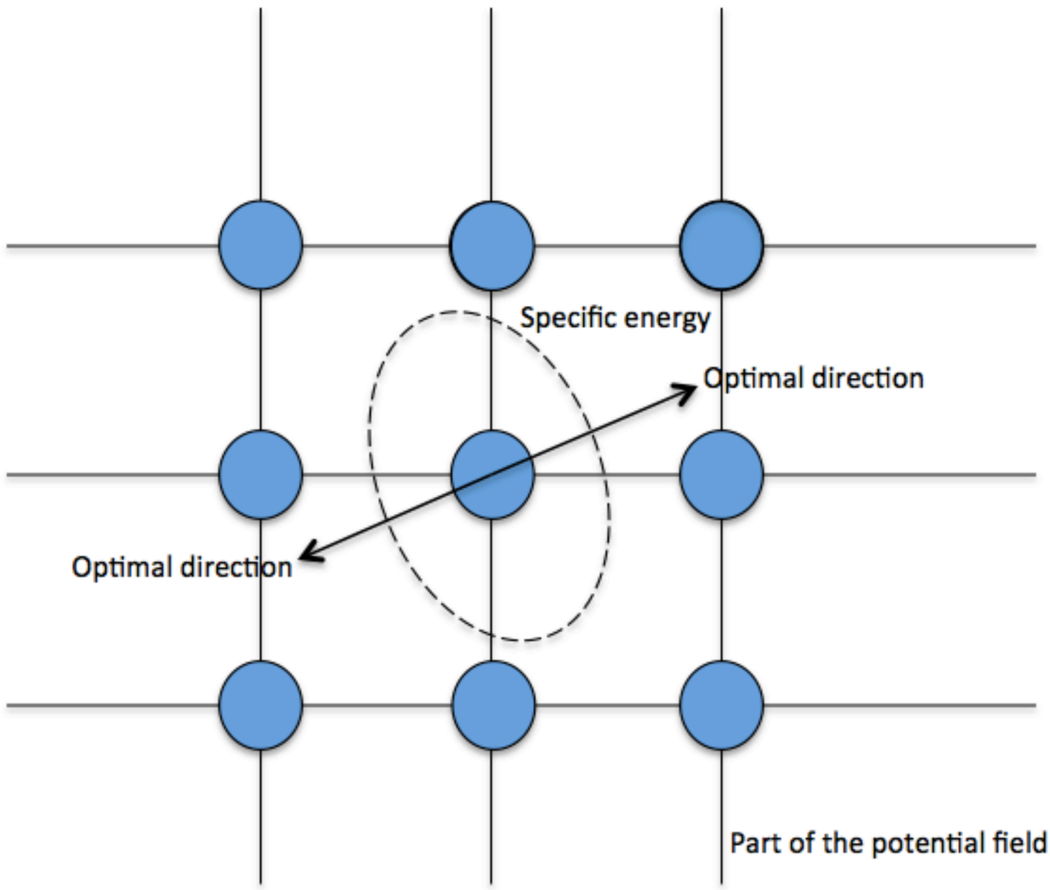

Figure 26 – Discrete the machine based energy potential field in the uv domain

The optimal feed direction f at the arbitrary $S(u, v)$ is directly obtained if using the minimum of the $2\pi/k$ values once u is calculated. By using this method, a principle CC curve can be obtained, which will be introduced in the next part.

2.3.1.5 Principle curve generation

Generally, the principle cutter contact curve is planned foremost to direct the general tendency of the subsequent cutter contact curve, which is expanded based on the distinct criteria that have been introduced in the sub-chapter 2.1 such as iso-parametric, iso-planar and iso-scallop.

The original principle curve is generated in the parametric uv domain of the known surface on which the machine based energy potential field is embedded. It can be started with a random initial point p_i, which related vector u_i and the optimal feed direction f_i of the machine based energy potential field on the sampled $N \times N$ grid are already known if this node can be obtained by Eq. (38). By continuous the steps from f_i with a forward step d_f in the workpiece coordinate system, the following CC point p_{i+1} can be calculated as shown:

$$p_{i+1} = p_i + \frac{d_f}{E(f_i \cdot \vec{u})^2 + 2F(f_i \cdot \vec{u})(f_i \cdot \vec{v}) + G(f_i \cdot \vec{v})^2} f_i \,, \tag{39}$$

where $\vec{u}$ and $\vec{v}$ are the fundamental unit vectors of the uv domain, as well as E, F, G are the modulus of the first basic form in differential geometry [59].

The principle curve can be generated in the forward step until reach the uv domain's boundary. Then it can be started the similar process from p_i to generate the backward step through the opposite direction of f_i. Finally, the whole principle curve can be fully generated by cascading the forward and backward part.

2.3.1.6 Expansion algorithm according to Iso-scallop height

After generating the principle curve, cutter contact curves can be expanded to its both sides in order to filling the whole surface. According to the iso-scallop height needs, the side step between the neighboring CC curves should be enlarged as more as possible, as much as possible the maximum scallop height.

If the tangent direction determines with the optimal feed direction at each CC point on the principle curve, the expansion of the CC curve is impossible. Fig. 27 shows how to generate the first expanded curve according to the traditional iso-scallop height expansion rules: shift a side step $d_s = w_i$ that perpendicular to the feed direction f_i for each CC point p_i on the principle curve.

Reference [56] provides the equation for the sake of calculating p_i as shown below:

$$|p_i p_i'| = w_i \,, \tag{40}$$

$$(p_i - p_i')(\frac{\partial S}{\partial u}\frac{du}{dt} + \frac{\partial S}{\partial v}\frac{dv}{dt}) = 0 \,, \tag{41}$$

where the differential form $\frac{\partial S}{\partial u}\frac{du}{dt} + \frac{\partial S}{\partial v}\frac{dv}{dt}$ is the feed direction f_i at p_i in theoretically.

The Taylor expansion can eliminate higher order terms of the value p_i':

$$p_i' = p_i + \frac{\partial S}{\partial u}\Delta u + \frac{\partial S}{\partial v}\Delta v \,, \tag{42}$$

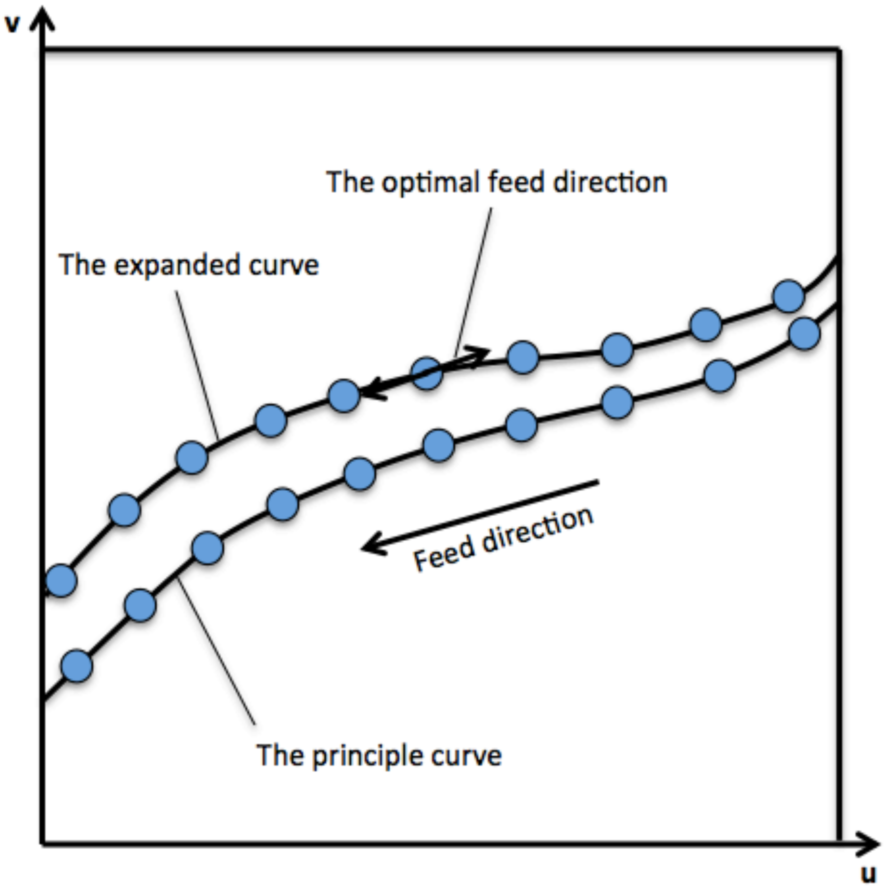

Figure 27 – The way to generate the first expanded curve according to the traditional iso-scallop height expansion rules

By utilization of the Eqs. (40)-(42), the parametric increment of p_i' can be calculated in order to match the key equations:

$$\Delta u = \frac{\pm w_i(F\frac{du}{dt} + G\frac{dv}{dt})}{\sqrt{(EG - F^2)(E(\frac{du}{dt})^2 + 2F\frac{du}{dt}\frac{dv}{dt} + G(\frac{dv}{dt})^2)}}, \quad (43)$$

$$\Delta v = \frac{\pm w_i(E\frac{du}{dt} + F\frac{dv}{dt})}{\sqrt{(EG - F^2)(E(\frac{du}{dt})^2 + 2F\frac{du}{dt}\frac{dv}{dt} + G(\frac{dv}{dt})^2)}}, \quad (44)$$

where $E = \frac{\partial s}{\partial u} \cdot \frac{\partial s}{\partial u}$, $F = \frac{\partial s}{\partial u} \cdot \frac{\partial s}{\partial v}$ and $G = \frac{\partial s}{\partial v} \cdot \frac{\partial s}{\partial v}$ are the factors of the first basic form in differential geometry.

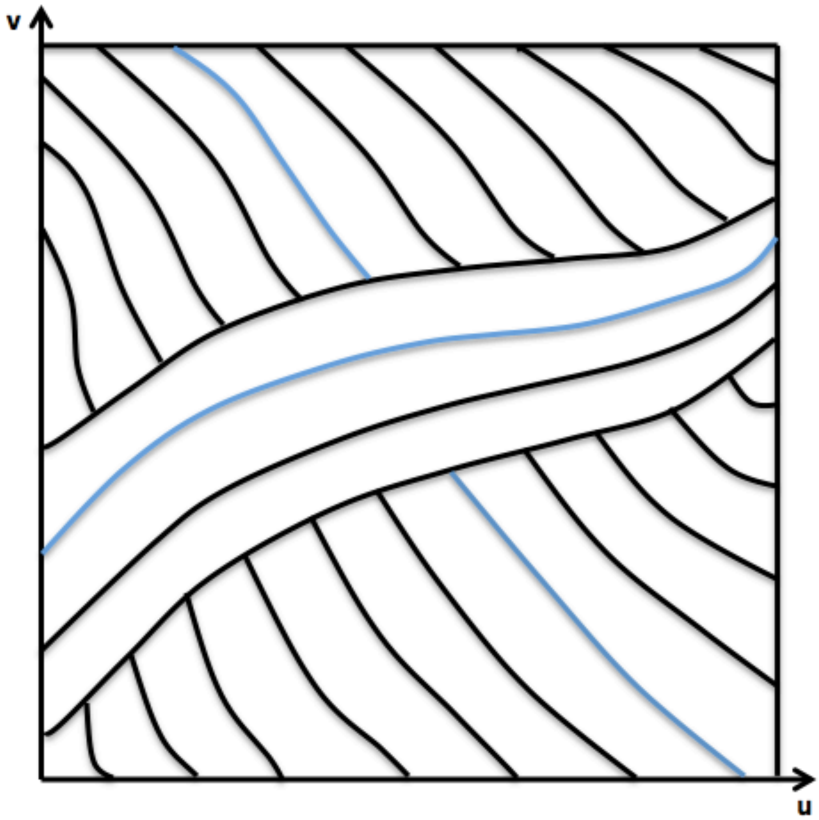

Figure 28 – Three expansion groups of cutter contact curves that mantle the whole surface domain

The bias between the optimal feed direction and the tangent direction of the expand curve will be extremely large if the expansion step have been finished and have the certain expanded curves. Then a concept of quality evaluation should be introduced, which will terminated the expansion when the deviation is exceeding a threshold that is expressed as the ratio:

$$\frac{\sum u_i - \sum u_{i0}}{\sum u_i},$$

where $\sum u_i$ is the sum of the machine based energy potential field value through the real feed direction at all the cutter contact points on the expanded curve, as well as $\sum u_{i0}$ is the sum of the optimal machine based energy potential field value at each CC point on the curve. It should be noted that the ratio should be 0 for a principle curve.

As Fig. 28 shown, three expansion groups with the principle curve coloured in blue can cover the entire surface domain. This sub-chapter has introduced a path generation considering the energy consumption, which will be selective utilized to the case study and the rest will be used to future work of research.

3 Case Study

The purpose of the case study section is that to find the most optimized solution of the target shape by researching and adjusting the G codes of the machining. Generally, the machining simulation software such as EdgeCAM will generate a default tool path that can process the target shape according to the blueprint. However, the default solution cannot meet our specific requirements in instance, for example surface smoothness requirements and machining time optimization needs etc.. In this master thesis, we will choose a surface shape that is shown in Fig. 29, which is chosen for the sake of easier observing and comparing intuitively.

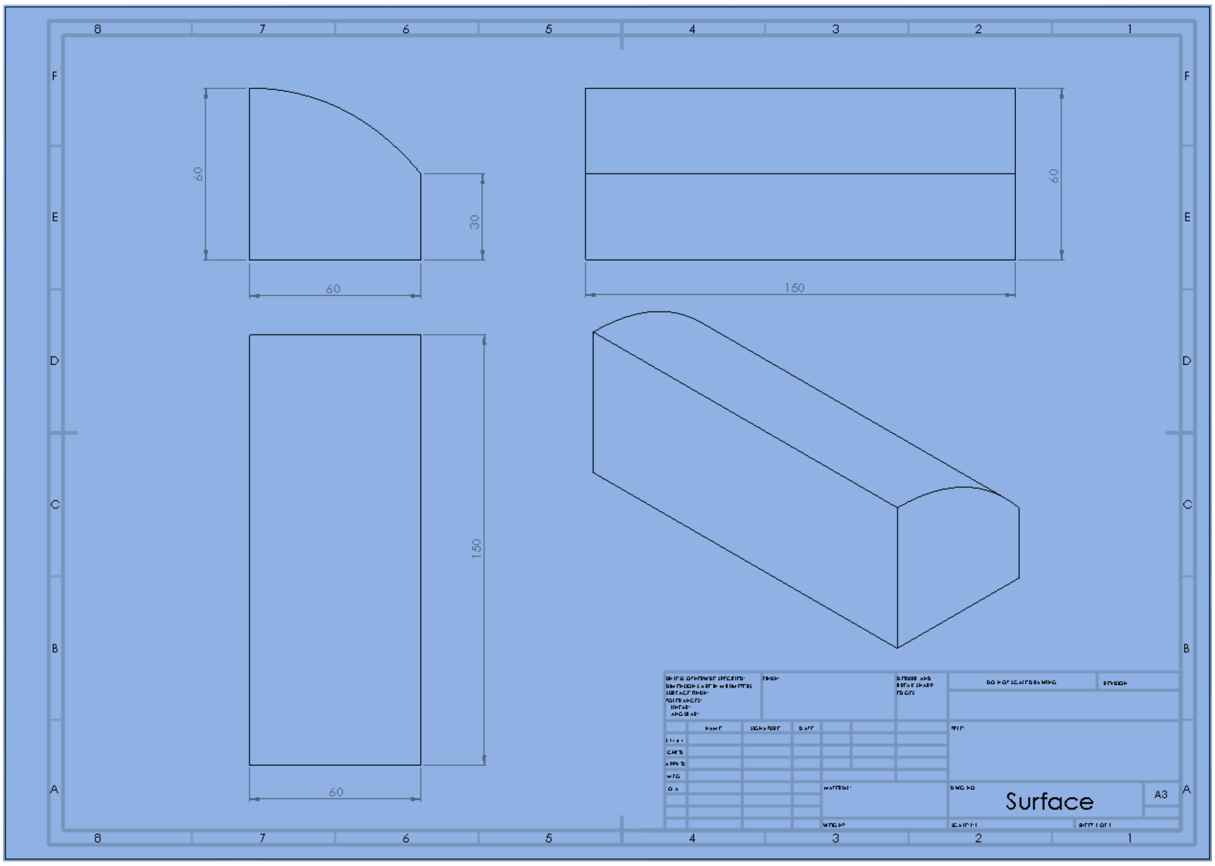

Figure 29 – The four views of the target stock and surface

We use EdgeCAM to plan the tool path, simulate and generate the G codes in this thesis. The G codes of all the methods and approaches are attached in the appendix part at the end of this paper. The illustration and investigation of the G codes will be conduct by the diagrammatic sketch in order to explain the codes in a simple and intuitive way.

In this chapter, we will first generate different types of tool path approaches and compare with them in the simulation software, and then the solution will be obtained by combining the optimized machining method. At the end of this chapter the final optimized solution will be conduct in the CNC machine and will be compared with the default case depends on the operation time and smoothness of working surface.

3.1 Analysis of Default Generation Path Based on G codes

As the above description, the tool path of the default solution can be read in the G code file and illustrated in the Fig. 30. The main tool path of the default one is moving in the y-axis direction (top figure of Fig. 30) and cutting layer by layer through the z-axis.

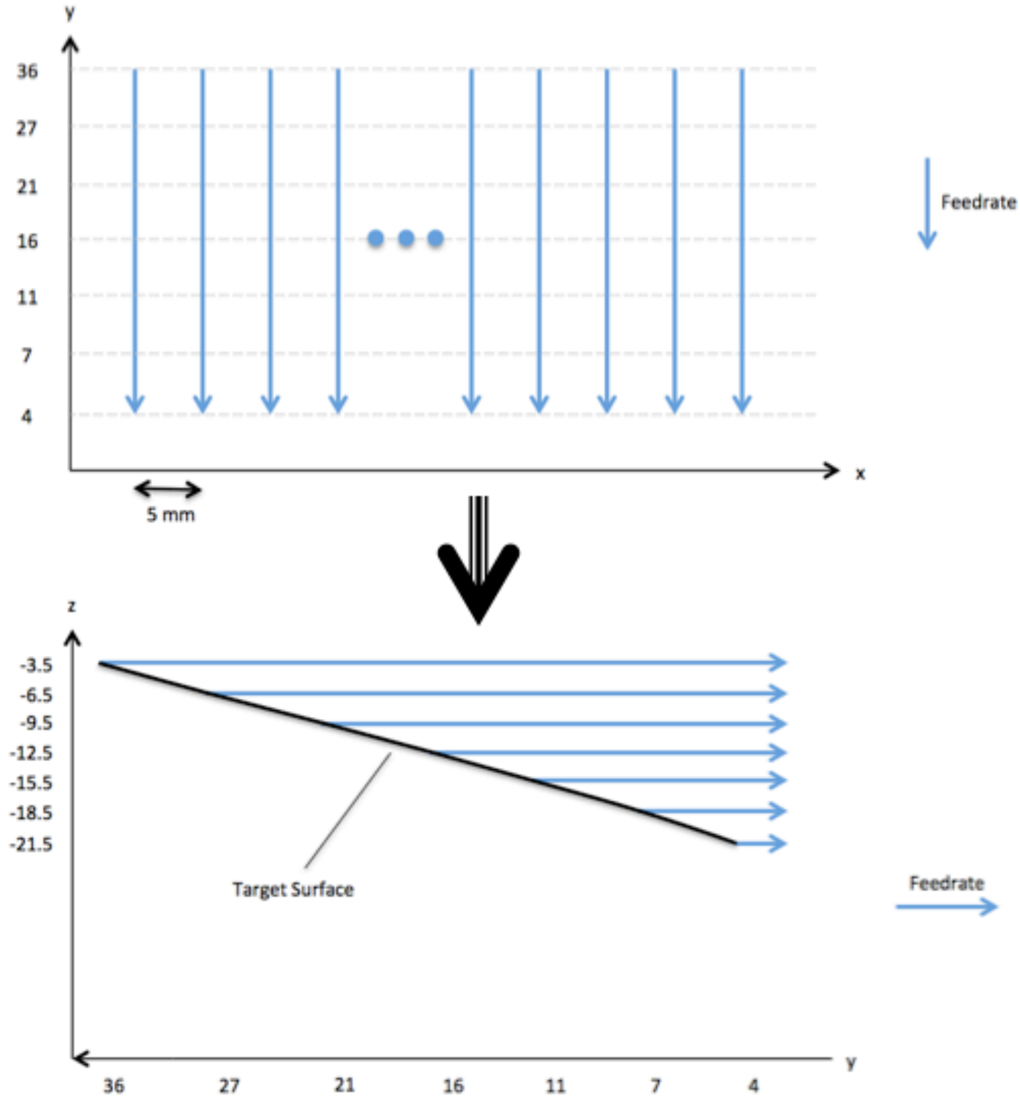

Figure 30 – The tool path illustration of default solution from EdgeCAM

Fig. 31 shows the tool path simulation by G code simulation software. The general shape of the target surface can be seen in this figure by the route of tool movement. The machining time is about 16 minutes and the surface is rough, which cannot meet our requirements in both smoothness and operation time. Therefore, the optimized solutions and approaches are proposed in the following sub chapters.

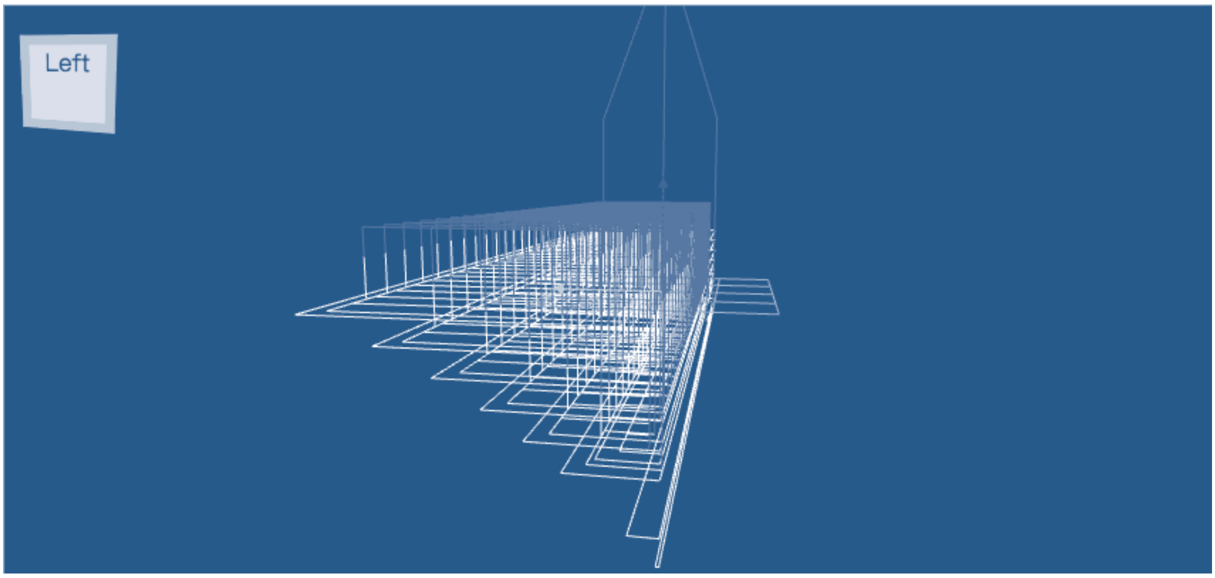

Figure 31 – Tool path simulation figure of the default case

3.2 Approaches to the Case Based on G codes (simulation)

It is obvious that the default solution mentioned above is not a satisfactory program. Therefore, several approaches in this section will be mentioned to optimize the surface machining. It should be mentioned that this section's research and comparison of the different approaches are based on the simulation software in order to save time and money, as well as comparison of different tool path's processing performance. There are four optimization approaches that will be investigate by analysing the G codes, which are attached in the appendix part and in the attachment as well.

In this thesis, we will propose a module method to optimize the tool path movement. The main module can be divided into two different machining ways:

1. Linear tool path movement module

2. 3D tool path movement module

Then we will optimize each module to produce the optimized module, and then combine the optimized module together to provide the final proposal of tool path optimization, which will be execute in the CNC machine.

3.2.1 Surface Machining Optimization Method 1: Linear Path only

Fig. 32 and Fig 33 show the tool path illustration by investigating of the G codes. The Rough milling will be the first step to mill the target stock in the x-axis, afterwards the profile milling will be conducted in order to fulfil the smoothness requirements.

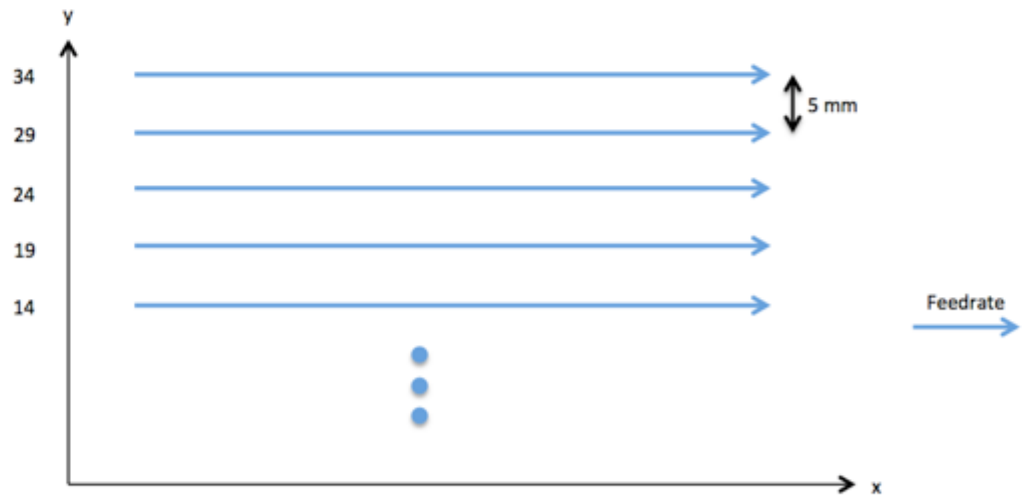

Figure 32 – Rough milling illustration of linear path only optimization solution (RM module)

Figure 33 – Profile milling illustration of linear path only optimization solution (PM module)

It should be mentioned that Fig. 32 and Fig. 33 are described the tool path movement in the top view of the stock. The interval between the adjacent tool paths can be seen from the G codes and illustrated in the Fig. 32 as well. However, in the profile milling stage, the neighboring tool paths are not in the same axis. In another word, each tool path is in the distinct depth, which is illustrated in the Fig. 34 (left view of the stock). The principle of the machining of surface is: through iterations of several small processing paths in the x-axis direction, the target surface will be formed by an infinite approximation of the shape of the surface.

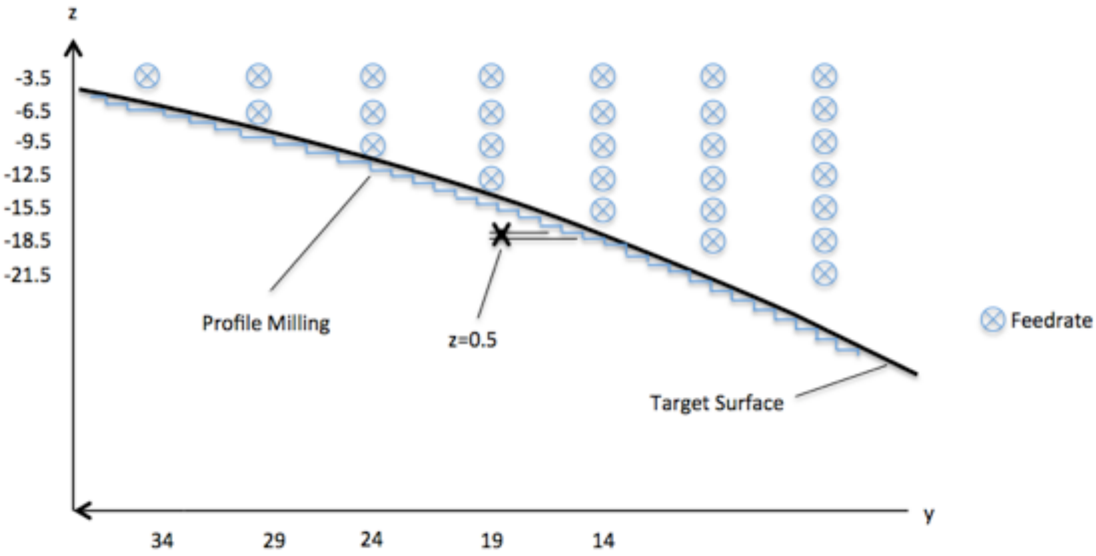

Figure 34 – Machining illustration of linear path only optimization solution based on left view of the stock

Fig. 35 is generated from the same G code simulation software. It can be seen from this figure that the surface smoothness is better than the default case. Nonetheless, the machining time is longer than the default case. We will compare the operation time of all the simulation approaches in the comparison section.

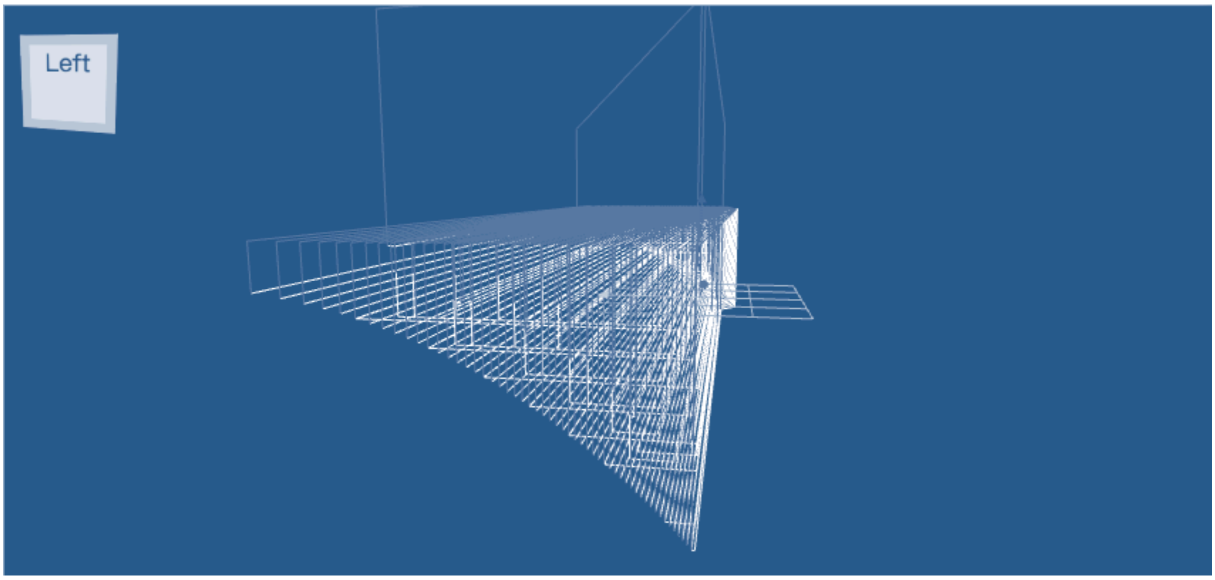

Figure 35 – Tool path simulation figure of the linear only optimization case

Method 1 is the original method to conduct the surface machining in linear way as we introduced in the previous section. In the next section we will propose a 3D machining method that has different tool path compare to the linear operation.

3.2.2 Surface Machining Optimization Method 2: Iso Scallop Method

This section will experiment the feasibility of the 3D machining method. Fig. 36 is the tool path illustration of the iso scallop method. The tool path is through the y-axis direction if we consider the tool route in the top view of the stock. The actual path is increment in the z-axis direction and moved in the y-axis, which is the reason we use the short line on the arrow to indicate the incremental change on the other axis.

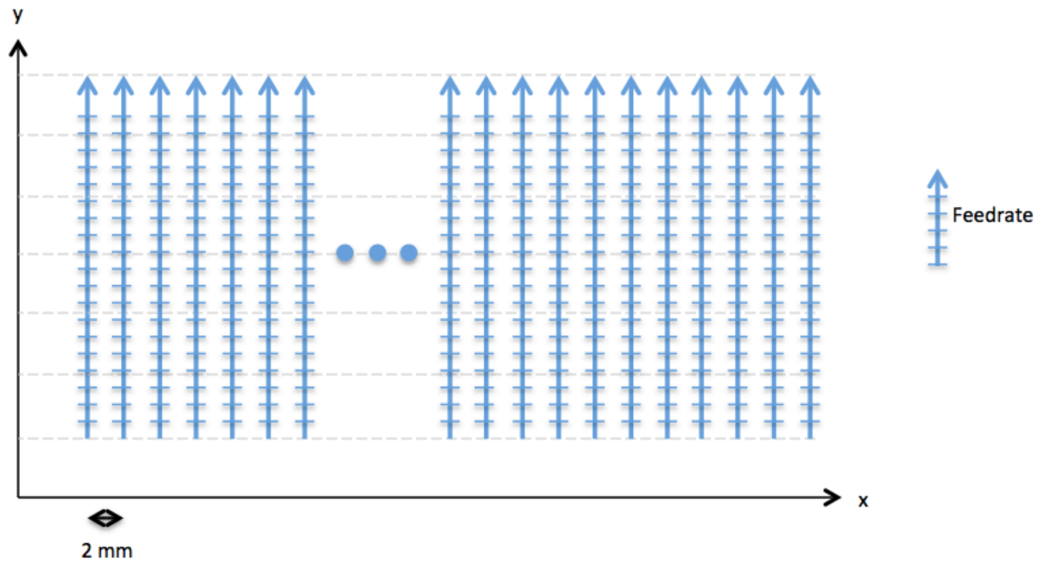

Figure 36 – Tool path illustration of iso scallop optimization solution (CM module)

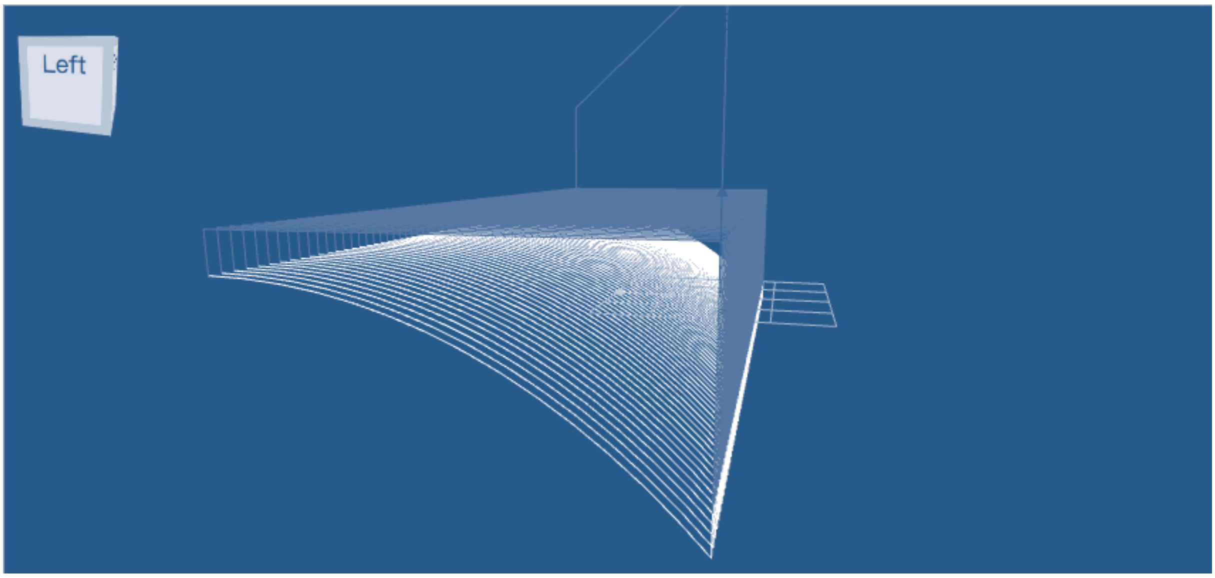

Figure 37 – Tool path simulation figure of the scallop optimization case

There is a serious problem in the machining of iso scallop method. We can read the start point of the tool path through the G codes. The path is from the bottom to the top of the surface. However, the vertical distance of the surface is 30mm, which is longer than the tool length. Moreover, the ball-end cutting tool cannot be perpendicular to the target plane in the real machining. Therefore, we need to purpose an optimization solution of this 3D machining method, which will be carried out in the next section.

3.2.3 Surface Machining Optimization: Optimization of Method 2

Due to the tool crash problem that has mentioned in the above section, we will add a rough milling step in the front of the method 2 in order to avoid tool damage.

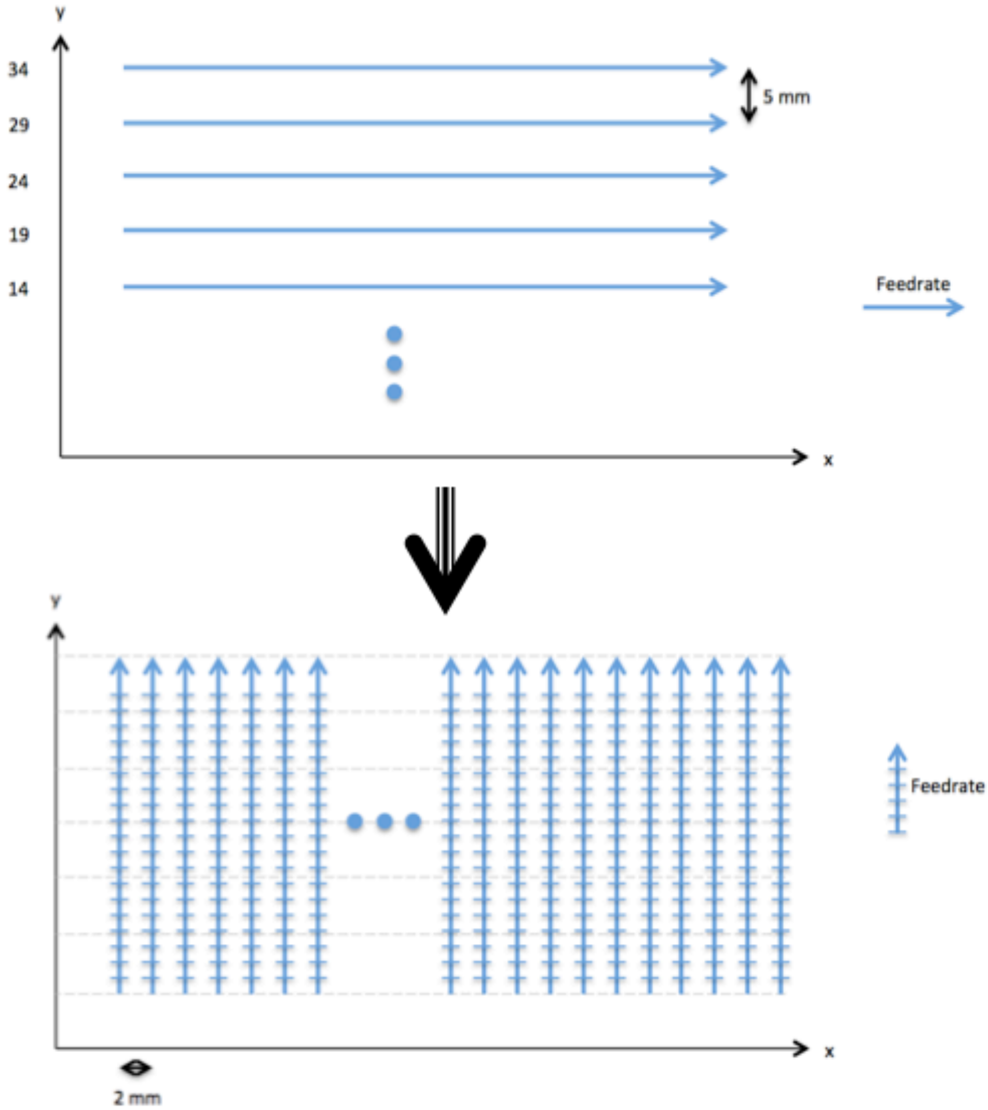

Figure 38 – Tool path illustration of combination of RM module & CM module (iso scallop)

Fig. 38 describes the tool movement of iso scallop method. It needs the rough milling before iso scallop machining. Like a double-edged sword, the iso scallop method provides better smoothness while also consuming more processing time due to the small step over in our simple surface case. The iso scallop method might has a better balance performance in the processing time and processing accuracy in the more complex cases. Due to this reason, we will make a more complex surface to test the different algorithms on five-axis CNC machine in the future works.

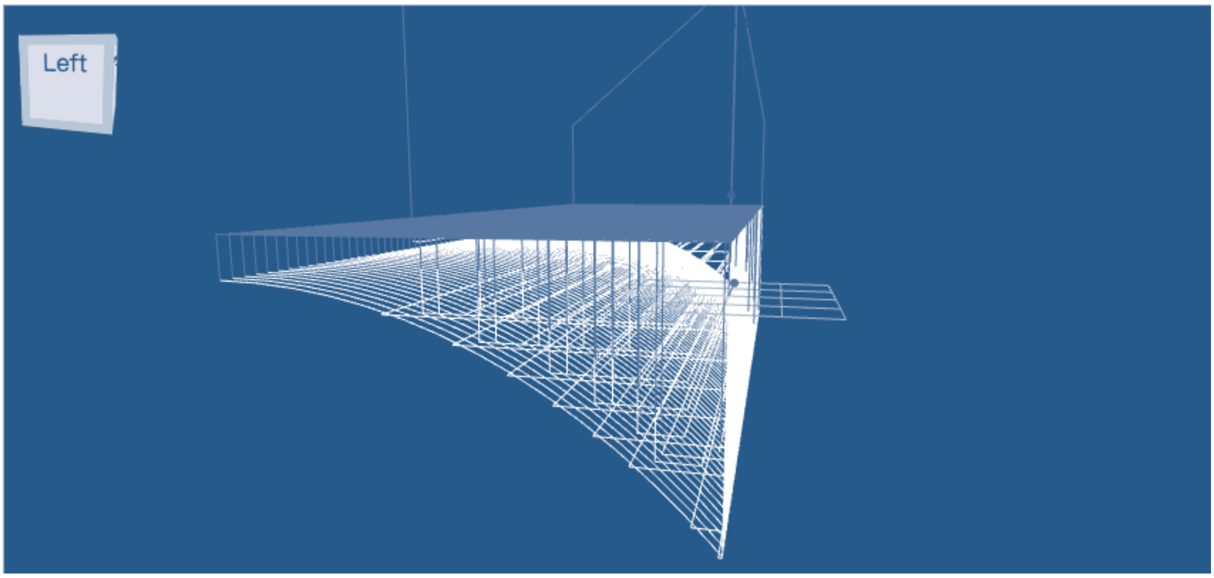

Figure 39 – Tool path simulation figure of combination of RM module & CM module (iso scallop) case

It can be seen in Fig.39 that the optimization of method 2 is avoiding the damage to the cutting tool and increasing the accuracy of processing at the same time, which means the 3D machining method is an optimized solution that can be considered in the real CNC machining (adjusting of the parameters such as feedrate and spindle speed will be conducted in the real processing in the following chapter).

3.2.4 Surface Machining Optimization: Optimization of Method 1

Method 1 is an approach that makes the tool travel in a linear way in x-axis direction. As the illustration Fig. 32 shown, the cutting tool needs to travel back to the previous x-axis coordinates so as to start the new cutting step. This travel time will probably waste the energy and total machining time. In order to optimize the linear method, the best solution is to make the tool path moving without the travelling time.

Fig. 40 shows the tool path of the optimization of method 1. The main difference between the optimized one and the origin one is the rough milling's tool path. The following machining can be profile milling or small step over rough milling so as to achieve the surface as close as possible to the final surface we want to process.

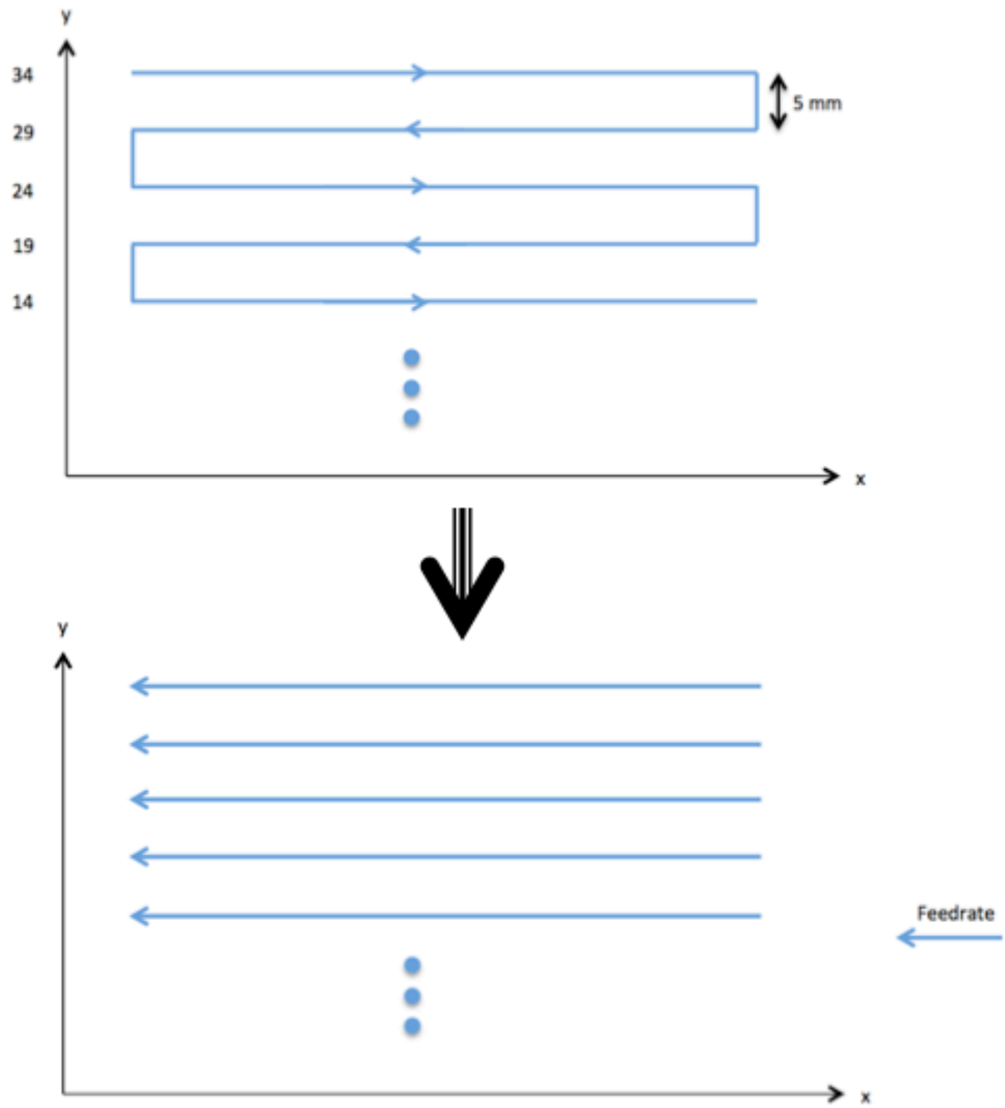

Figure 40 – Tool path illustration of optimization of method 1 (rough milling module optimization)

We can see from the Fig. 41 that the tool path is changed in the rough milling step. It should be mentioned that he path interval is not small enough in both the linear cutting and 3D cutting simulations. All the simulations are using the same parameters such as feedrate, path interval, cutting depth etc. to make the reasonable comparison, which will be made in the next section.

In the next part, the comparison through machining time, tool distance and program line will be made according to the four optimized approaches and the default case. Then the two real program proposals will be proposed so as to test the result of optimization method.

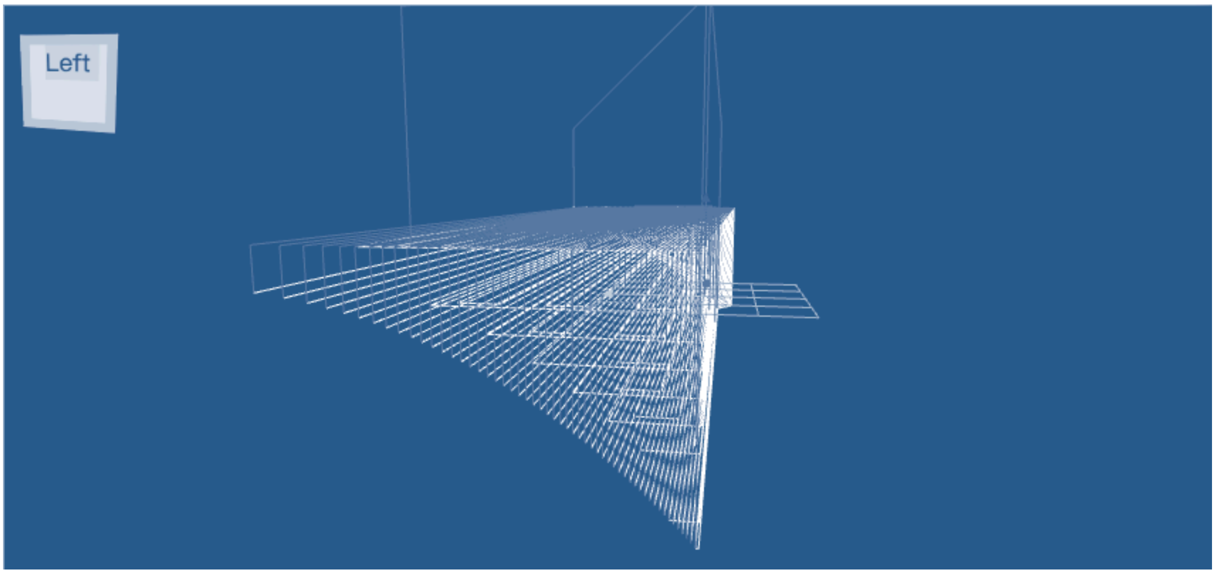

Figure 41 – Tool path simulation figure of optimized method 1 case

3.3 Comparison of the Different Approaches & Final Proposal

The data of Table 3 from left to right is arranged in the order in which they appear in the previous section and the resources of these data are attached in the appendix part.

Table 3 – Comparison of the five simulations

	DEFAULT CASE	LINEAR CASE	3D CASE	LINEAR+3D	OPT. LINEAR
MACHING TIME	16m00s	24m07s	07m01s	18m12s	20m53s
PATH DISTANCE	18561.22	32474.83	12619.95	25449.27	28749.98
FEEDRATE	1000	1000	1000	1000	1000
SPEED (RPM)	5730	6366	6366	6366	6366
PROGRAM LINE	1288	710	2262	2382	588
MACHINING TECHNOLOGY	Rough	Smooth	Tool Damage	Smooth	Smooth

There are four methods from the chart that can be considered to the comparison such as default case, linear case, linear + 3D case and optimized linear case except the tool damage approach (3D case). Then we ruled out rough case for machined faces (default case) and the most time consuming case (linear case). At the final stage, we have two optimized options (blue column) that need to implement in the real CNC machining so as to test the performance of this two methods.

As the comparison chart shows to us, although the simulation above is the most resource saving method and the results of the simulation can help us to choose what kind of program should be implement in the real case, but its limitations are obvious, that is, it can not be intuitive to reflect the specific performance of specific program. In order to make our research more practical, the experiment of comparing these two methods will be conducted in the next section. It should be noted that the machining parameters would be modified for the sake of achieving the highest performance of each method.

3.4 Experimental Results & Conclusion

3.4.1 Experimental Process & Results

Fig. 42 is the linear method surface, which will be the reference material compare with the linear + 3D method. In order to increase the contrast, our linear processing program is only used in the simulation part of the selected processing methods, which means the specific parameters are not optimized. The total operation time is about 22 minutes and the surface quality of this method is not satisfactory as shown in the figure.

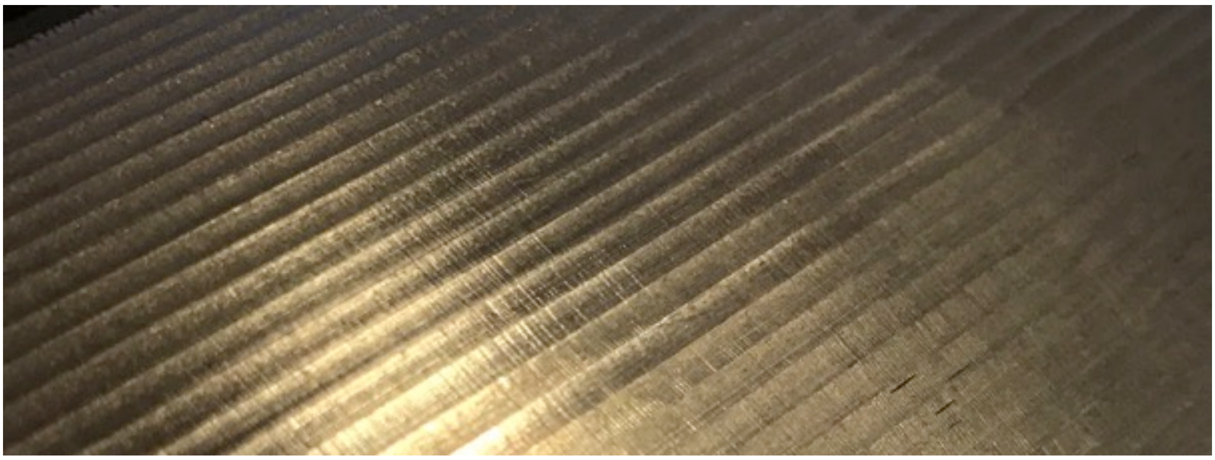

Figure 42 – Linear method surface

Then we plan to machine the surface by using linear + 3D approach. As we mentioned before, this method is using the iso scallop method (the path interval is 0.4mm) for the profile milling step and the parameters such as feedrate and spindle speed are calculated by following:

$$N = \frac{V_c}{\pi \cdot D}, \tag{45}$$

where N is the spindle speed, V_c is the specific speed that is selected depends on different materials and D is the diameter of the cutting tool.

$$f_r = N \cdot n \cdot f_z \,, \tag{46}$$

where f_r is the feedrate of each machining, n is the number of teeth and f_z is the ERC feed depends on different materials.

We also need the formula to calculate the material removal rate so as to compare the performance of distinct machining:

$$MRR = a_e \cdot a_p \cdot f_r \,, \tag{47}$$

where a_e is the width of cut and a_p is the depth of cut.

Then we can utilize Eq. (45) and Eq. (46) to calculate the parameters for our specific milling method (linear + 3D machining).

For the machining of first rough milling by using 12mm Flute End Mill:

$$N = \frac{V_c}{\pi \cdot D} = \frac{350}{\pi \cdot 0.012} = 9288RPM$$

$$f_r = N \cdot n \cdot f_z = 9288 \cdot 3 \cdot 0.1 = 2786\ mm/min$$

For the machining of second rough milling by using 12mm Flute End Mill:

$$f_r = N \cdot n \cdot f_z = 9288 \cdot 3 \cdot 0.14 = 3900\ mm/min$$

where f_z for each step is adjusted by different correction factor depends on distinct a_e.

For the machining of profile milling by using 10mm Ball Nose End Mill:

$$N = \frac{V_c}{\pi \cdot D} = \frac{440}{\pi \cdot 0.01} = 14012RPM$$

$$f_r = N \cdot n \cdot f_z = 14012 \cdot 2 \cdot 0.057 = 1597\ mm/min$$

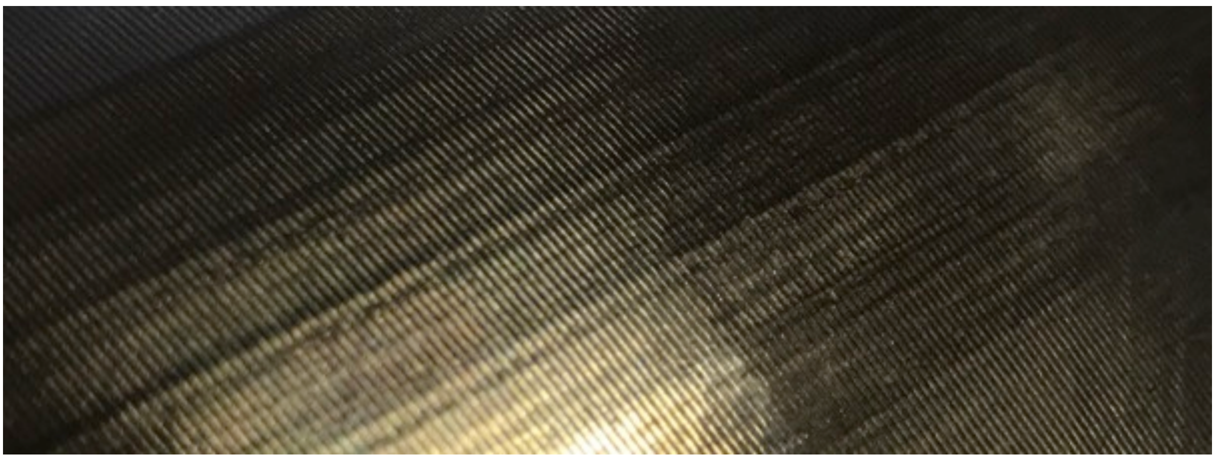

Figure 43 – Linear +3D method surface

After calculation of the specific parameters, we execute the machining by using these numbers. Then we obtain a smoother surface than the contrast surface as shown in Fig. 43 and the total machining time is about 30 minutes.

Table 4 – Comparison of the two real CNC machining

		LINEAR CASE	LINEAR + 3D CASE
MACHING TIME		22m	30m
FIRST STEP ROUGH	Feedrate (mm/min)	2250	2786
	Spindle Speed (RPM)	8000	9288
	MRR (mm^3/min)	32400	25074
SECOND STEP PROFILE	Feedrate (mm/min)	995	3900
	Spindle Speed (RPM)	9550	9288
	MRR (mm^3/min)	746	2808
THIRD STEP FINISH	Feedrate (mm/min)	N/A	1597
	Spindle Speed (RPM)	N/A	14012
	MRR (mm^3/min)	N/A	638

It is obvious that the optimized linear + 3D method can process more smoother surface without consuming too much time. More comparison of the two methods can be seen in table 4.

```
N26490 G0 Z5.0001
N26500 X86.322 Y8.5378
N26510 Z-17
N26520 G1 Z-18
N26530 G3 X84.8144 Y7.8903 CR=3
N26540 G1 X84.5687 Y7.6668
N26550 G2 X80.1142 Y5.6154 CR=6.224
N26560 G1 X0.005 Y5.6138
N26570 X-0.4947 Y5.6447
N26580 X-0.9914 Y5.7072
N26590 X-1.4831 Y5.8013
N26600 G3 X-3.0348 Y5.8627 CR=3
N26610 G0 Z5.0001
N26620 X87.1593 Y11.5474
N26630 Z-17.6
N26640 G1 Z-18.6
N26650 G3 X86.0916 Y10.025 CR=3
N26660 G1 X85.8341 Y9.0988
N26670 G2 X83.1103 Y5.7806 CR=6.2223
N26680 G1 X82.231 Y5.3044
N26690 G2 X79.4007 Y4.3258 CR=14.193
N26700 X75.4463 Y3.7475 CR=26.4408
N26710 X68.4515 Y3.5152 CR=111.8083
N26720 X44.4516 Y3.4869 CR=5301.8995
N26730 G1 X3.4516 Y3.4868
N26740 X2.452 Y3.5141
N26750 X1.4759 Y3.7316
N26760 X0.5517 Y4.1136
N26770 X-0.3016 Y4.6349
N26780 G3 X-1.3021 Y5.072 CR=3
```

(a) Linear arc

```
G1 X40.2 Y62.8665 Z-0.0018
G0 Z5
X40.6 Y-6.3581
Z-31.2411
G1 Y-3.3581
POLY PO[Y]=(-0.484,0,0.013) PO[Z]=(-27.931,0,-0.011)
PO[Y]=(0.234,0.007,0.005) PO[Z]=(-27.136,-0.007,-0.004)
PO[Y]=(3.108,-0.013,0.033) PO[Z]=(-24.155,0.012,-0.031)
PO[Y]=(3.827,0.017,-0.01) PO[Z]=(-23.428,-0.018,0.011)
PO[Y]=(7.419,-0.787,0.811) PO[Z]=(-20.081,-0.823,0.797)
PO[Y]=(11.011,-0.879,1.774) PO[Z]=(-17.08,-0.638,1.256)
PO[Y]=(11.73,-0.006,0.023) PO[Z]=(-16.522,0.007,-0.027)
PO[Y]=(15.322,-0.295,0.306) PO[Z]=(-13.865,-0.32,0.306)
PO[Y]=(19.633,-5.558,9.248) PO[Z]=(-11.074,-3.699,6.055)
PO[Y]=(22.507,-0.012,0.036) PO[Z]=(-9.429,0.019,-0.062)
PO[Y]=(23.943,0.005,0.008) PO[Z]=(-8.653,-0.011,-0.013)
PO[Y]=(26.817,-0.004,0.021) PO[Z]=(-7.233,0.007,-0.042)
PO[Y]=(28.254,0,0.013) PO[Z]=(-6.576,-0.002,-0.027)
PO[Y]=(31.128,-0.001,0.014) PO[Z]=(-5.371,0.002,-0.033)
PO[Y]=(36.876,-4.319,6.592) PO[Z]=(-3.362,-1.519,2.112)
PO[Y]=(39.75,-0.005,0.015) PO[Z]=(-2.56,0.017,-0.052)
PO[Y]=(41.187,0.007,-0.003) PO[Z]=(-2.186,-0.032,0.015)
PO[Y]=(45.497,-1.017,1.028) PO[Z]=(-1.273,-0.266,0.216)
PO[Y]=(49.808,-1.035,2.077) PO[Z]=(-0.626,-0.105,0.16)
PO[Y]=(51.245,-0.005,0.011) PO[Z]=(-0.478,0.035,-0.085)
PO[Y]=(54.837,0,0.002) PO[Z]=(-0.16,0.005,-0.02)
PO[Y]=(55.197,0,0) PO[Z]=(-0.139,0,-0.009)
PO[Y]=(59.867,0,0) PO[Z]=(-0.002,0,-0.01)
G1 X40.6 Y62.8666 Z-0.0018
G0 Z5
```

(b) Spline

```
N82380 G1 Y-3.3565
N82390 Y-0.4827 Z-27.9289
N82400 Y0.2358 Z-27.134
N82410 Y3.1096 Z-24.1539
N82420 Y3.8281 Z-23.427
N82430 Y7.4204 Z-20.0795
N82440 Y11.0127 Z-17.0791
N82450 Y11.7312 Z-16.5208
N82460 Y15.3235 Z-13.864
N82470 Y18.1974 Z-11.9816
N82480 Y19.6343 Z-11.073
N82490 Y22.5081 Z-9.4278
N82500 Y23.9451 Z-8.652
N82510 Y26.8189 Z-7.2321
N82520 Y28.2558 Z-6.5749
N82530 Y31.1297 Z-5.3699
N82540 Y32.5666 Z-4.8186
N82550 Y35.4404 Z-3.8189
N82560 Y36.8774 Z-3.3618
N82570 Y39.7512 Z-2.5591
N82580 Y41.1881 Z-2.1856
N82590 Y45.4989 Z-1.2725
N82600 Y49.8097 Z-0.626
N82610 Y51.2466 Z-0.4783
N82620 Y54.8389 Z-0.1602
N82630 Y55.1982 Z-0.1388
N82640 Y59.8682 Z-0.0017
N82650 Y62.8682
N82660 G0 Z5
N82670 X67.8 Y-6.3565
```

(c) None

Figure 44 – Three different NC programs

However, the surface is not smooth enough in the horizontal direction cause the output method of NC program. There are three types of NC program that we can select for the surface machining and these three programs are shown in Fig. 44. In the end we chose the none type NC program, which is the linear moving of the cutting tool. The chosen surface is not made with a circular radius so that it cannot be implemented as a linear arc NC program, as well as the spline NC program cannot be used causes limitation of the CNC machine.

3.4.2 Conclusion

According to the experimental results, the optimized method (linear + 3D solution) can get more than the previous surface several times the smoothness, while with only an increase of 36% of the processing time. Thus, through the whole research in the previous chapters and the case study, we can draw the following conclusions:

1. Only the path optimization tool path method that combines the machining parameters with the optimized calculation can achieve maximum optimization performance.

2. 3D machining methods such as iso parametric, iso scallop and iso planar methods might cost more processing time than the linear methods, but they can achieve a higher degree of smoothness. So in the surface processing methods, 3D processing methods have better overall performance than linear ones.

3. For the 3D machining step, the type of spline NC program should have the best performance and smoothness than the other two options.

According to the research previously, in the 3D machining methods, iso scallop might have the best performance in machining more complex free form surface. In the future work, we will investigate the application of iso scallop method in five axis CNC machine for machining more complicated free form surface compare with other optimization methods. Moreover, the future work will be an increased optimization level. We will focus on the overall energy consumption of the machining that is mentioned in the before chapter, to optimize the energy consumption of the entire process so as to achieve the ultimate goal of the optimization.

Reference

[1] Mattson M., "CNC Programming: Principles and Applications", Delmar Cengage Learning. USA, 2010

[2] Patrick Hood-Daniel and James Floyd Kelly, "Build Your Own CNC Machine", 2009

[3] Thomas H. Cormen, Charles E. Leiserson, Ronald L. Rivest, and Clifford Stein, "Introduction to Algorithms", Notes on Turing Machines, CS 4820, 2012

[4] Axelson Manufacturing Company, "Vertical Milling Machine", Division of U.S. Industries. Inc, 1987

[5] Y. Seok Suh and K. Lee, "NC milling tool path generation for arbitrary pockets defined by sculptured surfaces", Computer-Aided Design, vol. 22, pp. 273-284, 1990

[6] S. Ding, M. Mannan, A. Poo, D. Yang, and Z. Han, "Adaptive iso-planar tool path generation for machining of free-form surfaces", Computer-Aided Design, vol. 35, pp. 141-153, 2003

[7] H.Y. Feng and Z. Teng, "Iso-planar piecewise linear NC tool path generation from discrete measured data points", Computer-Aided Design, vol. 37, pp. 55-64, 2005

[8] Pengcheng Hu, Lufeng Chen, Kai Tang, "Efficiency-optimal iso-planar tool path generation for five-axis finishing machining of freeform surfaces", Computer-Aided Design, 2016

[9] Hon-yuen Tam, Haiyin Xu and Zude Zhou, "Iso-planar interpolation for the machining of implicit surfaces", Computer-Aided Design 34, pp. 125-136, 2002

[10] G. Elber and E. Cohen, "Toolpath generation for freeform surface models", Computer-Aided Design, vol. 26, pp. 490-496, 1994

[11] W. He, M. Lei, and H. Bin, "Iso-parametric CNC tool path optimization based on adaptive grid generation", The International Journal of Advanced Manufacturing Technology, vol. 41, pp. 538- 548, 2009

[12] P. Hu, L. Chen, J. Wang, and K. Tang, "Boundary-Conformed Tool Path Generation Based on Global Reparametrization", in International Conference on Computer-Aided Design and Computer Graphics, 2015

[13] K. Suresh and C. Yang, "Constant scallop-height machining of free-form surfaces", Journal of Engineering for Industry(Transactions of the ASME)(USA), vol. 116, pp. 253-259, 1994

[14] E. Lee, "Contour offset approach to spiral toolpath generation with constant scallop height", Computer-Aided Design, vol. 35, pp. 511-518, 2003

[15] A. Can and A. Ünüvar, "A novel iso-scallop tool-path generation for efficient five-axis machining of free-form surfaces", The International Journal of Advanced Manufacturing Technology, vol. 51, pp. 1083-1098, 2010

[16] J.-H. Yoon, "Fast tool path generation by the iso-scallop height method for ball-end milling of sculptured surfaces", International Journal of Production Research, vol. 43, pp. 4989-4998, 2005

[17] J. Xu, S. Zhang, J. Tan, and X. Liu, "Non-redundant tool trajectory generation for surface finish machining based on geodesic curvature matching", The International Journal of Advanced Manufacturing Technology, vol. 62, pp. 1169-1178, 2012

[18] Christophe Tournier and Claire Lartigue, "5-axis iso-scallop tool paths along parallel planes", CAD, pp. 278-286, 2008

[19] Qiang Zou, Juyong Zhang, Bailin Deng and Jibin Zhao, "Iso-level tool path planning for free-form surfaces", Computer-Aided Design 53, pp. 117-125, 2014

[20] J. C. J. Chiou, "Floor, wall and ceiling approach for ball-end tool pocket machining", Computer-Aided Design, vol. 37, pp. 373-385, 2005

[21] V. Pateloup, E. Duc, P. Ray, "Corner optimization for pocket machining, International Journal of Machine Tools and Manufacture", 44 (12), pp. 1343–1353, 2004

[22] Sata T Kimura, F Okada N, Hosaka M.; 1981. "A new method for NC interpolator for machining of sculpture surface", Computer Aided Design; 22 (5): pp. 273-283, 1981

[23] Chih-Ching Lo., "CNC machine tool surface interpolator for ball-end milling of free-form surfaces. ", International Journal of Machine Tools & Manufacture, 40: pp. 307-326, 2000

[24] Matthieu Rauch, Emmanuel Duc, Jean-YvesHascoet, "Improving trochoidal tool paths generation and implementation using process constraints modeling", International Journal of Machine Tools & Manufacture 49: pp. 375–383, 2009

[25] Altintas Y, Brecher C, Weck M, Witt S, "Virtual Machine Tool. CIRP Annals", 54(2): pp. 115–138, 2005

[26] Brecher C, Esser M, Witt S, "Interaction of Manufacturing Process and Machine Tool", CIRP Annals 58(2): pp. 588–607, 2009

[27] AltintasY, KerstingP, BiermannD, BudakE, DenkenaB, LazogluI, "Virtual Process Systems for Part Machining Operations", CIRP Annals 63(2): pp. 585–605, 2014

[28] Siller H, Rodriguez CA, Ahuett H, "Cycle Time Prediction in High Speed Milling Operations for Sculptured Surface Finishing", Journal of Materials Processing Technology 174: pp. 355–362, 2006

[29] Heo EY, Kim DW, Kim BH, Chen FF, "Estimation of NC Machining Time Using NC Block Distribution for Sculptured Surface Machining", Robotics and Computer-Integrated Manufacturing 22: pp. 437–446, 2006

[30] So BS, Jung YH, Park JW, Lee DW, "Five Axis Machining Time Estimation Algorithm Based on Machine Characteristics", Journal of Materials Processing Technology 187: pp. 37–40, 2007

[31] Altintas Y, Verl A, Brecher C, Uriarte L, Pritschow G, "Machine Tool Feed Drives", CIRP Annals 60(2): pp. 779–796, 2011

[32] ErkorkmazK, AltintasY, YeungCH, "Virtual Computer Numerical Control System", CIRP Annals 55(1): pp. 399–402, 2006

[33] Zhou, L., Li, J., Li, F., Meng, Q., Li, J., Xu, X., "Energy consumption model and energy efficiency of machine tools: a comprehensive literature review", J. Clean. Prod. 112, pp. 3721-3734, 2016

[34] Kordonowy, D.N., "A power assessment of machining tools", Mass. Inst. Technol, 2002

[35] Kara, S., Li, W., "Unit process energy consumption models for material removal processes", CIRP Annals-Manufacturing Technol. 60, pp. 37-40, 2011

[36] Draganescu, F., Gheorghe, M., Doicin, C., "Models of machine tool efficiency and specific consumed energy", J. Mater. Process. Technol. 141, pp. 9-15, 2003

[37] Aramcharoen, A., Mativenga, P.T., "Critical factors in energy demand modelling for CNC milling and impact of tool path strategy", J. Clean. Prod. 78, pp. 63-74, 2014

[38] Diaz, N., Helu, M., Jarvis, A., To€nissen, S., Dornfeld, D., Schlosser, R., "Strategies for Minimum Energy Operation for Precision Machining", 2009

[39] Quintana, G., Ciurana, J., Ribatallada, J., "Modelling power consumption in ball-end milling operations", Mater. Manuf. Process. 26, pp. 746-756, 2011

[40] Kant, G., Sangwan, K.S., "Predictive modelling for energy consumption in machining using artificial neural network", Procedia CIRP 37, pp. 205-210, 2015

[41] Dietmair, A., Verl, A., "Energy consumption forecasting and optimisation for tool machines", Energy 62, 63, 2009

[42] Balogun, V.A., Edem, I.F., Adekunle, A.A., Mativenga, P.T., "Specific energy based evaluation of machining efficiency", J. Clean. Prod, 2016

[43] Pavanaskar, S., Pande, S., Kwon, Y., Hu, Z., Sheffer, A., McMains, S., "Energy-efficient vector field based toolpaths for CNC pocketmachining", J. Manuf. Process. 20, pp. 314-320, 2015

[44] Mouzon, G., Yildirim, M.B., Twomey, J., "Operational methods for minimization of energy consumption of manufacturing equipment", Int. J. Prod. Res. 45, pp. 4247-4271, 2007

[45] Newman, S.T., Nassehi, A., Imani-Asrai, R., Dhokia, V., "Energy efficient process planning for CNC machining", CIRP J. Manuf. Sci. Technol. 5, pp. 127-136, 2012

[46] J.E. Bobrow, "NC machine tool path generation from CSG part representation", Computer-Aided Design 17 (2), pp. 69–76, 1985

[47] G.C. Loney, T.M. Ozsoy, "NC machining of free form surfaces", Computer-Aided Design 19 (2), pp. 85–90, 1987

[48] N. Shokrollahi and E. Shojaei, "Experimental comparison of Iso Scallop, Iso Planar and Iso parametric Algorithms in Machining Sculptured Surface", Indian J.Sci.Res. 1(2), pp. 475-481, 2014

[49] C.C. Lo, "Feedback interpolators for CNC machine tools", ASME Manufacturing Science and Engineering 119 (4), pp. 587–592, 1997

[50] I.D. Faux, M.J. Pratt, "Computational Geometry for Design and Manufacturing", John Wiley and Sons, 1981

[51] R.S. Lin, Y. Koren, "Efficient tool-path planning for machining free-form surfaces", ASME Journal of Engineering for Industry 118, pp. 20–28, 1996

[52] R.L. Burden, J.D. Faires, "Numerical Analysis", Brooks/Cole Publishing, 1997

[53] Erkorkmaz K, Altintas Y, "High Speed CNC System Design: Part I – Jerk Limited Trajectory Generation and Quintic Spline Interpolation", International Journal of Machine Tools and Manufacture 41(9), pp. 1323–1345, 2001

[54] Lo, C. C., "Efficient cutter-path planning for five-axis surface machining with a flat-end cutter", Computer-Aided Des. 31, pp. 557-566, 1999

[55] Park, C. W., Kwon, K. S., Kim, W. B., Min, B. K., Park, S. J., Sung, I. H., Yoon, Y. S., Lee, K. S., Lee, J. H., Seok, J., "Energy consumption reduction technology in manufacturing - A selective review of policies", standards and research. Int. J. Precis. Eng. Manuf. 10, pp. 151-173, 2009

[56] Yang, D., "Constant scallop-height machining of free-form surfaces", J. Eng. Ind. 116, pp. 253, 1994

[57] Makhanov, S., "Optimization and correction of the tool path of the five-axis milling machine: Part 1. Spatial optimization", Math. Comput. Simul. 75, pp. 210-230, 2007

[58] Kim, T., Sarma, S.E., "Toolpath generation along directions of maximum kinematic performance; a first cut at machine-optimal paths", Computer-Aided Des. 34, pp. 453-468, 2002

[59] Do Carmo, M.P., Do Carmo, M.P., "Differential Geometry of Curves and Surfaces", Prentice-hall Englewood Cliffs, 1976

[60] Y. Altintas, S. Tulsyan, "Prediction of part machining cycle times via virtual CNC", Manufacturing Technology 64, pp. 361-364, 2015

Appendix: Notes of Iso-Parametric Machining

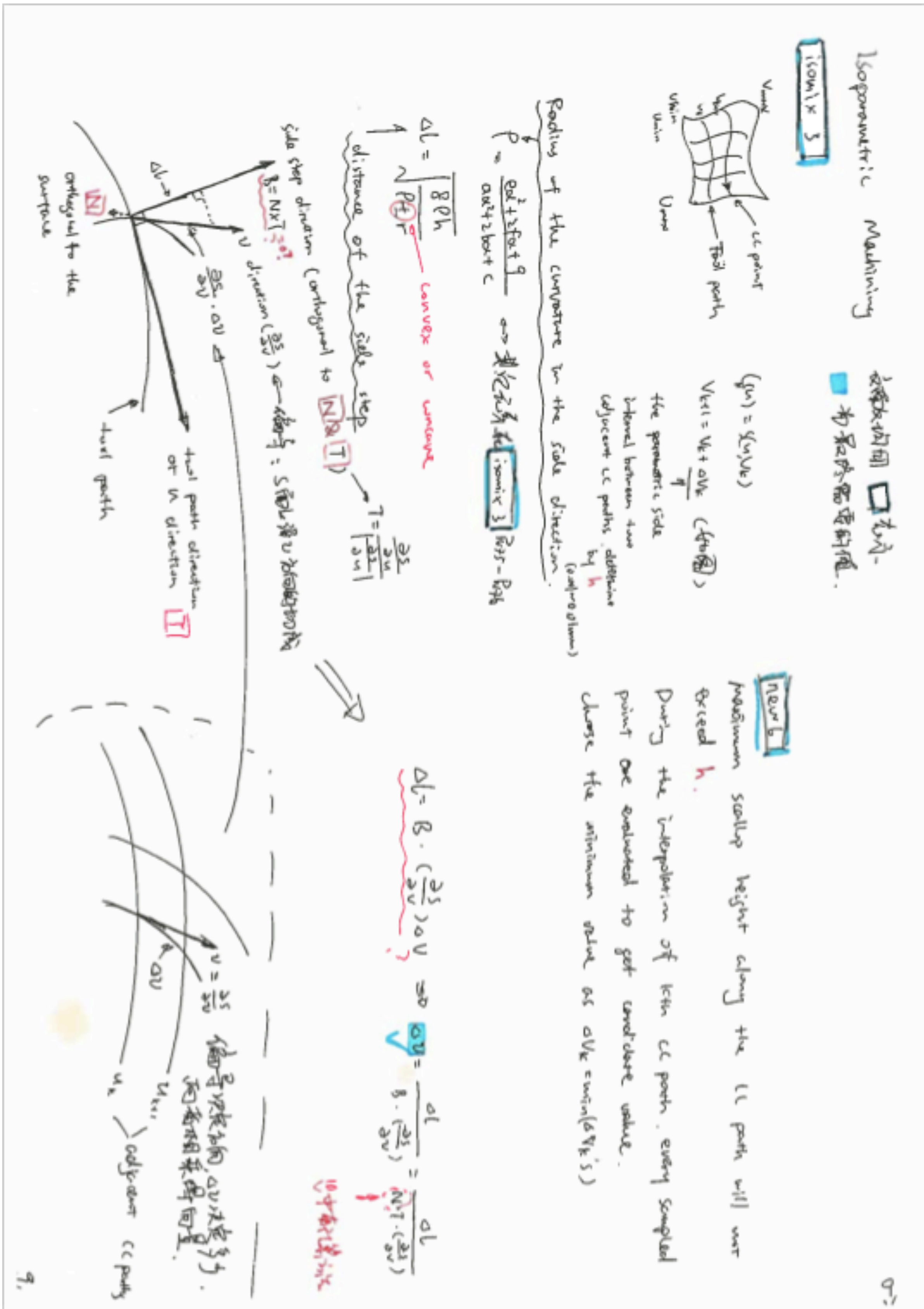

Appendix: Notes of Iso-Planar Machining

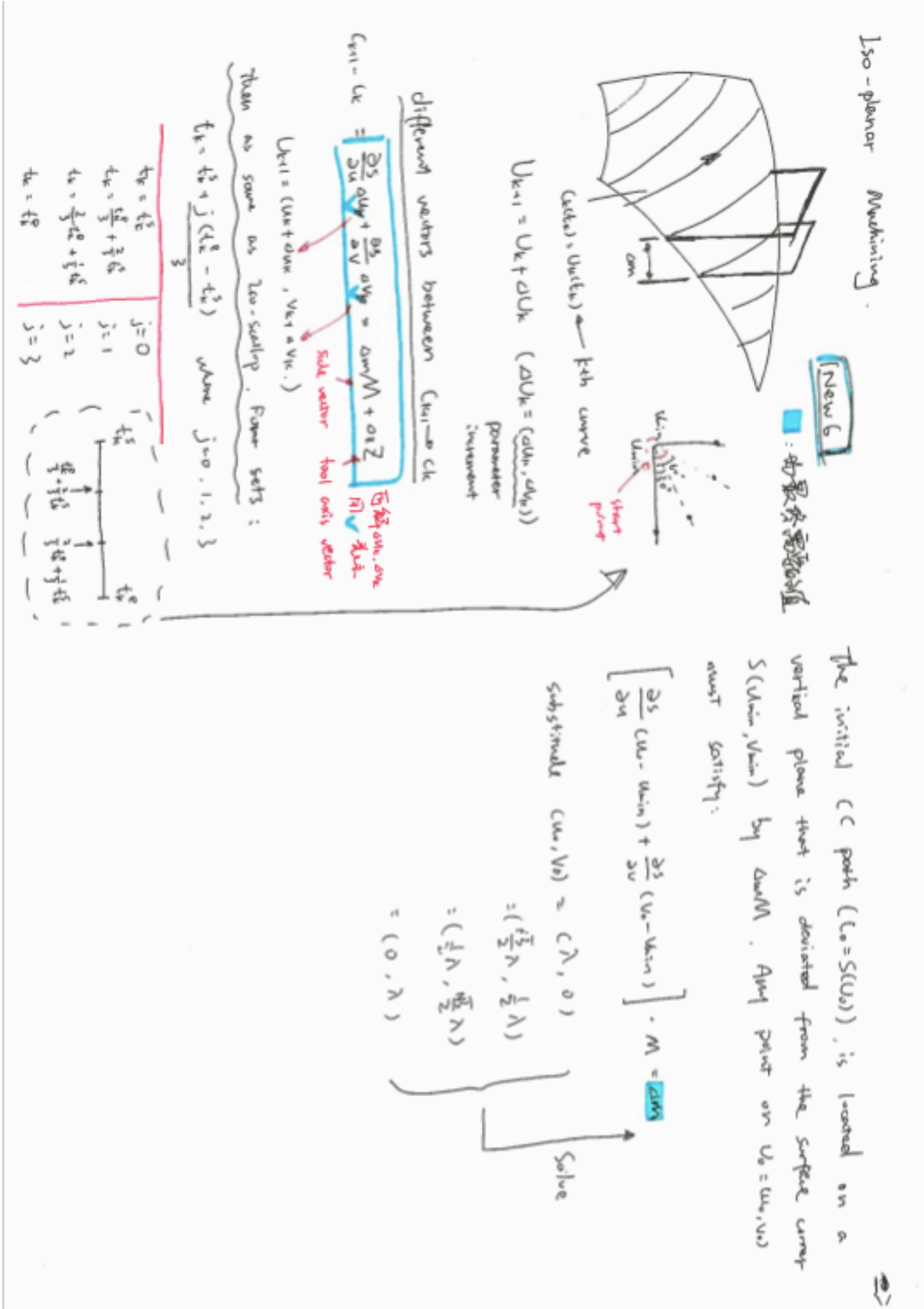

Appendix: Notes of Iso-Scallop Machining

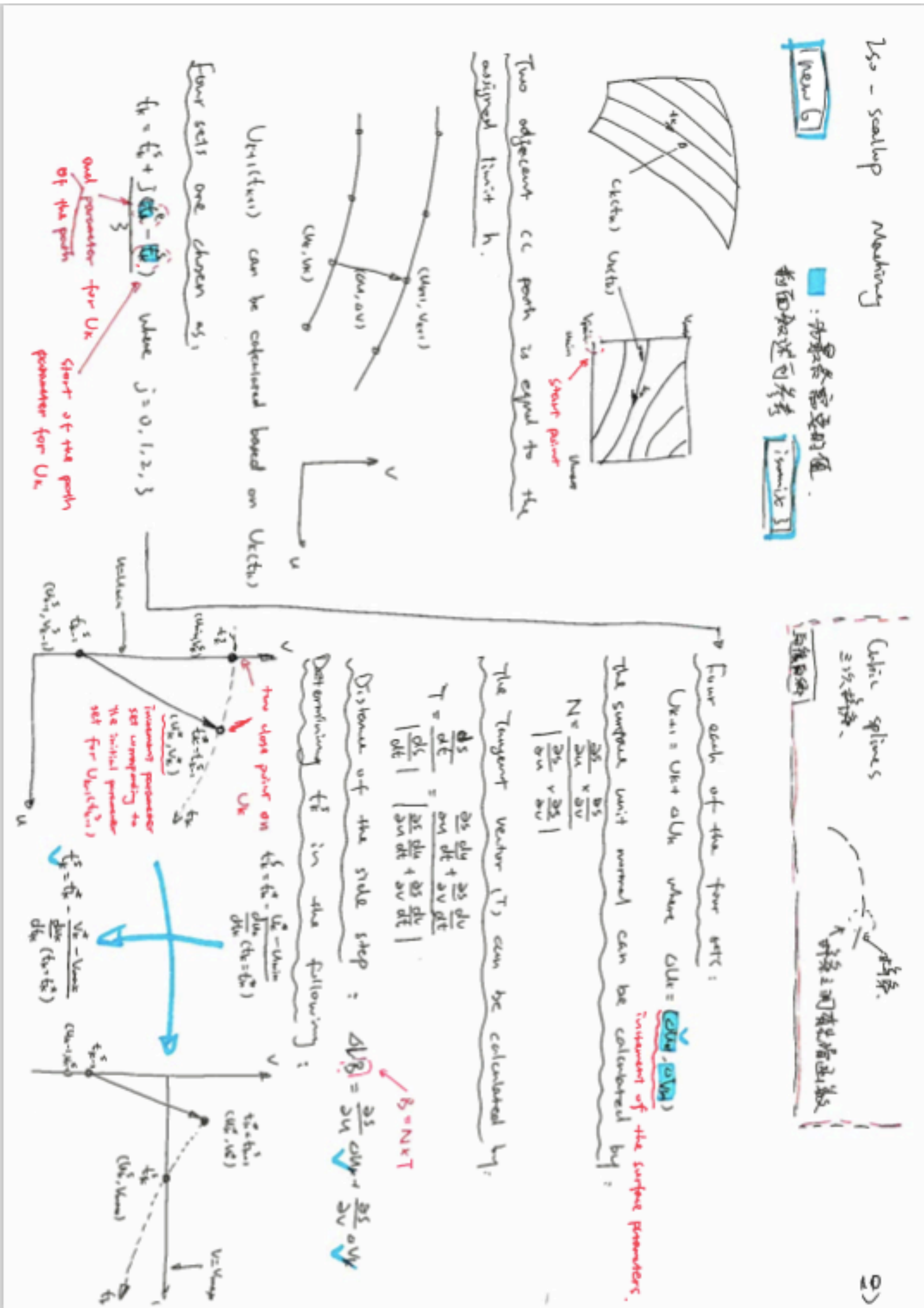

Appendix: Notes of Prediction model page 1

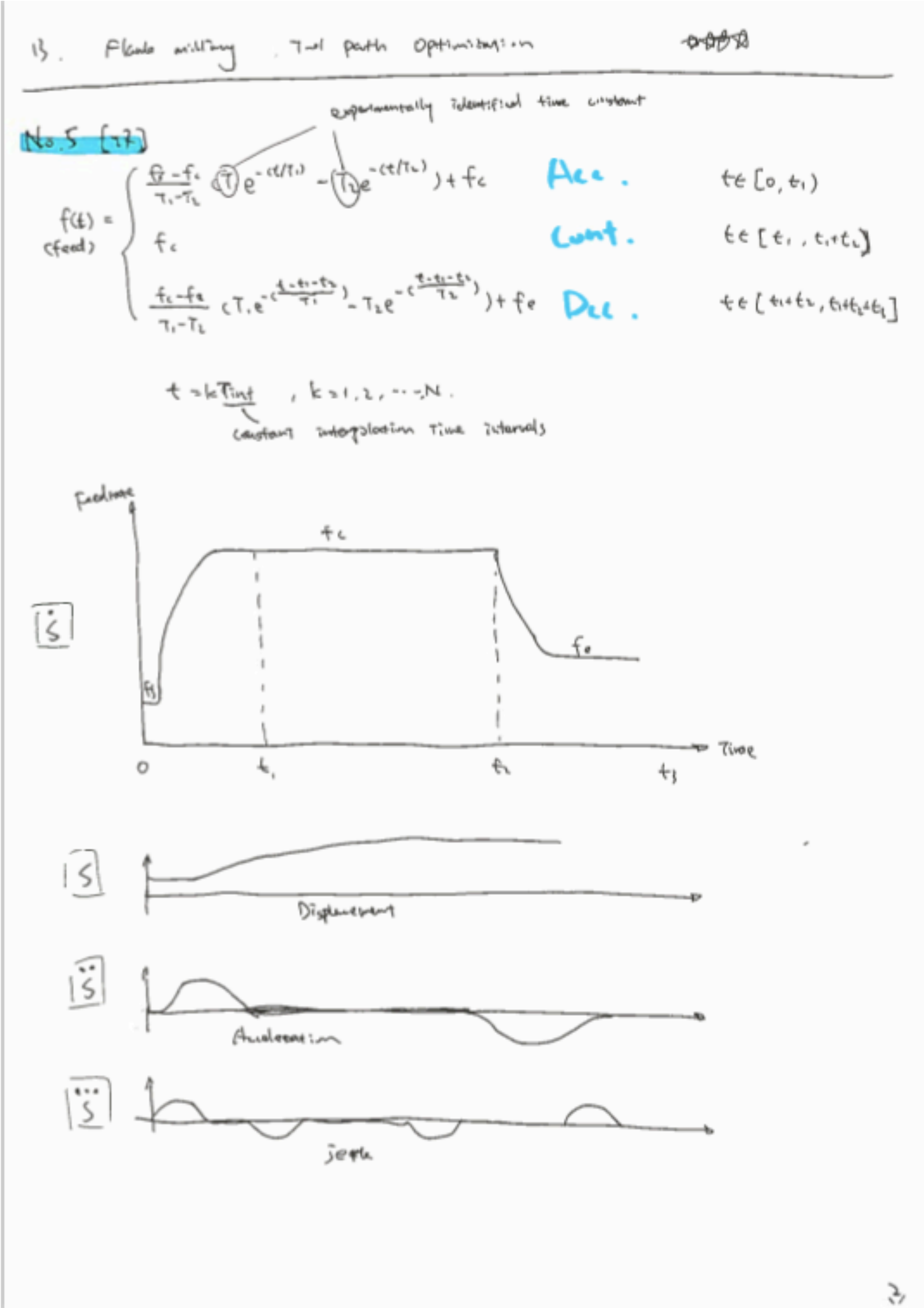

Appendix: Notes of Prediction model page 2

$$L(t) = \begin{cases} \frac{f_3 - f_2}{T_1 - T_2}\{T_1^2(1-e^{-(t/T_1)}) - T_2^2(1-e^{-(t/T_2)})\} + f_2 t + L(0) & t \in [0, t_1) \\ f_2(t - t_1) + L(t_1) & t \in [t_1, t_1+t_2) \\ \frac{f_2 - f_e}{T_1 - T_2}(T_1^2 - T_2^2 - T_1^2 e^{-(\frac{t-t_1-t_2}{T_1})} + T_2^2 e^{-(\frac{t-t_1-t_2}{T_2})}) + f_e(t - t_1 - t_2) + L(t_1+t_2) & t \in [t_1+t_2, t_1+t_2+t_3] \end{cases}$$

the corresponding travel length commands (obtain by integrating the feed in 3)

$$L = L(t_1 + t_2 + t_3)$$

Maching time affect by { Trajectory generation profile / proprietary corner smoothing algorithms.

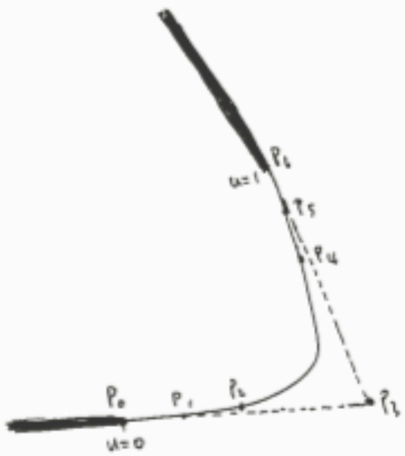

$$P(u) = \begin{cases} P_0 \sum_{n=0}^{5} C_{0n} u^n + \cdots + P_5 \sum_{n=5}^{5} C_{5n} u^n + P_6 \cdot 0 & 0 \le u \le 0.5 \\ P_0 \cdot 0 + \cdots + P_5 \sum_{n=1}^{5} D_{5n} u^n + P_6 \sum_{n=1}^{5} D_{6n} u^n & 0.5 \le u \le 1 \end{cases}$$

found in [12]

No. IV

Introduction. 1.1 Methods about Energy saving.

two deficiencies, (1) three axis (we need five-axis)

(2) only adjustable at the second or third stage

(e.g. feedrate, spindle speed have almost no room to adjust due to working constraints) but the tool path is fixed (unadjustable)

1.2 Tool path generation algorithm (Introduction of other methods)

Structure: 2. establish of energy potential field

3. tool path generation to find best fitting directions

4. physical cutting experiments & comparison

3/

Appendix: Notes of Tool path generation regard to energy consumption page 1

2.1 Pre-determination of tool orientation

Conclusion until page 3: According to Fig 1, 2, 3,
lead angle α should be positive if r_k is negative.

or — " — α — " — as small as 0 to achieve largest cutting width

Tool orientation

$$T_i = (a_i, b_i, c_i) = n\cos\alpha + f\sin\alpha\cos\beta - k\sin\alpha\sin\beta \ ?$$

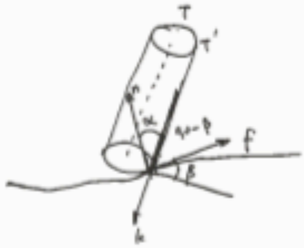

2.2. Energy consumption model

reference constant feed rate f.

$$E = (P_{idle} + P_T + P_D) \times \frac{\|P_{i+1} - P_i\|}{f}$$

P_{idle} → idle power demand; P_T → cutting power demand; P_D → driving power demand

$\|P_{i+1} - P_i\|$ → infinitesimal distance; $\frac{\|P_{i+1} - P_i\|}{f}$ → infinitesimal time, Δt

⇓ calibrated

$$E_T = P_T \times \frac{\|P_{i+1} - P_i\|}{f} = \int_0^{\Delta t}\int_0^{h_0} (F_t(h, t)\, r\, S)\, dh\, dt$$

r → tool radius; S → Spindle speed (rad/s); t → certain time; h → certain height

F_t → tangential force intensity 切向力强度

$(F_t(h,t)\, r\, S)\, dh$ → cutting power at Time t

AC - type tilting table with only two rotary axes. (Appendix)

$$\underbrace{(m_{i,1}, m_{i,2}, m_{i,3}, m_{i,4}, m_{i,5})}_{\text{movements}} = IKT(x_i, y_i, z_i, a_i, b_i, c_i)$$

$$V_k = \frac{(m_{i+1,k} - m_{i,k})}{\Delta t} \qquad a_k = \frac{(m_{i+1,k} - 2m_{i,k} + m_{i-1,k})}{\Delta t^2}, \quad k = 1, 2, 3, 4, 5$$

4

Appendix: Notes of Tool path generation regard to energy consumption page 2

$$E_D = P_D \Delta t = \sum_{k=1}^{5} (\mu_k J_k v_k \Delta t + F_k v_k^2 \Delta t + \{\tfrac{1}{2} J_k ((v_k + a_k \Delta t)^2 - v_k^2)\}) \text{ if } a_k > 0$$

(last term of the kinetic energy demand) → 0 if $a_k \le 0$

[due to the law of energy conservation]
能量守恒定律.

$$E = P_{idle} \Delta t + E_T + E_D$$

The area swept by cutter from P_i to P_{i+1}:

$$A_i = \frac{1}{2} (w_i + w_{i+1}) \|P_{i+1} - P_i\|$$

The quotient of energy consumed over the swept area:

$$U = \frac{E}{A} = \frac{P_{idle} \Delta t + E_T + E_D}{\frac{1}{2} (w_i + w_{i+1}) \|P_{i+1} - P_i\|}$$

Machine-based energy potential field (MBEPF)

Two properties: [Property 1] Each point has two opposite optimal directions. expection is rare and never happened.

[Property 2] Flow lines are continues and never self-interact.

Tool path should ~~try~~ be ~~possibility~~ match as much as possible individual optimal directions of MBEPF

3, Consumption energy based five-axis tool path generation

CC curves → tool orientation in sequently for each CC point →

CL curves based on CC curves → associated tool orientations

5

Appendix: Notes of Tool path generation regard to energy consumption page 3

Due to machining accuracy, two constraints:

① The maximum scallop height (残留高度) on the finish surface must stay below a threshold. 阈值.

② The chord error e of any two adjacent cc points must not exceed a given tolerance.

ds: Fig.8 $\quad w_i = \min(2r, \sqrt{8rh})$

df: Fig.8 $\quad df = \min(\sqrt{8e|r_f| - 4e^2}, df_0)$ ← manually set constant [illegible]

↑ Surface radius of curvature along the feed direction.

Satisfy: ds, df and minimize total energy consumption ← Target

3.1 Optimal feed direction

$$u = \frac{1}{\sum_{i=1}^{4} \frac{1}{\|P-\mu_i\|^2}} \sum_{i=1}^{4} \frac{u_i}{\|P-\mu_i\|^2}$$

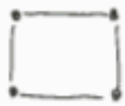

3.2 Principle curve generation

Next cc point P_{i+1}:

$$P_{i+1} = P_i + \frac{df}{E(f_i\cdot\vec{u})^2 + 2F(f_i\cdot\vec{u})(f_i\cdot\vec{v}) + G(f_i\cdot\vec{v})^2} f_i$$

3.3 Iso-scallop height based expansion algorithm

通过 ds 计算 [illegible]

P_i' calculation: $\quad |P_iP_i'| = w_i$

$$(P_i - P_i')\left(\frac{\partial s}{\partial u}\frac{du}{dt} + \frac{\partial s}{\partial v}\frac{dv}{dt}\right) = 0$$

↑ Theoretically the feed direction f_i at P_i

6

Appendix: Notes of Tool path generation regard to energy consumption page 4

By Taylor expansion:

$$P_i' = P_i + \frac{\partial S}{\partial u}\Delta u + \frac{\partial S}{\partial v}\Delta v$$

calculate Δu, Δv using equation (20–(22))

Measurement ratio $\frac{\sum u_i - \sum u_{i0}}{\sum u_i}$, which should be 0 on principle curve, not larger than 0.2 on expanded curve.

No. 10

3. DBSFs in five-axis machining.

Direction-Based Scalar Fields

3.1 . The modified cutting strip width → Fig. 2 $\alpha(\theta) \to d_{xq}(\theta) \to d_{xy}(\theta) \to d_w(\theta)$

3.2 The workpiece feed rate

↓

Fig. 4. P_w, T_w (WCS) —transfer→ M_{setup} (TCS) ∴ Eq 8 —IKT Eq 9 (inverse kinematic transformation)→ (MCS)

(WCS): workpiece coordinate system

(TCS): Table coordinate system

(MCS): Machine coordinate system

Appendix: Notes of Tool path generation regard to energy consumption page 5

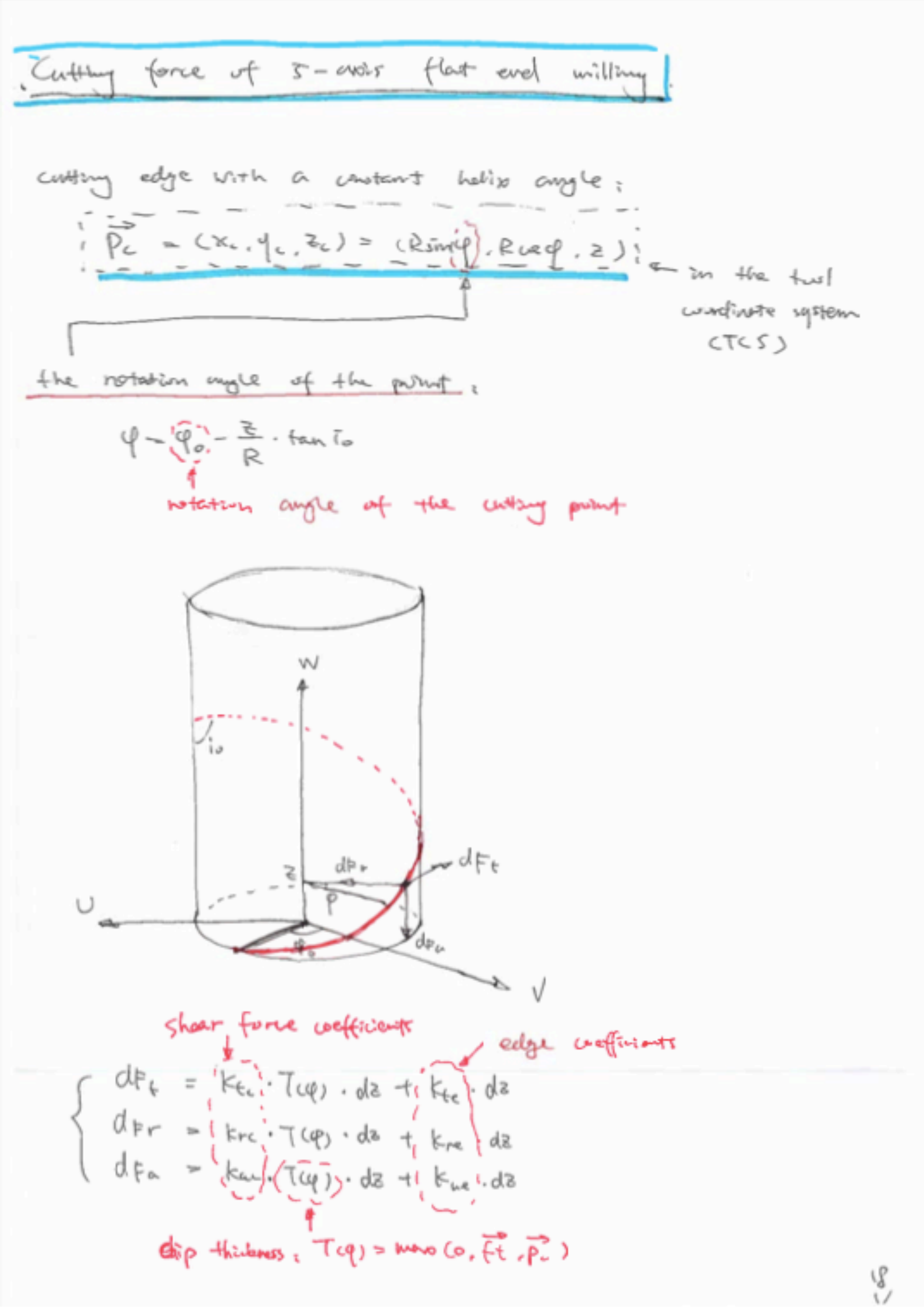

Appendix: Notes of Tool path generation regard to energy consumption page 6

To unify the different cutting force in a same working frame, the three components should be transformed back to the TCS.

$$\begin{bmatrix} dF_u \\ dF_v \\ dF_w \end{bmatrix} = \begin{bmatrix} -\sin(\varphi) & -\cos(\varphi) & 0 \\ -\cos(\varphi) & \sin(\varphi) & 0 \\ 0 & 0 & -1 \end{bmatrix} \begin{bmatrix} dF_r \\ dF_t \\ dF_a \end{bmatrix}$$

Inverse kinematics transformation of five-axis machine with a tilting table.

After the TCS moves into a new position $(x_i, y_i, z_i, a_i, b_i, c_i)$ it is necessary to calculate the relative movement $(m_{i,1}, m_{i,2}, m_{i,3}, m_{i,4}, m_{i,5}, m_{i,6})$

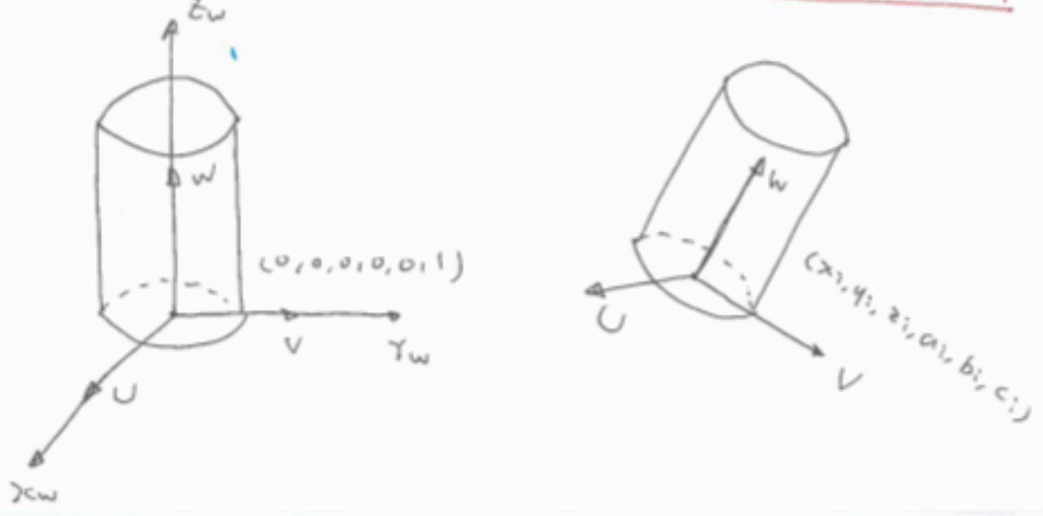

We should solve two rotation angles about axis Xw and Zw to determine the IKT.

next page

19

Appendix: Notes of Tool path generation regard to energy consumption page 7

$$[a_i, b_i, c_i, 1]^T = Rot(Z_w - m_{i,5}) \cdot Rot(X_w - m_{i,6}) \cdot [0, 0, 0, 1]^T$$

↓ Expand to

$$\begin{pmatrix} a_i \\ b_i \\ c_i \end{pmatrix} = \begin{pmatrix} \sin(m_{i,6}) * \sin(m_{i,5}) \\ \sin(m_{i,4}) * \cos(m_{i,5}) \\ \cos(m_{i,4}) \end{pmatrix}$$

With the two rotational coordinates obtained, the translational movement $(m_{i,1}, m_{i,2}, m_{i,3})$ of the TCS in terms of a rotated frame can be expressed as:

$$[m_{i,1}, m_{i,2}, m_{i,3}, 1]^T = Rot(X_w, m_{i,4}) \cdot Rot(Z_w, m_{i,5}) \cdot [x_i, y_i, z_i, 1]^T$$

Finally, the IKT solution $\{m_{i,1}, m_{i,2}, m_{i,3}, m_{i,4}, m_{i,5}, m_{i,6}\}$ is obtained

3. Singularity in inverse kinematics transformation

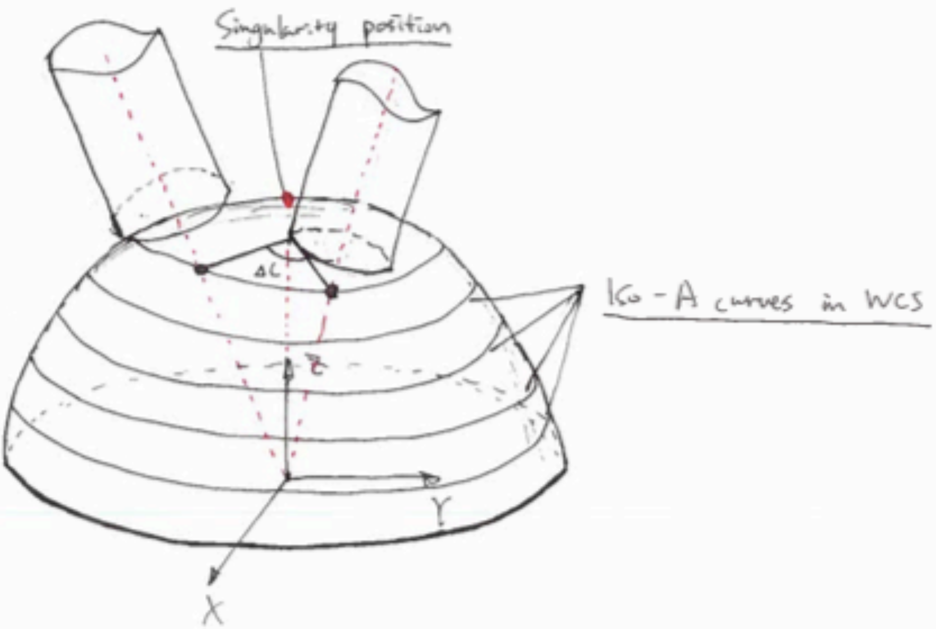

20

Appendix: G codes simple definition page 1

G-Codes simple definition

G00 Rapid traverse
G01 Linear interpolation with feedrate
G02 Circular interpolation (clockwise)
G03 Circular interpolation (counter clockwise)
G2/G3 Helical interpolation
G04 Dwell time in milliseconds
G05 Spline definition
G06 Spline interpolation
G07 Tangential circular interpolation / Helix interpolation / Polygon interpolation / Feedrate interpolation
G08 Ramping function at block transition / Look ahead "off"
G09 No ramping function at block transition / Look ahead "on"
G10 Stop dynamic block preprocessing
G11 Stop interpolation during block preprocessing
G12 Circular interpolation (cw) with radius
G13 Circular interpolation (ccw) with radius
G14 Polar coordinate programming, absolute
G15 Polar coordinate programming, relative
G16 Definition of the pole point of the polar coordinate system
G17 Selection of the X, Y plane
G18 Selection of the Z, X plane
G19 Selection of the Y, Z plane
G20 Selection of a freely definable plane
G21 Parallel axes "on"
G22 Parallel axes "off"
G24 Safe zone programming; lower limit values
G25 Safe zone programming; upper limit values
G26 Safe zone programming "off"
G27 Safe zone programming "on"
G33 Thread cutting with constant pitch
G34 Thread cutting with dynamic pitch
G35 Oscillation configuration
G38 Mirror imaging "on"
G39 Mirror imaging "off"
G40 Path compensations "off"
G41 Path compensation left of the work piece contour
G42 Path compensation right of the work piece contour
G43 Path compensation left of the work piece contour with altered approach
G44 Path compensation right of the work piece contour with altered approach
G50 Scaling
G51 Part rotation; programming in degrees
G52 Part rotation; programming in radians
G53 Zero offset off

Appendix: G codes simple definition page 2

G54	Zero offset #1
G55	Zero offset #2
G56	Zero offset #3
G57	Zero offset #4
G58	Zero offset #5
G59	Zero offset #6
G63	Feed / spindle override not active
G66	Feed / spindle override active
G70	Inch format active
G71	Metric format active
G72	Interpolation with precision stop "off"
G73	Interpolation with precision stop "on"
G74	Move to home position
G75	Curvature function activation
G76	Curvature acceleration limit
G78	Normalcy function "on" (rotational axis orientation)
G79	Normalcy function "off"
G80 - G89 for milling applications:	
G80	Canned cycle "off"
G81	Drilling to final depth canned cycle
G82	Spot facing with dwell time canned cycle
G83	Deep hole drilling canned cycle
G84	Tapping or Thread cutting with balanced chuck canned cycle
G85	Reaming canned cycle
G86	Boring canned cycle
G87	Reaming with measuring stop canned cycle
G88	Boring with spindle stop canned cycle
G89	Boring with intermediate stop canned cycle
G81 - G88 for cylindrical grinding applications:	
G81	Reciprocation without plunge
G82	Incremental face grinding
G83	Incremental plunge grinding
G84	Multi-pass face grinding
G85	Multi-pass diameter grinding
G86	Shoulder grinding
G87	Shoulder grinding with face plunge
G88	Shoulder grinding with diameter plunge
G90	Absolute programming
G91	Incremental programming
G92	Position preset
G93	Constant tool circumference velocity "on" (grinding wheel)
G94	Feed in mm / min (or inch / min)
G95	Feed per revolution (mm / rev or inch / rev)
G96	Constant cutting speed "on"

Appendix: G codes simple definition page 3

Note that some of the above G-codes are not standard. Specific control features, such as laser power control, enable those optional codes.

M codes simple definition

M00 Unconditional stop
M01 Conditional stop
M02 End of program
M03 Spindle clockwise
M04 Spindle counterclockwise
M05 Spindle stop
M06 Tool change (see Note below)
M19 Spindle orientation
M20 Start oscillation (configured by G35)
M21 End oscillation
M30 End of program
M40 Automatic spindle gear range selection
M41 Spindle gear transmission step 1
M42 Spindle gear transmission step 2
M43 Spindle gear transmission step 3
M44 Spindle gear transmission step 4
M45 Spindle gear transmission step 5
M46 Spindle gear transmission step 6
M70 Spline definition, beginning and end curve 0
M71 Spline definition, beginning tangential, end curve 0
M72 Spline definition, beginning curve 0, end tangential
M73 Spline definition, beginning and end tangential
M80 Delete rest of distance using probe function, from axis measuring input
M81 Drive On application block (resynchronize axis position via PLC signal during the block)
M101-M108 Turn off fast output byte bit 1 (to 8)
M109 Turn off all (8) bits in the fast output byte
M111-M118 Turn on fast output byte bit 1 (to 8)
M121-M128 Pulsate (on/off) fast output byte bit 1 (to 8)
M140 Distance regulation "on" (configured by G265)
M141 Distance regulation "off"
M150 Delete rest of distance using probe function, for a probe input (one of 16, M151-M168)
M151-M158 Digital input byte 1 bit 1 (to bit 8) is the active probe input
M159 PLC cannot define the bit mask for the probe inputs
M160 PLC can define the bit mask for the probe inputs (up to 16)
M161-M168 Digital input byte 2 bit 1 (to bit 8) is the active probe input

Appendix: G codes of default solution page 1

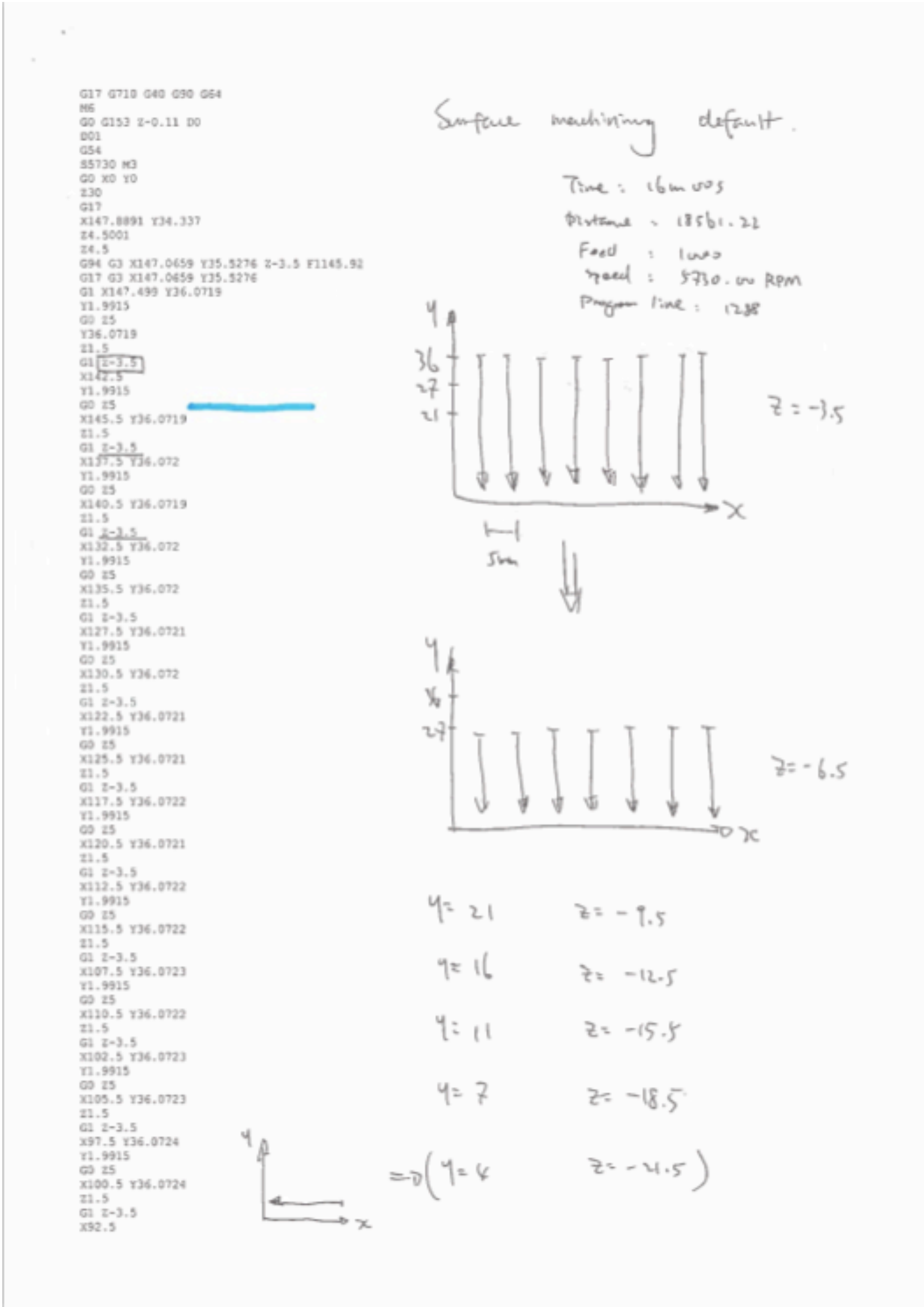


```
G17 G710 G40 G90 G64
M6
G0 G153 Z-0.11 D0
D01
G54
S5730 M3
G0 X0 Y0
Z30
G17
X147.8891 Y34.337
Z4.5001
Z4.5
G94 G3 X147.0659 Y35.5276 Z-3.5 F1145.92
G17 G3 X147.0659 Y35.5276
G1 X147.499 Y36.0719
Y1.9915
G0 Z5
Y36.0719
Z1.5
G1 Z-3.5
X142.5
Y1.9915
G0 Z5
X145.5 Y36.0719
Z1.5
G1 Z-3.5
X137.5 Y36.072
Y1.9915
G0 Z5
X140.5 Y36.0719
Z1.5
G1 Z-3.5
X132.5 Y36.072
Y1.9915
G0 Z5
X135.5 Y36.072
Z1.5
G1 Z-3.5
X127.5 Y36.0721
Y1.9915
G0 Z5
X130.5 Y36.072
Z1.5
G1 Z-3.5
X122.5 Y36.0721
Y1.9915
G0 Z5
X125.5 Y36.0721
Z1.5
G1 Z-3.5
X117.5 Y36.0722
Y1.9915
G0 Z5
X120.5 Y36.0721
Z1.5
G1 Z-3.5
X112.5 Y36.0722
Y1.9915
G0 Z5
X115.5 Y36.0722
Z1.5
G1 Z-3.5
X107.5 Y36.0723
Y1.9915
G0 Z5
X110.5 Y36.0722
Z1.5
G1 Z-3.5
X102.5 Y36.0723
Y1.9915
G0 Z5
X105.5 Y36.0723
Z1.5
G1 Z-3.5
X97.5 Y36.0724
Y1.9915
G0 Z5
X100.5 Y36.0724
Z1.5
G1 Z-3.5
X92.5
```

Appendix: G codes of default solution page 2

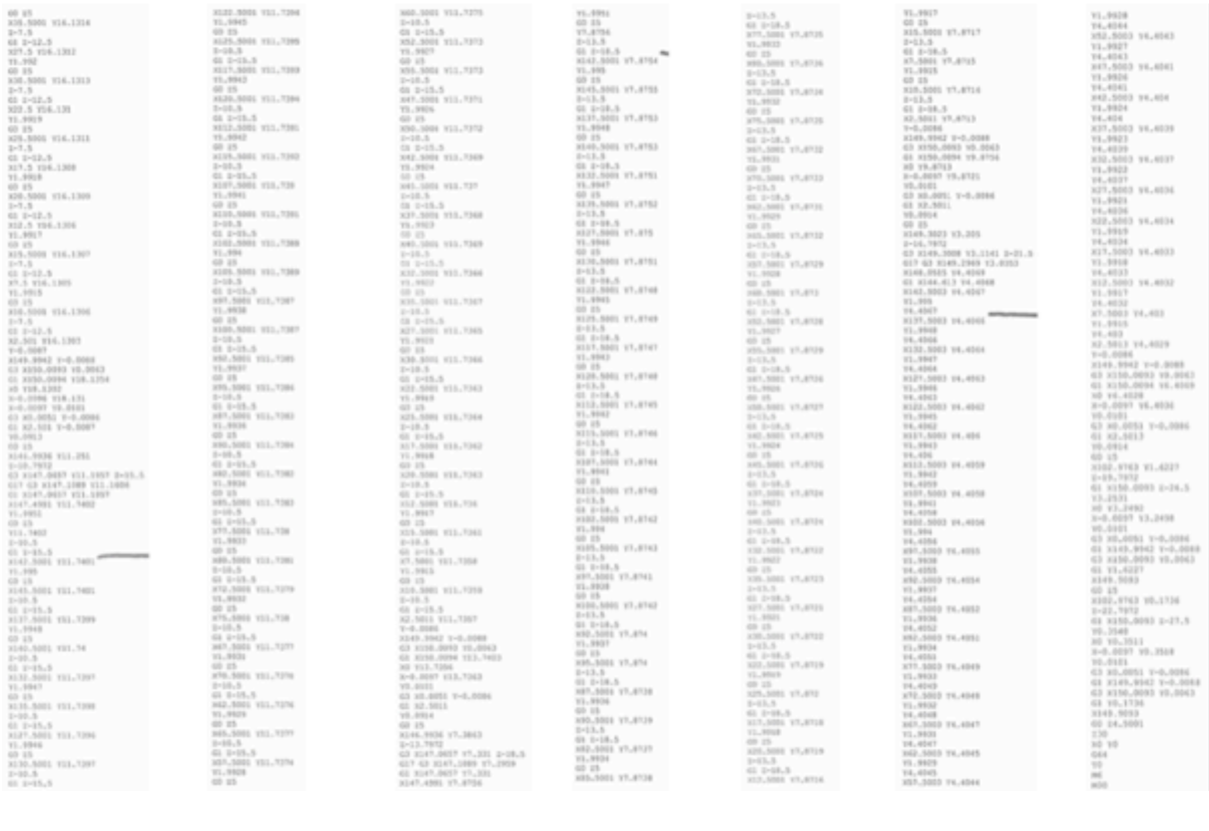

Appendix: G codes of linear path only page 1

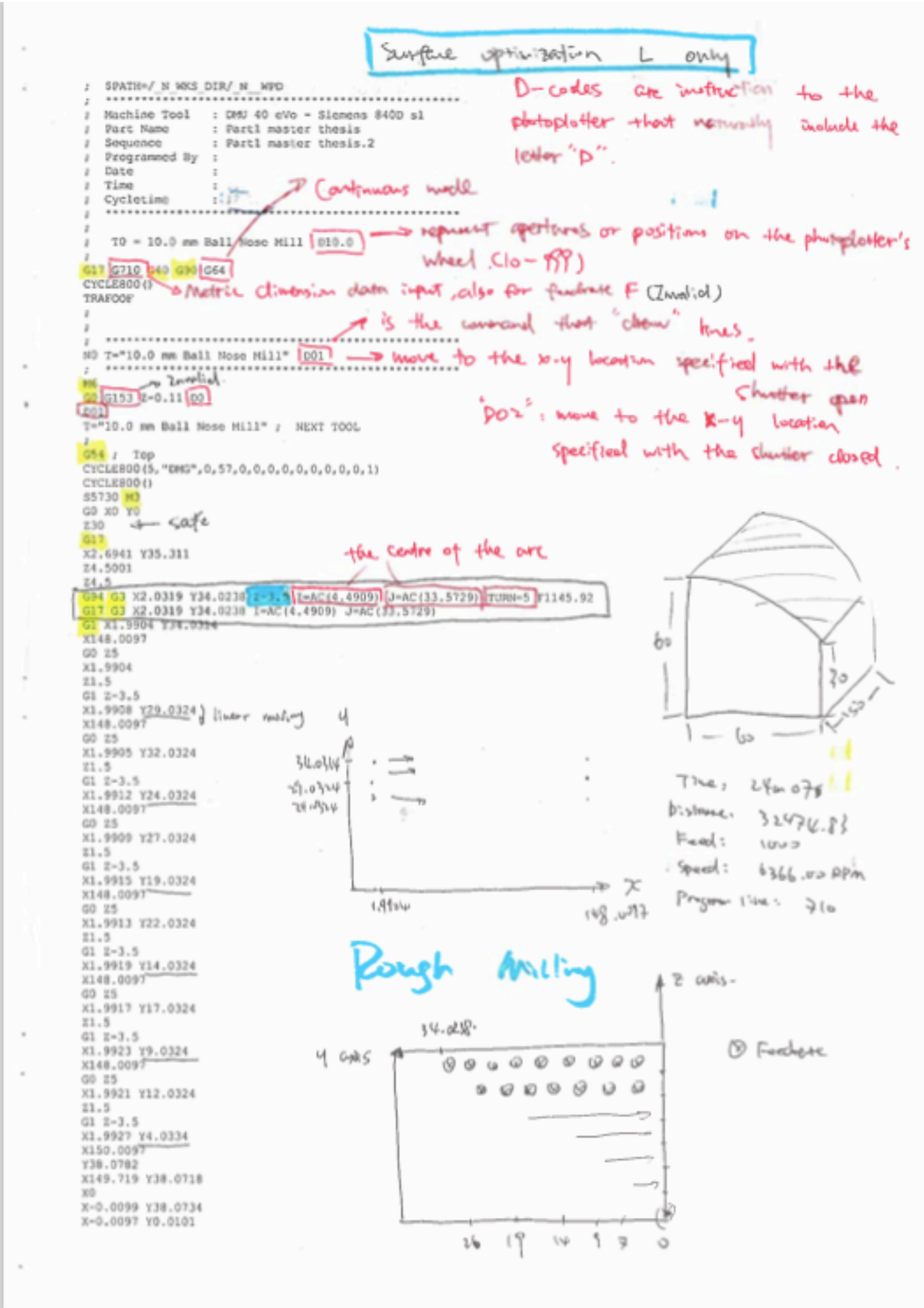

```
;  $PATH=/_N_WKS_DIR/_N__WPD
;  ************************************************************
;  Machine Tool      : DMU 40 eVo - Siemens 840D sl
;  Part Name         : Part1 master thesis
;  Sequence          : Part1 master thesis.2
;  Programmed By     :
;  Date              :
;  Time              :
;  Cycletime         :
;  ************************************************************
;
;   T0 = 10.0 mm Ball Nose Mill D10.0
;
G17 G710 G40 G90 G64
CYCLE800()
TRAFOOF
;
;
;  ************************************************************
N0 T="10.0 mm Ball Nose Mill" D01
;  ************************************************************
M6
G0 G153 Z-0.11 D0
D01
T="10.0 mm Ball Nose Mill" ;  NEXT TOOL
;
G54 ;  Top
CYCLE800(5,"DMG",0,57,0,0,0,0,0,0,0,0,0,1)
CYCLE800()
S5730 M3
G0 X0 Y0
Z30
G17
X2.6941 Y35.311
Z4.5001
Z4.5
G94 G3 X2.0319 Y34.0238 Z-3.5 I=AC(4.4909) J=AC(33.5729) TURN=5 F1145.92
G17 G3 X2.0319 Y34.0238 I=AC(4.4909) J=AC(33.5729)
G1 X1.9904 Y34.0324
X148.0097
G0 Z5
X1.9904
Z1.5
G1 Z-3.5
X1.9908 Y29.0324
X148.0097
G0 Z5
X1.9905 Y32.0324
Z1.5
G1 Z-3.5
X1.9912 Y24.0324
X148.0097
G0 Z5
X1.9909 Y27.0324
Z1.5
G1 Z-3.5
X1.9915 Y19.0324
X148.0097
G0 Z5
X1.9913 Y22.0324
Z1.5
G1 Z-3.5
X1.9919 Y14.0324
X148.0097
G0 Z5
X1.9917 Y17.0324
Z1.5
G1 Z-3.5
X1.9923 Y9.0324
X148.0097
G0 Z5
X1.9921 Y12.0324
Z1.5
G1 Z-3.5
X1.9927 Y4.0334
X150.0097
Y38.0782
X149.719 Y38.0718
X0
X-0.0099 Y38.0734
X-0.0097 Y0.0101
```

Appendix: G codes of linear path only page 2

```
G3 X0.0096 Y-0.0092 CR=0.0198
G1 X149.9903
G3 X150.0097 Y0.0102 CR=0.0199
G1 Y4.0314
X149.9097
G0 Z5
X2.5629 Y26.6465
Z-1.7972
G3 X2.622 Y26.7155 Z-6.5 I=AC(4.4913) J=AC(25.0555) TURN=2
G17 G3 X2.6594 Y26.7567 I=AC(4.4913) J=AC(25.0555)
G1 X2.622 Y26.7155
X1.9906 Y27.2761
X148.0095
G0 Z5
X1.9906
Z-1.5
G1 Z-6.5
X1.9911 Y22.2771
X148.0095
G0 Z5
X1.9908 Y25.2771
Z-1.5
G1 Z-6.5
X1.9916 Y17.2771
X148.0094
G0 Z5
X1.9913 Y20.2771
Z-1.5
G1 Z-6.5
X1.9921 Y12.2771
X148.0094
G0 Z5
X1.9918 Y15.2771
Z-1.5
G1 Z-6.5
X1.9925 Y7.2771
X148.0094
G0 Z5
X1.9922 Y10.2771
Z-1.5
G1 Z-6.5
X1.993 Y2.2781
X150.0093
X150.0095 Y29.5629
X0 Y29.5558
X-0.0096 Y29.5569
X-0.0097 Y0.0101
G3 X0.0051 Y-0.0087 CR=0.0206
G1 X149.9942 Y-0.0088
G3 X150.0093 Y0.0063 CR=0.0208
G1 Y2.2781
X149.9093
G0 Z5
X2.0067 Y19.031
Z-4.7972
G3 X2.0184 Y19.1211 Z-9.5 I=AC(4.4914) J=AC(18.7547) TURN=2
G17 G3 X2.0372 Y19.2309 I=AC(4.4914) J=AC(18.7547)
G1 X2.0272 Y19.1761
X2.0184 Y19.1211
X1.9909 Y19.1252
X148.0094
G0 Z5
X1.9909
Z-4.5
G1 Z-9.5
X1.9915 Y14.1262
X148.0094
G0 Z5
X1.9911 Y17.1262
Z-4.5
G1 Z-9.5
X1.9921 Y9.1262
X148.0094
G0 Z5
X1.9917 Y12.1262
Z-4.5
G1 Z-9.5
X1.9927 Y4.1272
X150.0093
X150.0095 Y23.261
X0 Y23.2551
```

Radius for circular interpolation

Cycle

Appendix: G codes of linear path only page 3

```
X-0.0096 Y23.256
X-0.0097 Y0.0101
G3 X0.0051 Y-0.0086 CR=0.0206
G1 X149.9942 Y-0.0088
G3 X150.0093 Y0.0063 CR=0.0208
G1 Y4.1272
X149.9093
G0 Z5
X2.0143 Y13.9662
Z-7.7972
G3 X2.0281 Y14.056 Z-12.5 I=AC(4.4916) J=AC(13.6299) TURN=2
G17 G3 X2.0383 Y14.1107 I=AC(4.4916) J=AC(13.6299)
G1 X2.0281 Y14.056
X1.991 Y14.0624
X148.0094
G0 Z5
X1.991
Z-7.5
G1 Z-12.5
X1.9918 Y9.0634
X148.0094
G0 Z5
X1.9913 Y12.0634
Z-7.5
G1 Z-12.5
X1.9926 Y4.0644
X150.0093
X150.0094 Y18.1354
X0 Y18.1302
X-0.0096 Y18.131
X-0.0097 Y0.0101
G3 X0.0051 Y-0.0086 CR=0.0206
G1 X149.9942 Y-0.0088
G3 X150.0093 Y0.0063 CR=0.0208
G1 Y4.0644
X149.9093
G0 Z5
X1.9921 Y9.2738
Z-10.7972
G3 X1.9951 Y9.3646 Z-15.5 I=AC(4.4918) J=AC(9.2353) TURN=2
G17 G3 X1.9951 Y9.3646 I=AC(4.4918) J=AC(9.2353)
G1 X1.9912 Y9.3648
X148.0094
G0 Z5
X1.9913
Z-10.5
G1 Z-15.5
X1.9923 Y4.3668
X150.0093
X150.0094 Y13.7403
X0 Y13.7356
X-0.0097 Y13.7363
Y0.0101
G3 X0.0051 Y-0.0086 CR=0.0206
G1 X149.9942 Y-0.0088
G3 X150.0093 Y0.0063 CR=0.0208
G1 Y4.3668
X149.9093
G0 Z5
X2.5065 Y6.8899
Z-13.7972
G3 X2.563 Y6.961 Z-18.5 I=AC(4.4921) J=AC(5.3709) TURN=2
G17 G3 X2.6358 Y7.0454 I=AC(4.4921) J=AC(5.3709)
G1 X2.5989 Y7.0036
X2.563 Y6.961
X1.991 Y7.4325
X148.0094
G0 Z5
X1.991
Z-13.5
G1 Z-18.5
X1.9925 Y2.4345
X150.0093
X150.0094 Y9.8756
X0 Y9.8713
X-0.0097 Y9.8721
Y0.0101
G3 X0.0051 Y-0.0086 CR=0.0206
G1 X149.9942 Y-0.0088
G3 X150.0093 Y0.0063 CR=0.0208
G1 Y2.4345
```

Appendix: G codes of linear path only page 4

```
X149.9093
G0 Z5
X4.4062 Y0.6985
Z-16.7972
G3 X4.3155 Y0.7032 [illegible] I=AC(4.4918) J=AC(3.197) TURN=2
G17 G3 X4.2761 Y0.7063 CR=2.5
X5.6556 Y2.0202 CR=1.25
G2 X6.9036 Y3.2001 CR=1.25
G1 X1.9918
X150.0093
X150.0094 Y6.4069
X0 Y6.4028
X-0.0097 Y6.4036
Y0.0101
G3 X0.0051 Y-0.0086 CR=0.0206
G1 X149.9942 Y-0.0088
G3 X150.0093 Y0.0063 CR=0.0208
G1 Y3.2001
X149.9093
G0 Z5
X102.9763 Y1.6227
Z-19.7972
G1 X150.0093 Z-24.5
Y3.2531
X0 Y3.2492
X-0.0097 Y3.2498
Y0.0101
G3 X0.0051 Y-0.0086 CR=0.0206
G1 X149.9942 Y-0.0088
G3 X150.0093 Y0.0063 CR=0.0208
G1 Y1.6227
X149.9093
G0 Z5
X102.9763 Y0.1736
Z-22.7972
G1 X150.0093 Z-27.5
Y0.3548
X0 Y0.3511
X-0.0097 Y0.3518
Y0.0101
G3 X0.0051 Y-0.0086 CR=0.0206
G1 X149.9942 Y-0.0088
G3 X150.0093 Y0.0063 CR=0.0208
G1 Y0.1736
X149.9093
G0 Z4.5001
Z30
X0 Y0
MSG ("DEFINE OPERATION : PROFILE MILL OPERATION")
M5 M9
G0 G153 Z-0.11 D0
G0 G153 X-449.76 Y-378.77
D01
;
;  ***************************************************
N0 T="10.0 mm Ball Nose Mill"  D01
;  ***************************************************
M6
G0 G153 Z-0.11 D0
D01
T="10.0 mm Ball Nose Mill" ;  NEXT TOOL
;
S6366 M3
G0 X-0.2301 Y-0.7809
Z30
G17
X156.5212 Y48.43
Z4.5
G1 Z-1 F1782.54
G3 X150 Y51.1638 CR=5 F1336.91
G1 X149.6019 Y51.0009 F1782.54
X0
G3 X-5 Y46.0009 CR=5 F1336.91
G0 Z5
X156.0426 Y43.7384
Z4.5
G1 Z-1.5 F1782.54
G3 X150 Y47.4109 CR=5 F1336.91
G1 X149.6019 Y47.3137 F1782.54
X0
G3 X-5 Y42.3137 CR=5 F1336.91
```

↑ rough milling

↓ profile milling

M9 → Coolant off

profile milling

Z30 ← safe

G17 ← x, y plane

F1782.54 ← cutting start point

Appendix: G codes of linear path only page 5

```
G0 Z5
X155.7803 Y40.3961
Z4.5
G1 Z-2 F1782.54
G3 X150 Y44.469 CR=5 F1336.91
G1 X149.6019 Y44.4 F1782.54
X0
G3 X-5 Y39.4 CR=5 F1336.91
G0 Z5
X155.7795 Y38.0521
Z4.5
G1 Z-2.5 F1782.54
G3 X150 Y42.126 CR=5 F1336.91
G1 X149.6019 Y42.0571 F1782.54
X0
G3 X-5 Y37.0571 CR=5 F1336.91
G0 Z5
X155.6359 Y35.7494
Z4.5
G1 Z-3 F1782.54
G3 X150 Y40.0199 CR=5 F1336.91
G1 X149.6019 Y39.965 F1782.54
X0
G3 X-5 Y34.965 CR=5 F1336.91
G0 Z5
X155.6219 Y33.937
Z4.5
G1 Z-3.5 F1782.54
G3 X150 Y38.2259 CR=5 F1336.91
G1 X149.6019 Y38.1723 F1782.54
X0
G3 X-5 Y33.1723 CR=5 F1336.91
G0 Z5
X155.5793 Y32.1291
Z4.5
G1 Z-4 F1782.54
G3 X150 Y36.4732 CR=5 F1336.91
G1 X149.6019 Y36.4237 F1782.54
X0
G3 X-5 Y31.4237 CR=5 F1336.91
G0 Z5
X155.5172 Y30.5408
Z4.5
G1 Z-4.5 F1782.54
G3 X150 Y34.9635 CR=5 F1336.91
G1 X149.6019 Y34.9196 F1782.54
X0
G3 X-5 Y29.9196 CR=5 F1336.91
G0 Z5
X155.5172 Y29.1034
Z4.5
G1 Z-5 F1782.54
G3 X150 Y33.5261 CR=5 F1336.91
G1 X149.6019 Y33.4823 F1782.54
X0
G3 X-5 Y28.4823 CR=5 F1336.91
G0 Z5
X155.5186 Y27.6697
Z4.5
G1 Z-5.5 F1782.54
G3 X150 Y32.0908 CR=5 F1336.91
G1 X149.6019 Y32.0468 F1782.54
X0
G3 X-5 Y27.0468 CR=5 F1336.91
G0 Z5
X155.4612 Y26.3665
Z4.5
G1 Z-6 F1782.54
G3 X150 Y30.8583 CR=5 F1336.91
G1 X149.6019 Y30.8195 F1782.54
X0
G3 X-5 Y25.8195 CR=5 F1336.91
G0 Z5
X155.4435 Y25.1509
Z4.5
G1 Z-6.5 F1782.54
G3 X150 Y29.664 CR=5 F1336.91
G1 X149.6019 Y29.6268 F1782.54
X0
G3 X-5 Y24.6268 CR=5 F1336.91
G0 Z5
```

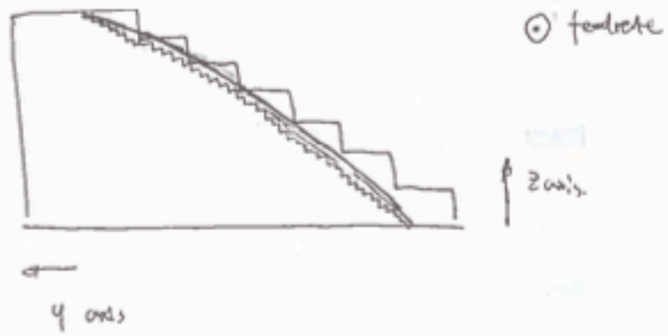

Appendix: G codes of linear path only page 6

```
X155.4435 Y23.9586
Z4.5
G1 Z-7 F1782.54
G3 X150 Y28.4717 CR=5 F1336.91
G1 X149.6019 Y28.4345 F1782.54
X0
G3 X-5 Y23.4345 CR=5 F1336.91
G0 Z5
X155.4072 Y22.7877
Z4.5
G1 Z-7.5 F1782.54
G3 X150 Y27.3443 CR=5 F1336.91
G1 X149.6019 Y27.3103 F1782.54
X0
G3 X-5 Y22.3103 CR=5 F1336.91
G0 Z5
X155.39 Y21.7322
Z4.5
G1 Z-8 F1782.54
G3 X150 Y26.3091 CR=5 F1336.91
G1 X149.6019 Y26.2766 F1782.54
X0
G3 X-5 Y21.2766 CR=5 F1336.91
G0 Z5
X155.3907 Y20.7209
Z4.5
G1 Z-8.5 F1782.54
G3 X150 Y25.297 CR=5 F1336.91
G1 X149.6019 Y25.2644 F1782.54
X0
G3 X-5 Y20.2644 CR=5 F1336.91
G0 Z5
X155.3904 Y19.7087
Z4.5
G1 Z-9 F1782.54
G3 X150 Y24.2851 CR=5 F1336.91
G1 X149.6019 Y24.2526 F1782.54
X0
G3 X-5 Y19.2526 CR=5 F1336.91
G0 Z5
X155.3741 Y18.7187
Z4.5
G1 Z-9.5 F1782.54
G3 X150 Y23.3142 CR=5 F1336.91
G1 X149.6019 Y23.2831 F1782.54
X0
G3 X-5 Y18.2831 CR=5 F1336.91
G0 Z5
X155.3493 Y17.7866
Z4.5
G1 Z-10 F1782.54
G3 X150 Y22.411 CR=5 F1336.91
G1 X149.6019 Y22.382 F1782.54
X0
G3 X-5 Y17.382 CR=5 F1336.91
G0 Z5
X155.3493 Y16.913
Z4.5
G1 Z-10.5 F1782.54
G3 X150 Y21.5374 CR=5 F1336.91
G1 X149.6019 Y21.5085 F1782.54
X0
G3 X-5 Y16.5085 CR=5 F1336.91
G0 Z5
X155.3498 Y16.0401
Z4.5
G1 Z-11 F1782.54
G3 X150 Y20.6639 CR=5 F1336.91
G1 X149.6019 Y20.6349 F1782.54
X0
G3 X-5 Y15.6349 CR=5 F1336.91
G0 Z5
X155.3376 Y15.1592
Z4.5
G1 Z-11.5 F1782.54
G3 X150 Y19.7971 CR=5 F1336.91
G1 X149.6019 Y19.7692 F1782.54
X0
G3 X-5 Y14.7692 CR=5 F1336.91
G0 Z5
X155.3396 Y14.3249
Z4.5
G1 Z-12 F1782.54
G3 X150 Y18.9606 CR=5 F1336.91
G1 X149.6019 Y18.9325 F1782.54
X0
G3 X-5 Y13.9325 CR=5 F1336.91
G0 Z5
X155.318 Y13.5352
Z4.5
G1 Z-12.5 F1782.54
G3 X150 Y18.1955 CR=5 F1336.91
G1 X149.6019 Y18.1692 F1782.54
X0
G3 X-5 Y13.1692 CR=5 F1336.91
G0 Z5
X155.318 Y12.7717
Z4.5
G1 Z-13 F1782.54
G3 X150 Y17.432 CR=5 F1336.91
G1 X149.6019 Y17.4058 F1782.54
X0
G3 X-5 Y12.4058 CR=5 F1336.91
G0 Z5
X155.318 Y12.0085
Z4.5
G1 Z-13.5 F1782.54
G3 X150 Y16.6688 CR=5 F1336.91
G1 X149.6019 Y16.6425 F1782.54
X0
G3 X-5 Y11.6425 CR=5 F1336.91
G0 Z5
X155.3079 Y11.2353
Z4.5
G1 Z-14 F1782.54
G3 X150 Y15.9071 CR=5 F1336.91
G1 X149.6019 Y15.8817 F1782.54
X0
G3 X-5 Y10.8817 CR=5 F1336.91
G0 Z5
X155.3168 Y10.5084
Z4.5
G1 Z-14.5 F1782.54
G3 X150 Y15.1701 CR=5 F1336.91
G1 X149.6019 Y15.144 F1782.54
X0
G3 X-5 Y10.144 CR=5 F1336.91
G0 Z5
X155.293 Y9.7896
Z4.5
G1 Z-15 F1782.54
G3 X150 Y14.4783 CR=5 F1336.91
G1 X149.6019 Y14.4542 F1782.54
X0
G3 X-5 Y9.4542 CR=5 F1336.91
G0 Z5
X155.293 Y9.1159
Z4.5
G1 Z-15.5 F1782.54
G3 X150 Y13.8046 CR=5 F1336.91
G1 X149.6019 Y13.7806 F1782.54
X0
G3 X-5 Y8.7806 CR=5 F1336.91
G0 Z5
X155.293 Y8.4421
Z4.5
G1 Z-16 F1782.54
G3 X150 Y13.1308 CR=5 F1336.91
G1 X149.6019 Y13.1067 F1782.54
X0
G3 X-5 Y8.1067 CR=5 F1336.91
G0 Z5
X155.2934 Y7.7688
Z4.5
G1 Z-16.5 F1782.54
G3 X150 Y12.4571 CR=5 F1336.91
G1 X149.6019 Y12.4329 F1782.54
X0
G3 X-5 Y7.4329 CR=5 F1336.91
G0 Z5
X155.2849 Y7.0925
Z4.5
G1 Z-17 F1782.54
G3 X150 Y11.7903 CR=5 F1336.91
G1 X149.6019 Y11.7669 F1782.54
X0
G3 X-5 Y6.7669 CR=5 F1336.91
G0 Z5
X155.2932 Y6.4543
Z4.5
G1 Z-17.5 F1782.54
G3 X150 Y11.1428 CR=5 F1336.91
G1 X149.6019 Y11.1186 F1782.54
X0
G3 X-5 Y6.1186 CR=5 F1336.91
G0 Z5
X155.2739 Y5.8205
Z4.5
G1 Z-18 F1782.54
G3 X150 Y10.5306 CR=5 F1336.91
G1 X149.6019 Y10.5082 F1782.54
X0
G3 X-5 Y5.5082 CR=5 F1336.91
G0 Z5
X155.2736 Y5.2209
Z4.5
G1 Z-18.5 F1782.54
G3 X150 Y9.9315 CR=5 F1336.91
G1 X149.6019 Y9.909 F1782.54
X0
G3 X-5 Y4.909 CR=5 F1336.91
G0 Z5
X155.2736 Y4.6215
Z4.5
G1 Z-19 F1782.54
G3 X150 Y9.3321 CR=5 F1336.91
G1 X149.6019 Y9.3097 F1782.54
X0
G3 X-5 Y4.3097 CR=5 F1336.91
G0 Z5
X155.2735 Y4.0223
Z4.5
G1 Z-19.5 F1782.54
G3 X150 Y8.7329 CR=5 F1336.91
G1 X149.6019 Y8.7105 F1782.54
X0
G3 X-5 Y3.7105 CR=5 F1336.91
G0 Z5
X155.2735 Y3.423
Z4.5
G1 Z-20 F1782.54
G3 X150 Y8.1337 CR=5 F1336.91
G1 X149.6019 Y8.1112 F1782.54
X0
G3 X-5 Y3.1112 CR=5 F1336.91
G0 Z5
X155.2652 Y2.8373
Z4.5
G1 Z-20.5 F1782.54
G3 X150 Y7.5572 CR=5 F1336.91
G1 X149.6019 Y7.5355 F1782.54
X0
G3 X-5 Y2.5355 CR=5 F1336.91
G0 Z5
X155.2683 Y2.2726
Z4.5
G1 Z-21 F1782.54
G3 X150 Y6.9891 CR=5 F1336.91
G1 X149.6019 Y6.9671 F1782.54
X0
G3 X-5 Y1.9671 CR=5 F1336.91
G0 Z5
X155.2576 Y1.7235
Z4.5
G1 Z-21.5 F1782.54
G3 X150 Y6.4519 CR=5 F1336.91
G1 X149.6019 Y6.4308 F1782.54
X0
G3 X-5 Y1.4308 CR=5 F1336.91
G0 Z5
X155.2576 Y1.1874
Z4.5
G1 Z-22 F1782.54
G3 X150 Y5.9157 CR=5 F1336.91
G1 X149.6019 Y5.8946 F1782.54
X0
G3 X-5 Y0.8946 CR=5 F1336.91
G0 Z5
X155.2576 Y0.6511
Z4.5
G1 Z-22.5 F1782.54
G3 X150 Y5.3794 CR=5 F1336.91
G1 X149.6019 Y5.3583 F1782.54
X0
G3 X-5 Y0.3583 CR=5 F1336.91
G0 Z5
X155.2576 Y0.1149
Z4.5
G1 Z-23 F1782.54
G3 X150 Y4.8433 CR=5 F1336.91
G1 X149.6019 Y4.8222 F1782.54
X0
G3 X-5 Y-0.1778 CR=5 F1336.91
G0 Z4.9983
X155.2576 Y-0.4214
Z4.5
G1 Z-23.5 F1782.54
G3 X150 Y4.307 CR=5 F1336.91
G1 X149.6019 Y4.2859 F1782.54
X0
G3 X-5 Y-0.7141 CR=5 F1336.91
G0 Z4.9738
X155.2425 Y-0.9589
Z4.5
G1 Z-24 F1782.54
G3 X150 Y3.7862 CR=5 F1336.91
G1 X149.6019 Y3.7664 F1782.54
X0
G3 X-5 Y-1.2336 CR=5 F1336.91
G0 Z4.9227
X155.249 Y-1.4504
Z4.5
G1 Z-24.5 F1782.54
G3 X150 Y3.2876 CR=5 F1336.91
G1 X149.6019 Y3.2672 F1782.54
X0
G3 X-5 Y-1.7328 CR=5 F1336.91
G0 Z4.8474
X155.2447 Y-1.9468
Z4.5
G1 Z-25 F1782.54
G3 X150 Y2.7958 CR=5 F1336.91
G1 X149.6019 Y2.7758 F1782.54
X0
G3 X-5 Y-2.2242 CR=5 F1336.91
G0 Z4.7478
X155.2445 Y-2.4293
Z4.5
G1 Z-25.5 F1782.54
G3 X150 Y2.3136 CR=5 F1336.91
G1 X149.6019 Y2.2936 F1782.54
X0
G3 X-5 Y-2.7064 CR=5 F1336.91
G0 Z4.6248
X155.2443 Y-2.9116
Z4.5
G1 Z-26 F1782.54
G3 X150 Y1.8315 CR=5 F1336.91
G1 X149.6019 Y1.8115 F1782.54
X0
G3 X-5 Y-3.1885 CR=5 F1336.91
G0 Z4.5
X155.2443 Y-3.3938
G1 Z-26.5 F1782.54
G3 X150 Y1.3493 CR=5 F1336.91
G1 X149.6019 Y1.3293 F1782.54
X0
G3 X-5 Y-3.6707 CR=5 F1336.91
G0 Z4.5
X155.2446 Y-3.8755
G1 Z-27 F1782.54
G3 X150 Y0.8673 CR=5 F1336.91
G1 X149.6019 Y0.8473 F1782.54
X0
G3 X-5 Y-4.1527 CR=5 F1336.91
G0 Z4.5
X155.2468 Y-4.3549
G1 Z-27.5 F1782.54
G3 X150 Y0.3855 CR=5 F1336.91
G1 X149.6019 Y0.3653 F1782.54
X0
G3 X-5 Y-4.6347 CR=5 F1336.91
G0 Z4.5
Z30
X-0.2301 Y-0.7809
G64
TRAFOOF
ROT
TRANS
CYCLE800()
T0
M6
M30
```

Appendix: G codes of iso scallop crash page 1

```
G17 G710 G40 G90 G64
M6
G0 G153 Z-0.11 D0
D01
G54
S6366 M3
G0 X1.0009 Y0.1008
Z30
G17
Z5
Z-22.7741
G1 G94 Z-27.7741 F1782.54
Y3.6599 Z-24.086
Y7.219 Z-20.7653
Y7.9308 Z-20.1506
Y10.7781 Z-17.7749
Y11.4899 Z-17.1999
Y15.049 Z-14.5587
Y15.7608 Z-14.0775
Y18.6081 Z-12.2126
Y20.0317 Z-11.3455
Y22.879 Z-9.7155
Y24.3026 Z-8.9753
Y27.1499 Z-7.5686
Y28.5735 Z-6.9417
Y31.4208 Z-5.7478
Y32.8444 Z-5.2219
Y35.6917 Z-4.2315
Y37.1154 Z-3.7954
Y39.9626 Z-3.0001
Y41.3863 Z-2.6433
Y44.2335 Z-2.0356
Y45.6572 Z-1.7485
Y49.9281 Z-1.1082
Y51.3517 Z-0.969
Y54.9108 Z-0.6539
Y55.6226 Z-0.6264
Y59.8935 Z-0.5011
G0 Z5
X2.9999 Y0.1008
Z-22.774
G1 Z-27.774
Y3.6599 Z-24.086
Y7.219 Z-20.7652
Y7.9308 Z-20.1505
Y10.7781 Z-17.7749
Y11.4899 Z-17.1998
Y15.049 Z-14.5587
Y15.7608 Z-14.0775
Y18.6081 Z-12.2126
Y20.0318 Z-11.3454
Y22.879 Z-9.7155
Y24.3027 Z-8.9753
Y27.15 Z-7.5686
Y28.5736 Z-6.9417
Y31.4209 Z-5.7478
Y32.8445 Z-5.2219
Y35.6918 Z-4.2315
Y37.1154 Z-3.7954
Y39.9627 Z-3.0001
Y41.3863 Z-2.6433
Y44.2336 Z-2.0356
Y45.6572 Z-1.7485
Y49.9282 Z-1.1082
Y51.3518 Z-0.9689
Y54.9109 Z-0.6539
Y55.6227 Z-0.6264
Y59.8936 Z-0.5011
G0 Z5
X4.9999 Y0.1009
Z-22.7739
G1 Z-27.7739
Y3.66 Z-24.0859
Y7.2191 Z-20.7652
Y7.9309 Z-20.1505
Y10.7782 Z-17.7748
Y11.49 Z-17.1998
Y15.0491 Z-14.5586
Y15.7609 Z-14.0775
Y18.6082 Z-12.2125
Y20.0318 Z-11.3454
```

Surface iso scallop crash

Time: 7m.01s
Distance: 12619.85
Feed: 1000
Speed: 6366.00 RPM
Program line: 2262

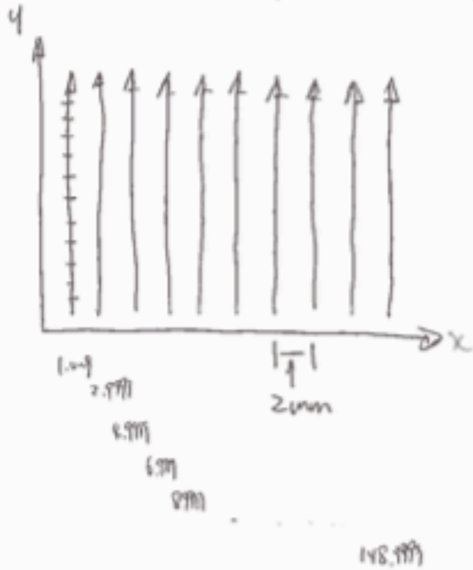

Appendix: G codes of iso scallop crash page 2

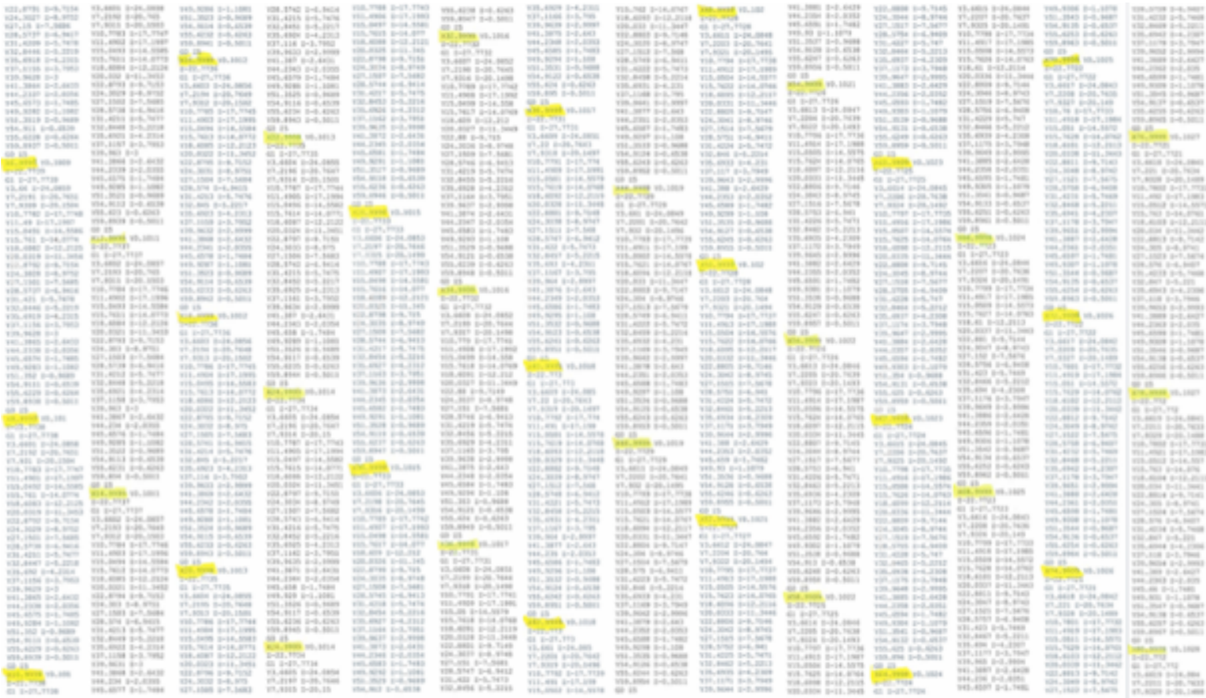

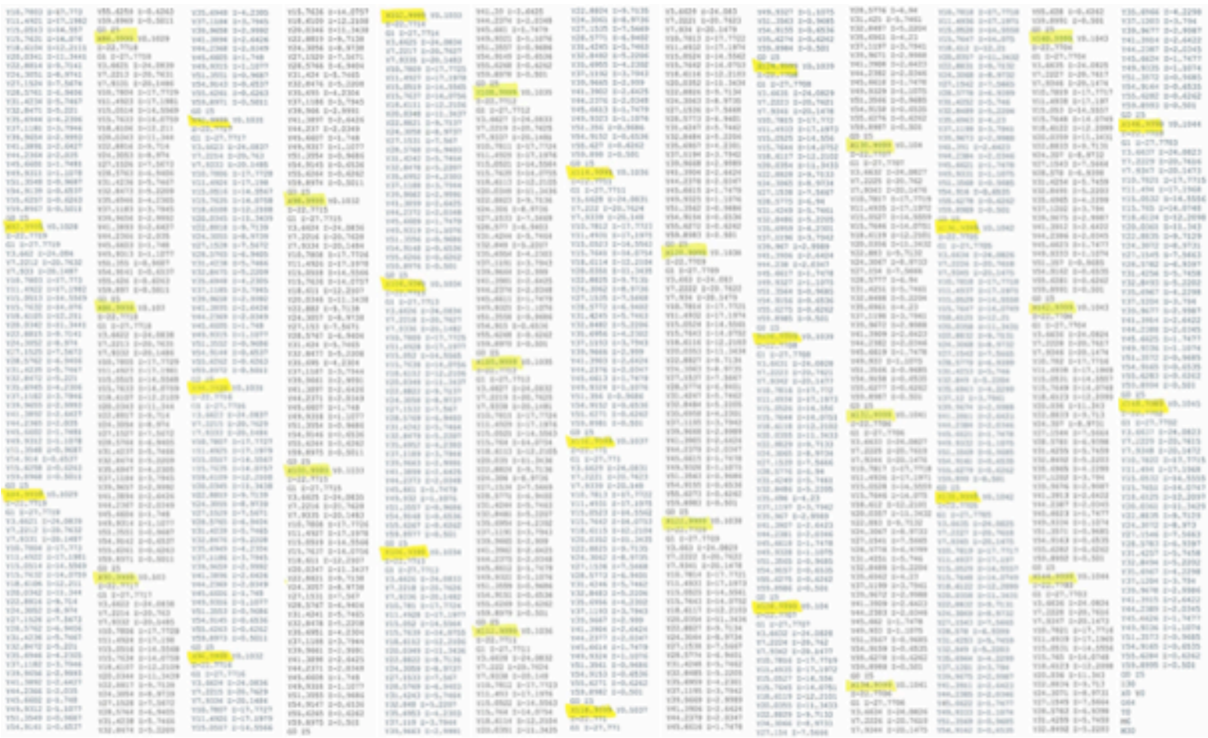

Appendix: G codes of linear path + iso scallop page 1

```
G17 G710 G40 G90 G64
M6
G0 G153 Z-0.11 D0
D01
G54
S5730 M3
G0 X0 Y0
Z30
G17
X2.6941 Y35.311
Z4.5001
Z4.5
G94 G3 X2.0319 Y34.0238 Z-3.5 F1145.92
G17 G3 X2.0319 Y34.0238
G1 X1.9904 Y34.0314
X148.0097
G0 Z5
X1.9904
Z1.5
G1 Z-3.5
X1.9908 Y29.0324
X148.0097
G0 Z5
X1.9905 Y32.0324
Z1.5
G1 Z-3.5
X1.9912 Y24.0324
X148.0097
G0 Z5
X1.9909 Y27.0324
Z1.5
G1 Z-3.5
X1.9915 Y19.0324
X148.0097
G0 Z5
X1.9913 Y22.0324
Z1.5
G1 Z-3.5
X1.9919 Y14.0324
X148.0097
G0 Z5
X1.9917 Y17.0324
Z1.5
G1 Z-3.5
X1.9923 Y9.0324
X148.0097
G0 Z5
X1.9921 Y12.0324
Z1.5
G1 Z-3.5
X1.9927 Y4.0334
X150.0097
Y38.0782
X149.719 Y38.0718
X0
X-0.0099 Y38.0734
X-0.0097 Y0.0101
G3 X0.0096 Y-0.0092
G1 X149.9903
G3 X150.0097 Y0.0102
G1 Y4.0334
X149.9097
G0 Z5
X2.5629 Y26.6465
Z-1.7972
G3 X2.622 Y26.7155 Z-6.5
G17 G3 X2.6594 Y26.7567
G1 X2.622 Y26.7155
X1.9906 Y27.2761
X148.0095
G0 Z5
X1.9906
Z-1.5
G1 Z-6.5
X1.9911 Y22.2771
X148.0095
G0 Z5
X1.9908 Y25.2771
Z-1.5
G1 Z-6.5
X1.9916 Y17.2771
```

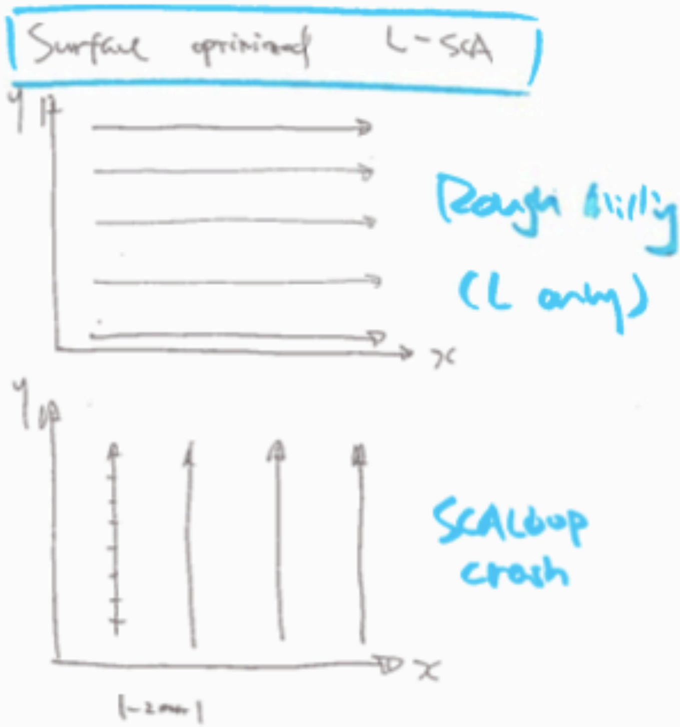

Time: 18m 12s

Distance: 25449.27

Feed: 1000

Speed: 6366.00 RPM

Program line: 238~

Appendix: G codes of linear path + iso scallop page 2

Appendix: G codes of optimized method 1 page 1

```
G17 G710 G40 G90 G64
M6
G0 G153 Z-0.11 D0
D01
G54
S5730 M3
G0 X0 Y0
Z30
G17
X2.1942 Y32.5854
Z4.5001
Z4.5
G94 G2 X2.0319 Y34.0238 Z-3.5 F1145.92
G17 G2 X2.0225 Y33.9689
G1 X2.0319 Y34.0238
X1.9904 Y34.0314
X148.0097
Y29.0324
X1.9908
X1.9912 Y24.0324
X148.0097
Y19.0324
X1.9915
X1.9919 Y14.0324
X148.0097
Y9.0324
X1.9923
X1.9927 Y4.0334
X150.0097
Y38.0782
X149.719 Y38.0718
X0
X-0.0099 Y38.0734
X-0.0097 Y0.0101
G3 X0.0096 Y-0.0092
G1 X149.9903
G3 X150.0097 Y0.0102
G1 Y4.0334
X149.9097
G0 Z5
X147.4398 Y26.6503
Z-1.7972
G2 X147.3808 Y26.7195 Z-6.5
G17 G2 X147.3434 Y26.7607
G1 X147.3808 Y26.7195
X148.0095 Y27.2761
X1.9906
X1.9911 Y22.2771
X148.0095
X148.0094 Y17.2771
X1.9916
X1.9921 Y12.2771
X148.0094
Y7.2771
X1.9925
X1.993 Y2.2781
X150.0093
X150.0095 Y29.5629
X0 Y29.5558
X-0.0096 Y29.5569
X-0.0097 Y0.0101
G3 X0.0051 Y-0.0087
G1 X149.9942 Y-0.0088
G3 X150.0093 Y0.0063
G1 Y2.2781
X149.9093
G0 Z5
X147.9942 Y19.0312
Z-4.7972
G2 X147.9828 Y19.1213 Z-9.5
G17 G2 X147.9741 Y19.1763
G1 X147.9828 Y19.1213
X148.0094 Y19.1252
X1.9909
X1.9915 Y14.1262
X148.0094
Y9.1262
X1.9921
X1.9927 Y4.1272
X150.0093
X150.0095 Y23.261
```

Surface optimization L5

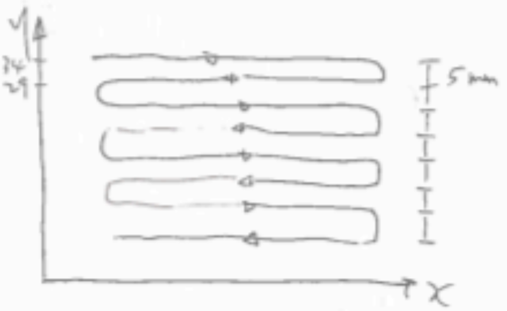

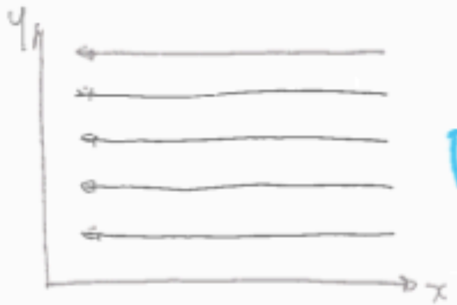

Profile Milling (L only)

Time: 20m 53s
Distance: 28249.98
Feed: 1000
Speed: 6366.00 RPM
Program line: 568

Appendix: G codes of optimized method 1 page 2

```
X0 Y23.2551
X-0.0096 Y23.256
X-0.0097 Y0.0101
G3 X0.0051 Y-0.0086
G1 X149.9942 Y-0.0088
G3 X150.0093 Y0.0063
G1 Y4.1272
X149.9093
G0 Z5
X2.0453 Y14.1452
Z-7.7972
G2 X2.0281 Y14.056 [Z-12.5]
G17 G2 X2.0193 Y14.001
G1 X2.0281 Y14.056
X1.991 Y14.0624
X148.0094
Y9.0634
X1.9918
X1.9926 Y4.0644
X150.0093
X150.0094 Y18.1354
X0 Y18.1302
X-0.0096 Y18.131
X-0.0097 Y0.0101
G3 X0.0051 Y-0.0086
G1 X149.9942 Y-0.0088
G3 X150.0093 Y0.0063
G1 Y4.0644
X149.9093
G0 Z5
X148.0086 Y9.2738
Z-10.7972
G2 X148.0057 Y9.3646 [Z-15.5]
G17 G2 X148.0057 Y9.3646
G1 X148.0094 Y9.3648
X1.9912
X1.9923 Y4.3668
X150.0093
X150.0094 Y13.7403
X0 Y13.7356
X-0.0097 Y13.7363
Y0.0101
G3 X0.0051 Y-0.0086
G1 X149.9942 Y-0.0088
G3 X150.0093 Y0.0063
G1 Y4.3668
X149.9093
G0 Z5
X147.4958 Y6.8923
Z-13.7972
G2 X147.4393 Y6.9635 [Z-18.5]
G17 G2 X147.3667 Y7.0479
G1 X147.4035 Y7.0061
X147.4393 Y6.9635
X148.0094 Y7.4325
X1.991
X1.9925 Y2.4345
X150.0093
X150.0094 Y9.8756
X0 Y9.8713
X-0.0097 Y9.8721
Y0.0101
G3 X0.0051 Y-0.0086
G1 X149.9942 Y-0.0088
G3 X150.0093 Y0.0063
G1 Y2.4345
X149.9093
G0 Z5
X4.225 Y0.7113
Z-16.7972
G2 X4.3155 Y0.7032 [Z-21.5]
G17 G2 X4.3549 Y0.7008
X3.1539 Y1.9744
X4.4036 Y3.2001
G1 X1.9918
X150.0093
X150.0094 Y6.4069
X0 Y6.4028
X-0.0097 Y6.4036
Y0.0101
G3 X0.0051 Y-0.0086
G1 X149.9942 Y-0.0088
G3 X150.0093 Y0.0063
G1 Y3.2001
X149.9093
G0 Z5
X102.9763 Y1.6227
Z-19.7972
G1 X150.0093 [Z-24.5]
Y3.2531
X0 Y3.2492
X-0.0097 Y3.2498
Y0.0101
G3 X0.0051 Y-0.0086
G1 X149.9942 Y-0.0088
G3 X150.0093 Y0.0063
G1 Y1.6227
X149.9093
G0 Z5
X102.9763 Y0.1736
Z-22.7972
G1 X150.0093 [Z-27.5]
Y0.3548
X0 Y0.3511
X-0.0097 Y0.3518
Y0.0101
G3 X0.0051 Y-0.0086
G1 X149.9942 Y-0.0088
G3 X150.0093 Y0.0063
G1 Y0.1736
X149.9093
G0 Z4.5001
Z30
X0 Y0 → safe point
M5 M9
G0 G153 Z-0.11 D0
G0 G153 X-449.76 Y-378.77
D01
M6
G0 G153 Z-0.11 D0
D01
S6366 M3
G0 X-0.2301 Y-0.7809
Z30
G17
X156.5212 Y48.43
Z4.5
G1 Z-1 F1782.54
G3 X150 Y51.1638 F1336.91
G1 X149.6019 Y51.0009 F1782.54
X0
G3 X-5 Y46.0009 F1336.91
G0 Z4.5
X156.0426 Y43.7384
G1 Z-1.5 F1782.54
G3 X150 Y47.4109 F1336.91
G1 X149.6019 Y47.3137 F1782.54
X0
G3 X-5 Y42.3137 F1336.91
G0 Z4.5
X155.7803 Y40.3961
G1 Z-2 F1782.54
G3 X150 Y44.469 F1336.91
G1 X149.6019 Y44.4 F1782.54
X0
G3 X-5 Y39.4 F1336.91
G0 Z4.5
X155.7795 Y38.0521
G1 Z-2.5 F1782.54
G3 X150 Y42.126 F1336.91
G1 X149.6019 Y42.0571 F1782.54
X0
G3 X-5 Y37.0571 F1336.91
G0 Z4.5
X155.6359 Y35.7494
G1 Z-3 F1782.54
G3 X150 Y40.0199 F1336.91
G1 X149.6019 Y39.965 F1782.54
X0
G3 X-5 Y34.965 F1336.91
G0 Z4.5
X155.6219 Y33.937
G1 Z-3.5 F1782.54
G3 X150 Y38.2259 F1336.91
G1 X149.6019 Y38.1723 F1782.54
X0
G3 X-5 Y33.1723 F1336.91
G0 Z4.5
X155.5793 Y32.1291
G1 Z-4 F1782.54
G3 X150 Y36.4732 F1336.91
G1 X149.6019 Y36.4237 F1782.54
X0
G3 X-5 Y31.4237 F1336.91
G0 Z4.5
X155.5172 Y30.5408
G1 Z-4.5 F1782.54
G3 X150 Y34.9635 F1336.91
G1 X149.6019 Y34.9196 F1782.54
X0
G3 X-5 Y29.9196 F1336.91
G0 Z4.5
X155.5172 Y29.1034
G1 Z-5 F1782.54
G3 X150 Y33.5261 F1336.91
G1 X149.6019 Y33.4823 F1782.54
X0
G3 X-5 Y28.4823 F1336.91
G0 Z4.5
X155.5186 Y27.6697
G1 Z-5.5 F1782.54
G3 X150 Y32.0908 F1336.91
G1 X149.6019 Y32.0468 F1782.54
X0
G3 X-5 Y27.0468 F1336.91
G0 Z4.5
X155.4612 Y26.3665
G1 Z-6 F1782.54
G3 X150 Y30.8583 F1336.91
G1 X149.6019 Y30.8195 F1782.54
X0
G3 X-5 Y25.8195 F1336.91
G0 Z4.5
X155.4435 Y25.1509
G1 Z-6.5 F1782.54
G3 X150 Y29.664 F1336.91
G1 X149.6019 Y29.6268 F1782.54
X0
G3 X-5 Y24.6268 F1336.91
G0 Z4.5
X155.4435 Y23.9586
G1 Z-7 F1782.54
G3 X150 Y28.4717 F1336.91
G1 X149.6019 Y28.4345 F1782.54
X0
G3 X-5 Y23.4345 F1336.91
G0 Z4.5
X155.4072 Y22.7877
G1 Z-7.5 F1782.54
G3 X150 Y27.3443 F1336.91
G1 X149.6019 Y27.3103 F1782.54
X0
G3 X-5 Y22.3103 F1336.91
G0 Z4.5
X155.39 Y21.7322
G1 Z-8 F1782.54
G3 X150 Y26.3091 F1336.91
G1 X149.6019 Y26.2766 F1782.54
X0
G3 X-5 Y21.2766 F1336.91
G0 Z4.5
X155.3907 Y20.7209
G1 Z-8.5 F1782.54
G3 X150 Y25.297 F1336.91
G1 X149.6019 Y25.2644 F1782.54
X0
G3 X-5 Y20.2644 F1336.91
G0 Z4.5
X155.3904 Y19.7087
G1 Z-9 F1782.54
G3 X150 Y24.2851 F1336.91
G1 X149.6019 Y24.2526 F1782.54
X0
G3 X-5 Y19.2526 F1336.91
G0 Z4.5
X155.3741 Y18.7187
G1 Z-9.5 F1782.54
G3 X150 Y23.3142 F1336.91
G1 X149.6019 Y23.2831 F1782.54
X0
G3 X-5 Y18.2831 F1336.91
G0 Z4.5
X155.3493 Y17.7866
G1 Z-10 F1782.54
G3 X150 Y22.411 F1336.91
G1 X149.6019 Y22.382 F1782.54
X0
G3 X-5 Y17.382 F1336.91
G0 Z4.5
X155.3493 Y16.913
G1 Z-10.5 F1782.54
G3 X150 Y21.5374 F1336.91
G1 X149.6019 Y21.5085 F1782.54
X0
G3 X-5 Y16.5085 F1336.91
G0 Z4.5
X155.3498 Y16.0401
G1 Z-11 F1782.54
G3 X150 Y20.6639 F1336.91
G1 X149.6019 Y20.6349 F1782.54
X0
G3 X-5 Y15.6349 F1336.91
G0 Z4.5
X155.3376 Y15.1592
G1 Z-11.5 F1782.54
G3 X150 Y19.7971 F1336.91
G1 X149.6019 Y19.7692 F1782.54
X0
G3 X-5 Y14.7692 F1336.91
G0 Z4.5
X155.3396 Y14.3249
G1 Z-12 F1782.54
G3 X150 Y18.9606 F1336.91
G1 X149.6019 Y18.9325 F1782.54
X0
G3 X-5 Y13.9325 F1336.91
G0 Z4.5
X155.318 Y13.5352
G1 Z-12.5 F1782.54
G3 X150 Y18.1955 F1336.91
G1 X149.6019 Y18.1692 F1782.54
X0
G3 X-5 Y13.1692 F1336.91
G0 Z4.5
X155.318 Y12.7717
G1 Z-13 F1782.54
G3 X150 Y17.432 F1336.91
G1 X149.6019 Y17.4058 F1782.54
X0
G3 X-5 Y12.4058 F1336.91
G0 Z4.5
X155.318 Y12.0085
G1 Z-13.5 F1782.54
G3 X150 Y16.6688 F1336.91
G1 X149.6019 Y16.6425 F1782.54
X0
G3 X-5 Y11.6425 F1336.91
G0 Z4.5
X155.3079 Y11.2353
G1 Z-14 F1782.54
G3 X150 Y15.9071 F1336.91
G1 X149.6019 Y15.8817 F1782.54
X0
G3 X-5 Y10.8817 F1336.91
G0 Z4.5
X155.3168 Y10.5084
G1 Z-14.5 F1782.54
G3 X150 Y15.1701 F1336.91
G1 X149.6019 Y15.144 F1782.54
X0
G3 X-5 Y10.144 F1336.91
G0 Z4.5
X155.293 Y9.7896
G1 Z-15 F1782.54
```

Appendix: G codes of optimized method 1 page 3

```
G3 X150 Y14.4783 F1336.91
G1 X149.6019 Y14.4542 F1782.54
X0
G3 X-5 Y9.4542 F1336.91
G0 Z4.5
X155.293 Y9.1159
G1 Z-15.5 F1782.54
G3 X150 Y13.8046 F1336.91
G1 X149.6019 Y13.7806 F1782.54
X0
G3 X-5 Y8.7806 F1336.91
G0 Z4.5
X155.293 Y8.4421
G1 Z-16 F1782.54
G3 X150 Y13.1308 F1336.91
G1 X149.6019 Y13.1067 F1782.54
X0
G3 X-5 Y8.1067 F1336.91
G0 Z4.5
X155.2934 Y7.7688
G1 Z-16.5 F1782.54
G3 X150 Y12.4571 F1336.91
G1 X149.6019 Y12.4329 F1782.54
X0
G3 X-5 Y7.4329 F1336.91
G0 Z4.5
X155.2849 Y7.0925
G1 Z-17 F1782.54
G3 X150 Y11.7903 F1336.91
G1 X149.6019 Y11.7669 F1782.54
X0
G3 X-5 Y6.7669 F1336.91
G0 Z4.5
X155.2932 Y6.4543
G1 Z-17.5 F1782.54
G3 X150 Y11.1428 F1336.91
G1 X149.6019 Y11.1186 F1782.54
X0
G3 X-5 Y6.1186 F1336.91
G0 Z4.5
X155.2739 Y5.8205
G1 Z-18 F1782.54
G3 X150 Y10.5306 F1336.91
G1 X149.6019 Y10.5082 F1782.54
X0
G3 X-5 Y5.5082 F1336.91
G0 Z4.5
X155.2736 Y5.2209
G1 Z-18.5 F1782.54
G3 X150 Y9.9315 F1336.91
G1 X149.6019 Y9.909 F1782.54
X0
G3 X-5 Y4.909 F1336.91
G0 Z4.5
X155.2736 Y4.6215
G1 Z-19 F1782.54
G3 X150 Y9.3321 F1336.91
G1 X149.6019 Y9.3097 F1782.54
X0
G3 X-5 Y4.3097 F1336.91
G0 Z4.5
X155.2735 Y4.0223
G1 Z-19.5 F1782.54
G3 X150 Y8.7329 F1336.91
G1 X149.6019 Y8.7105 F1782.54
X0
G3 X-5 Y3.7105 F1336.91
G0 Z4.5
X155.2735 Y3.423
G1 Z-20 F1782.54
G3 X150 Y8.1337 F1336.91
G1 X149.6019 Y8.1112 F1782.54
X0
G3 X-5 Y3.1112 F1336.91
G0 Z4.5
X155.2652 Y2.8373
G1 Z-20.5 F1782.54
G3 X150 Y7.5572 F1336.91
G1 X149.6019 Y7.5355 F1782.54
X0
G3 X-5 Y2.5355 F1336.91
G0 Z4.5
X155.2683 Y2.2726
G1 Z-21 F1782.54
G3 X150 Y6.9891 F1336.91
G1 X149.6019 Y6.9671 F1782.54
X0
G3 X-5 Y1.9671 F1336.91
G0 Z4.5
X155.2576 Y1.7235
G1 Z-21.5 F1782.54
G3 X150 Y6.4519 F1336.91
G1 X149.6019 Y6.4308 F1782.54
X0
G3 X-5 Y1.4308 F1336.91
G0 Z4.5
X155.2576 Y1.1874
G1 Z-22 F1782.54
G3 X150 Y5.9157 F1336.91
G1 X149.6019 Y5.8946 F1782.54
X0
G3 X-5 Y0.8946 F1336.91
G0 Z4.5
X155.2576 Y0.6511
G1 Z-22.5 F1782.54
G3 X150 Y5.3794 F1336.91
G1 X149.6019 Y5.3583 F1782.54
X0
G3 X-5 Y0.3583 F1336.91
G0 Z4.5
X155.2576 Y0.1149
G1 Z-23 F1782.54
G3 X150 Y4.8433 F1336.91
G1 X149.6019 Y4.8222 F1782.54
X0
G3 X-5 Y-0.1778 F1336.91
G0 Z4.5
X155.2576 Y-0.4214
G1 Z-23.5 F1782.54
G3 X150 Y4.307 F1336.91
G1 X149.6019 Y4.2859 F1782.54
X0
G3 X-5 Y-0.7141 F1336.91
G0 Z4.5
X155.2425 Y-0.9589
G1 Z-24 F1782.54
G3 X150 Y3.7862 F1336.91
G1 X149.6019 Y3.7664 F1782.54
X0
G3 X-5 Y-1.2336 F1336.91
G0 Z4.5
X155.249 Y-1.4504
G1 Z-24.5 F1782.54
G3 X150 Y3.2876 F1336.91
G1 X149.6019 Y3.2672 F1782.54
X0
G3 X-5 Y-1.7328 F1336.91
G0 Z4.5
X155.2447 Y-1.9468
G1 Z-25 F1782.54
G3 X150 Y2.7958 F1336.91
G1 X149.6019 Y2.7758 F1782.54
X0
G3 X-5 Y-2.2242 F1336.91
G0 Z4.5
X155.2445 Y-2.4293
G1 Z-25.5 F1782.54
G3 X150 Y2.3136 F1336.91
G1 X149.6019 Y2.2936 F1782.54
X0
G3 X-5 Y-2.7064 F1336.91
G0 Z4.5
X155.2443 Y-2.9116
G1 Z-26 F1782.54
G3 X150 Y1.8315 F1336.91
G1 X149.6019 Y1.8115 F1782.54
X0
G3 X-5 Y-3.1885 F1336.91
G0 Z4.5
X155.2443 Y-3.3938
G1 Z-26.5 F1782.54
G3 X150 Y1.3493 F1336.91
G1 X149.6019 Y1.3293 F1782.54
X0
G3 X-5 Y-3.6707 F1336.91
G0 Z4.5
X155.2446 Y-3.8755
G1 Z-27 F1782.54
G3 X150 Y0.8673 F1336.91
G1 X149.6019 Y0.8473 F1782.54
X0
G3 X-5 Y-4.1527 F1336.91
G0 Z4.5
X155.2468 Y-4.3549
G1 Z-27.5 F1782.54
G3 X150 Y0.3855 F1336.91
G1 X149.6019 Y0.3653 F1782.54
X0
G3 X-5 Y-4.6347 F1336.91
G0 Z4.5
Z30
X-0.2301 Y-0.7809
G64
T0
M6
M30
```

Appendix: Simulation data of five methods

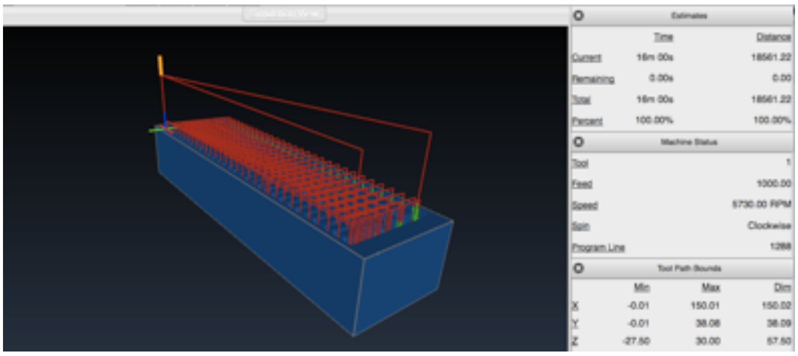

Result of default case

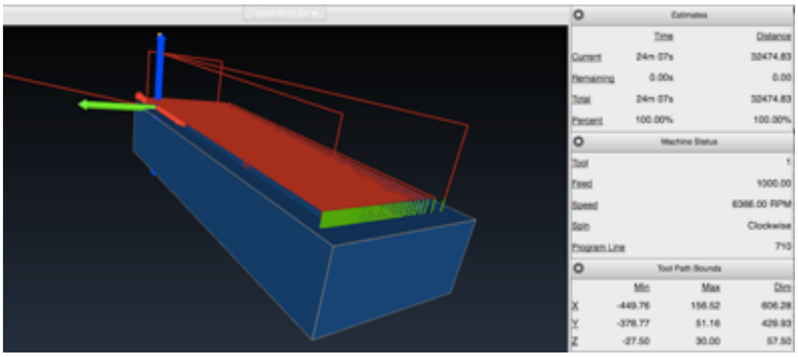

Result of linear case

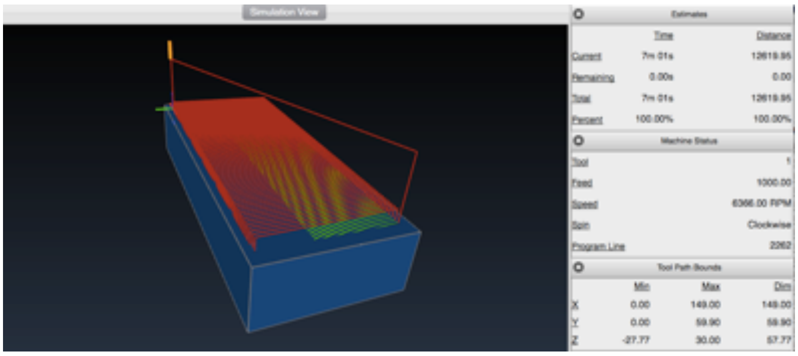

Result of 3D crash case

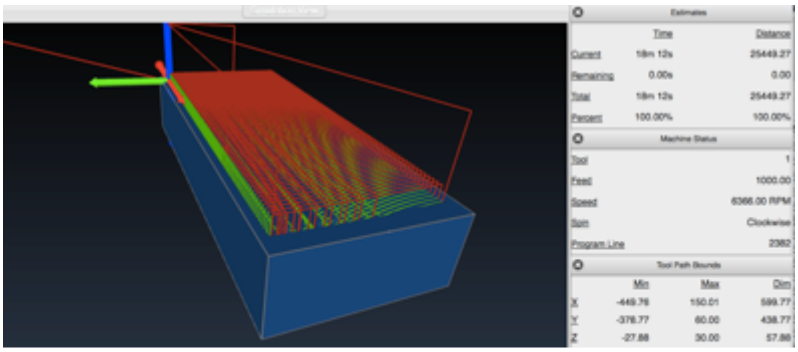

Result of linear+3D case

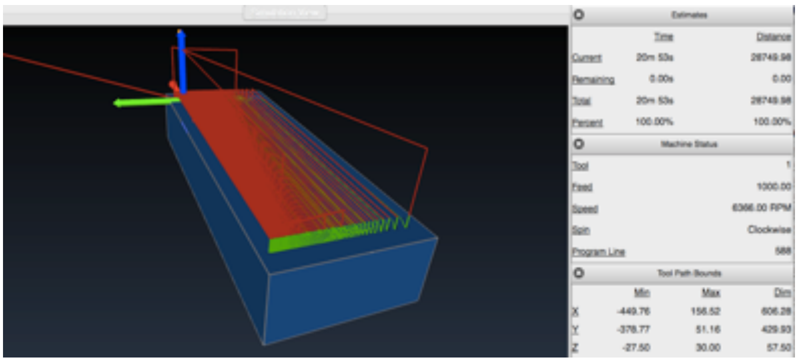

Result of optimized linear case